JAERI-Research
98-053

IRRADIATION EFFECTS ON PLASMA DIAGNOSTIC COMPONENTS

October 1998

Takeo NISHITANI(Editor), Toshiyuki IIDA*, Yujiro IKEDA, Etsuo ISHITSUKA,
Tsunemi KAKUTA, Satoshi KASAI, Hiroshi KAWAMURA, Yosuke MORITA,
Akira NAGASHIMA, Masaru NAKAMICHI, Tetsuya NAKAZAWA, Kenji NODA,
Yukio OYAMA, Hisashi SAGAWA, Fuminobu SATO*, Tatsuo SHIKAMA**,
Tatsuo SUGIE, Daiki YAMAKI and Shin YAMAMOTO

日本原子力研究所
Japan Atomic Energy Research Institute

本レポートは，日本原子力研究所が不定期に公刊している研究報告書です。
入手の問合わせは，日本原子力研究所研究情報部研究情報課（〒319-1195　茨城県那珂郡東海村）あて，お申し越しください。なお，このほかに財団法人原子力弘済会資料センター〒319-1195　茨城県那珂郡東海村日本原子力研究所内）で複写による実費領布をおこなっております。

This report is issued irregularly.
Inquiries about availability of the reports should be addressed to Research Information Division, Department of Intellectual Resources, Japan Atomic Energy Research Institute, Tokai-mura, Naka-gun, Ibaraki-ken 319-1195, Japan.

編集兼発行　日本原子力研究所

Irradiation Effects on Plasma Diagnostic Components

Takeo NISHITANI(Editor), Toshiyuki IIDA*, Yujiro IKEDA[+1], Etsuo ISHITSUKA[+2], Tsunemi KAKUTA[+3], Satoshi KASAI[+4], Hiroshi KAWAMURA[+2], Yosuke MORITA[+5], Akira NAGASHIMA[+6], Masaru NAKAMICHI[+2], Tetsuya NAKAZAWA[+7], Kenji NODA[+8], Yukio OYAMA[+1], Hisashi SAGAWA[+2], Fuminobu SATO*, Tatsuo SHIKAMA**, Tatsuo SUGIE, Daiki YAMAKI[+7] and Shin YAMAMOTO[+9]

Department of Fusion Plasma Research
Naka Fusion Research Establishment
Japan Atomic Energy Research Institute
Naka-machi, Naka-gun, Ibaraki-ken

(Received August 21, 1998)

One of the most important issues to develop the diagnostics for the experimental thermonuclear reactor such as ITER is the irradiation effects on the diagnostics components. Typical neutron flux and fluence on the first wall are 1 MW/m^2 and 1MWa/m^2, respectively for ITER. In such radiation condition, most of the present diagnostics could not survive so that those will be planed to be installed far from the vacuum vessel. However, some diagnostics sensors such as bolometers and magnetic probes still have to be install inside vessel. And many transmission components for lights, wave and electric signals are inevitable even inside vessel. As a part of this R&D program of the ITER Engineering Design Activities (EDA), we carried out the irradiation tests on the basic materials of the transmission components and in-vessel diagnostics sensors in order to identify radiation hardened materials that can be used for diagnostic systems. Optical elements are the most sensitive to radiation damages among the transmission components. In optical fibers and windows, radiation induced luminescence and transmission loss are severe problem for spectrometric diagnostics. Also the change of the reflection coefficient is important in mirrors or reflectors.

This work is conducted as an ITER Engineering Design Activities and this report corresponds to ITER Technical R&D Task Agreement on "Irradiation Tests on Diagnostics Components" (T246).

+1 Center for Neutron Science, Tokai Research Establishment
+2 Department of JMTR, Oarai Research Establishment
+3 Department of Nuclear Energy System, Tokai Research Establishment
+4 Department of Fusion Engineering Research
+5 Department of Material Development, Takasaki Radiation Chemistry Research Establishment
+6 Advanced Photon Research Center, Kansai Research Establishment
+7 Department of Materials Science, Tokai Research Establishment
+8 Office of Planning
+9 Department of ITER Project
* Osaka University
** Tohoku University

The radiation induced luminescence and transmission loss of optical fibers are investigated for ^{60}Co gamma-rays, 14 MeV neutrons and in the Japan Material Testing Reactor (JMTR). We carried out in-situ test of the window and reflectors in JMTR. Bolometers are installed inside the vacuum vessel to measure the whole radiation losses. First of all we have to demonstrate the bolometric measurement in the nuclear radiation condition. We investigated the performance of the JT-60 type bolometer with polyimide substrate under the ^{60}Co gamma-rays. We carried out in-situ test of the new bolometer with AlN substrate in ^{60}Co gamma-rays and JMTR. Magnetic probes are also installed inside the vacuum vessel to measure the magnetic field, which is very important for the plasma control. The magnetic probe made of the MI(Mineral Insulated) cable has been irradiated in JMTR with in-situ measurements.

Keywords: Irradiation Effect, ITER, Diagnostics, Ceramics, Windows, Fiber Optics, Reflector, Bolometer, Magnetic Coil, JMTR, FNS

プラズマ計測機器要素に対する照射効果

日本原子力研究所那珂研究所炉心プラズマ研究部

西谷　健夫（編集）・飯田　敏行*・池田裕二郎[+1]・石塚　悦男[+2]・角田　恒己[+3]
河西　敏[+4]・河村　弘[+2]・森田　洋右[+5]・長島　章[+6]・中道　勝[+2]・中沢　哲也[+7]
野田　健治[+8]・大山　幸夫[+1]・佐川　尚司[+2]・佐藤　文信*・四竈　樹男**・杉江　達夫
八巻　大樹[+7]・山本　新[+9]

（1998年８月２１日受理）

ＩＴＥＲをはじめとする核融合実験炉用計測装置の開発において最も重要な課題の一つは計測機器要素の放射線照射効果である。ＩＴＥＲでは第１壁における中性子束及び中性子フルエンスはそれぞれ熱負荷換算で1 MW/m^2 及び 1MWa/m^{2}にも達する。現在使われているほとんどのプラズマ計測装置はこのような放射線環境下で使用することはできないため、真空容器の外側に移さざるを得ない。しかし、ボロメータや磁気プローブのようにどうしても真空容器内に取り付ける必要があるものもある。また計測装置本体が真空容器外であっても、光、電磁波、電気信号などを伝送する機器は真空容器内に設置する必要がある。そこで、ＩＴＥＲの工学設計活動（ＥＤＡ）の工学Ｒ＆Ｄの一環として、耐放射線性を有した計測機器用材料を開発することを目的として、伝送機器の基本材料や炉内センサーの照射試験を行った。光学機器要素は伝送機器の中でもっとも放射線損傷を受け易い。特に光ファイバーや窓材では、放射線による透過損失と発光が分光測定において問題となる。そこで光ファイバーと窓材に対し、放射線による透過損失と発光の測定を^{60}Co γ 線、14 MeV中性子照射施設及びJMTRにおいて行った。また窓材と反射鏡の照射効果のその場測定をJMTRで行った。ボロメータはプラズマからの放射損失を測定するもので、

本研究はＩＴＥＲ工学設計活動の一環として実施したもので、本報告は工学R&Dタスク協定(T246)に基づくものである。

那珂研究所：〒311-0193　茨城県那珂郡那珂町向山801-1
+1　東海研究所中性子科学研究センター
+2　大洗研究所材料試験炉部
+3　東海研究所エネルギーシステム研究部
+4　核融合工学部
+5　高崎研究所材料開発部
+6　関西研究所光量子科学センター
+7　東海研究所物質科学研究部
+8　企画室
+9　ITER開発室
*　大阪大学
**　東北大学

真空容器内に取り付けられる。まずボロメータがＩＴＥＲのような放射線環境下で正常に動作することを確認する必要がある。そこでポリイミド薄膜を使用したJT-60型ボロメータに対し、^{60}Coγ線照射下にける動作特性を調べた。さらに新たに開発した窒化アルミ薄膜を使用したボロメータに対し、^{60}Coγ線及びJMTRにおける照射試験を行った。またプラズマ制御に必要な磁気プローブも真空容器内に取り付ける必要がある。そこで無機絶縁（MI）ケーブルを用いた磁気プローブのその場測定をJMTRで行った。

Contents

目　　次

1. Introduction

Takeo Nishitani and Shin Yamamoto

One of the most important issues to develop the diagnostics for the experimental thermonuclear reactor such as ITER is the irradiation effects on the diagnostics components. Typical neutron flux and fluence on the first wall are 1 MW/m^2 and $1MWa/m^2$, respectively for ITER. In such radiation condition, most of the present diagnostics could not survive so that those will be planed to be installed far from the vacuum vessel. However, some diagnostics sensors such as bolometers and magnetic probes still have to be install inside vessel. And many transmission components for lights, wave and electric signals are inevitable even inside vessel.

In this task carried out the irradiation tests on the basic materials of the transmission components such as ceramics, windows, fiber optics and mirrors, and in-vessel diagnostics sensors such as magnetic probes and bolometers.

Ceramics will be used as general insulating materials. They will be required in feedthroughs, connectors, mechanical supports and general standoffs, mineral insulated (MI) cables and their seals, substrates (bolometers), and other sensor devices such as pressure gauges. It is now also considered essential that only ITER relevant insulating materials be employed in components to be tested. For ceramics radiation induced conductivity (RIC) and radiation induced electrical degradation (RIED) are important issues under ac/dc electrical fields. Here we investigated RIC effect of a ceramics for 14 MeV neutrons. We confirmed that the RIC due to 14 MeV neutrons is similar to that due to other ionizing radiation such as electrons and gamma-rays.

Optical elements are the most sensitive to radiation damages among the transmission components. In optical fibers and windows, radiation induced luminescence and transmission loss are severe problem for spectrometric diagnostics. Also the change of the reflection coefficient is important in mirrors or reflectors. We carried out in-situ test of the windows and reflectors in JMTR.

Bolometers are installed inside the vacuum vessel to measure the whole radiation losses in the range infra red to soft x-ray. Those radiation power is much less than nuclear radiation (neutrons and gammas) in ITER. First of all we have to demonstrate the bolometric measurement in the nuclear radiation condition. We confirmed the performance of the JT-60 type bolometer under the ^{60}Co gamma-rays. We carried out in-situ test of the new bolometer based on ceramics in ^{60}Co gamma-rays and JMTR.

Magnetic probes are also installed inside the vacuum vessel to measure the magnetic field, which is very important for the kinetic control of the plasma. The magnetic probe made of the MI cable has been irradiated in JMTR with in-situ measurements.

2. Ceramics

2.1 Radiation Induced Conductivities of Ceramics for 14 MeV Neutrons

Kenji Noda, Tetsuya Nakazawa, Yukio Oyama, Daiki Yamaki and
Yujiro Ikeda

2.1.1 Experimental object

RIC(Radiation Induced Conductivity): To obtain experimental data on electrical resistivity of various ceramic materials at various temperatures under 14MeV neutron irradiation.

2.1.2 Specimen

(1) Material
Specimens used are high purity Al_2O_3 single crystal disks. Impurities in the specimens are as follows; Mg=22 ppm, Ca=3 ppm, Ti=54 ppm, Mn=10 ppm, Fe=20 ppm, W<1 ppm, C<1 ppm, Ni<1 ppm, V<1 ppm, Mo<1 ppm, Zn<1 ppm.

(2) Sample dimension:diameter=10mm, thickness=0.5mm

2.1.3 Experimental Condition

(1) Irradiation facility:

An irradiation by 14 MeV neutrons was performed at Fusion Neutronics Source (FNS) in Japan Atomic Energy Research Institute (JAERI). The FNS generates neutrons by D-T reactions using a 350keV deuteron accelerator. The accelerated beam current is up to 25mA and bombarded at 37 TBq of tritium-titanium target. The neutron production yield is 3×10^{12} n/s. The target is located inside a room of 5 m cubic surrounded by thick concrete shield wall.

(2) Irradiation conditions

Neutron flux was in the range from 10^{11} to 10^{15} $n.m^{-2}s^{-1}$ (neutron dose rate range 10^{-4} to 1 $Gy.s^{-1}$), temperature range 300 to 570K (i.e., 300, 490, 570K), and atmosphere a vacuum of 6×10^{-6} torr.

(3) Experimental devices

An irradiation chamber used for in-situ electrical resistivity is schematically shown in Fig.2.1.1[2.1.1]. A specimen is set to a specimen stage positioned to the target of FNS as closely as possible. In order to measure the resistivity of the specimen during the irradiation appropriately, the large ratio of electrical resistance between the specimens and insulators for the electrodes can be realized during irradiation by separating the insulators from the specimen position in the neutron irradiation field with a large neutron flux gradient. In the irradiation chamber, high vacuum can be attained using a turbo molecular pump system to avoid influence due to the ionization of surrounding gas for the

specimens. Temperature of the specimens can be varied in the range 300 to 870K by a heater attached.

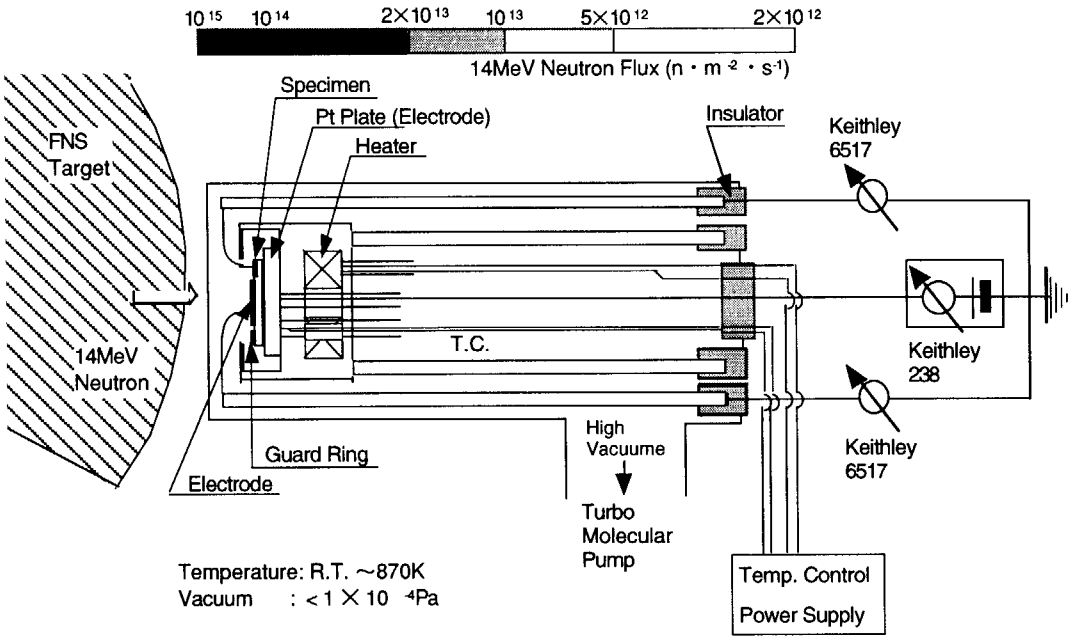

Fig. 2.1.1 Schematic illustrations of irradiation chamber for in-situ measurements of electrical resistivity of ceramic insulator materials and electric diagram of the measurement system.

The three terminal DC method was used for measurements of the resistivity of the specimens. For the measurements at 300K, platinum was deposited in vacuum on a surface of the Al_2O_3 crystal disk specimen to form a guard ring (inner diameter; 6 mm, outer diameter; 10 mm) and a center electrode (diameter; 4mm) with a 1.0 mm gap between the center electrode and the guard ring. On the other side surface of the specimen for the measurements at 300K, another electrode (high side electrode) was also made using the same method. Gold lead wires (diameter; 30mm) were attached on the platinum electrodes by wire bonding machine. In case of the specimens for the measurements at 490 and 570K, the center electrode and the guard ring were formed by painting platinum paste and heating at about 1270K for several hours. Then, another electrode (high side electrode) was made by the above-mentioned procedure using platinum paste.

The electrical diagram of the electrical resistivity measurement system for the measurement at 300K is also shown in Fig.2.1.1. A Keithley 238 Source Measure Unit was used to supply the specimen voltage and measured the specimen current (i.e., the current through the high side electrode and Pt plate in fig. 1). The guard ring current (i.e., the current through the guard ring) and the center electrode currents (i.e., the current through the center electrode) were measured by two Keithley 6517 high-resistance electrometers. For the

measurements at 490 and 570 K, only the center electrode current was measured with HP 4339A high resistance meter.

(4) Measurement:

The center electrode, the guard ring and the specimen currents for irradiation experiments at 300K, and the center electrode current for the experiments at 490 and 570 K were measured with an applied DC voltage of 105 V (i.e., electrical field of 210 $V.mm^{-1}$) in the irradiation chamber before, during and after irradiation. Neutron flux was measured by a 232T fission counter, calibrated by measuring alpha particles generated from DT fusion reactions with a SSD (solid State Detector) at the low neutron flux.

2.1.4 Experimental results and discussion

14 MeV neutron irradiation experiments for each irradiation period of a few minutes were carried out at 300, 490 and 570 K in the neutron flux range 10^{11} to 10^{15} $n.m^{-2}.s^{-1}$ (corresponding dose rates;10^{-4} to 10^{0} Gy. s^{-1}) for Al_2O_3[2.1.1]. The resistivity of a Al_2O_3 single crystal specimen was measured before, during and after each irradiation. Fig. 2.1.2 shows a typical example of the center electrode, the guard ring and the specimen currents in the in-situ measurements at 300 K. These currents increased at once just after the start of the neutron irradiation and constant values of the currents were immediately attained. The constant currents were kept with a constant neutron flux. When the neutron irradiation was stopped, the currents were immediately decreased. Such behavior of the currents was observed in the neutron flux range 10^{11} to 10^{15} $n.cm^{-2}.s^{-1}$. In case of the measurements at 490 and 570K, essentially similar behavior of the center current was also observed in the examined neutron flux range. The electrical resistivity of the specimens was evaluated from the center current values.

Fig. 2.1.3 shows the electrical conductivity of the Al_2O_3 single crystal specimen under irradiation at 300, 490 and 570 K versus 14 MeV neutron dose rate in a log-log plot. The conductivity of ceramic insulator materials under irradiation, σ, can be expressed by

$$\sigma = \sigma_0 + KR^d, \qquad (2.1.1)$$

where σ_0 is the conductivity in the absence of irradiation and KR^d is contribution due to RIC. R is the ionization dose rate, and K and d are constants strongly depending on materials (d is generally 0.5-1.0) [2.1.2].

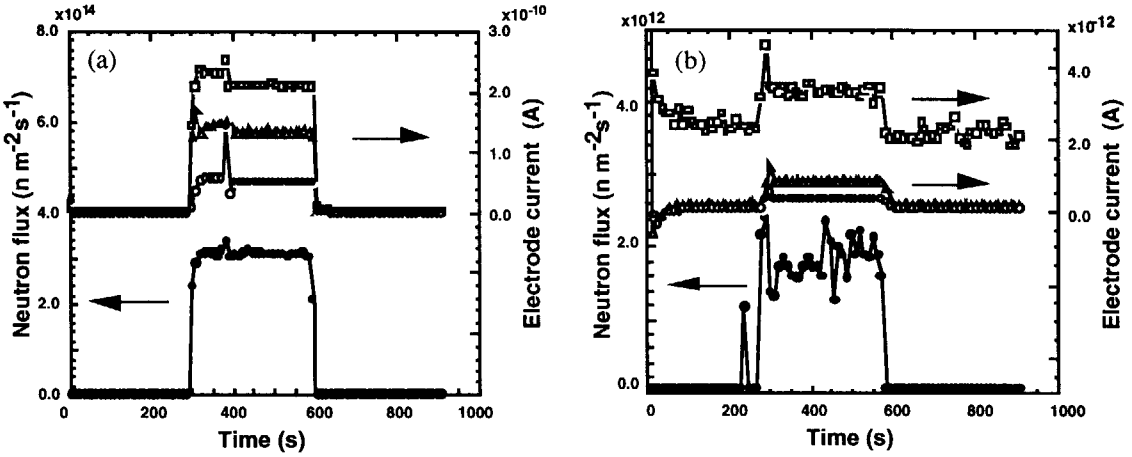

Fig. 2.1.2 Electric currents measured at 105V during neutron irradiation.
[—□—: specimen current, —△—: guard current, —○—: center current, —●—: neutron flux]

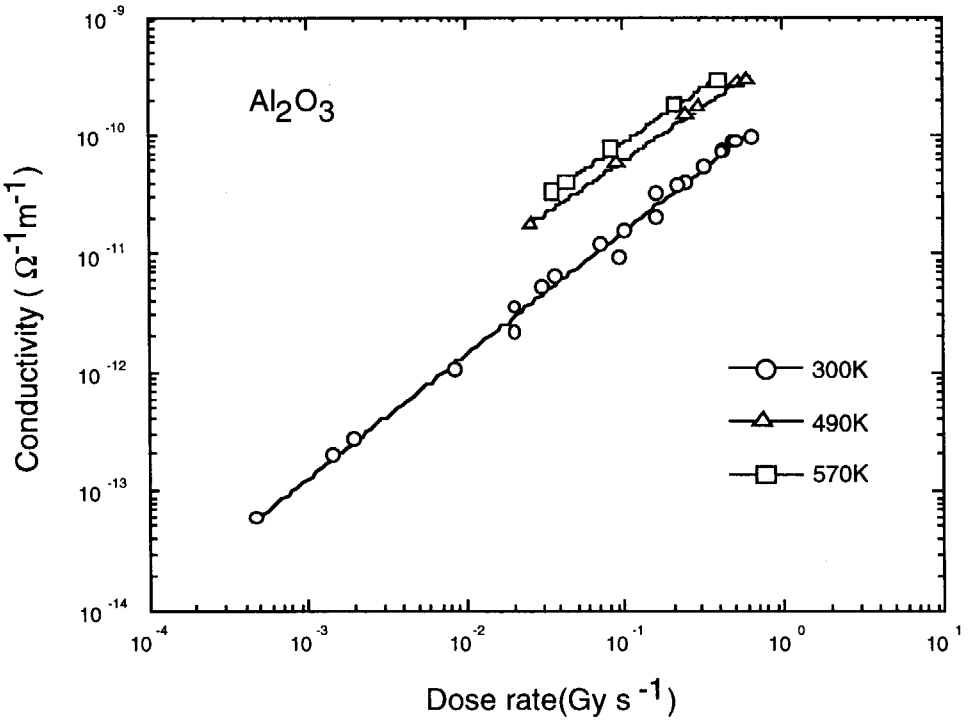

Fig. 2.1.3 Electrical conductivity of Al $_2O_3$ specimen under irradiation at 300, 490 and 570 K as a function of 14 MeV neutron dose rate.

Some recent studies indicated possibility of occurrence of permanent increase of in the electrical conductivity of ceramic insulators, i.e., radiation-induced electrical degradation (RIED) in the temperature range 470 to 870 K even for small damage level of 10^{-5} to 10^{-1} dpa, if an electrical field is applied during irradiation [2.1.2, 2.1.3, 2.1.4-6]. In this experiment, RIED, i.e., change of σ_0, was not observed, because of the negligibly small damage level due to the very low neutron flux level and the short irradiation period.

The dose rate exponent factors, d, for Al_2O_3 under 14 MeV neutron irradiation in the neutron flux range 10^{12} to 10^{15} n m^{-2} s^{-1} (i.e., 10^{-3} to 10^{0} Gy.s^{-1}) were evaluated to be in the range 0.9 to 1 at temperature from 300 to 570 K. The values of d were almost the same as the dose rate exponent for 0.004 wt % Cr_2O_3 doped Linde Al_2O_3 in the temperature range 300 to 570 K under electron irradiation (d=0.95) [2.1.7], in which impurities levels were considered to be similar to those in this study.

In in-situ resistivity measurements for ceramic materials in fission reactors, the measured currents were affected in some cases by leak current due to photoelectrons through ionized gas, which led overestimation of RIC of the specimen [2.1.8-10]. Such influence due to the leak current was substantially suppressed by changing electrical potential applied to the specimen from positive potential to negative potential [2.1.8, 2.1.9]. In this experiment, positive potential was applied to the specimen. However, the influence of the leak current is considered to be very small, since the measurements were carried out in a high vacuum. This is supported by the measured current behavior at 300K in Fig. 2.1.2: If the influence is not very small level, the number of photoelectrons from the capsule wall to the high side electrode with the high potential is much larger than the numbers from the capsule wall to the center electrode and the guard ring of which the potential is almost the same as that of the capsule wall, i.e., the specimen current is much larger than the center and the guard ring currents. However, the specimen current is almost identical to the sum of the center and guard currents. This means that the influence of the leak current through ionized gas is negligibly small. The influence of such leak current was also considered to be negligibly small for the measurements at 490 and 570K, since the measurements were carried out in a high vacuum of the same grade.

Although the measurements of the currents under irradiation were tried to be performed at temperatures higher than 570 K, the currents were not measured appropriately. This was considered to be attributed to contamination of the specimen surface during heating at high temperatures [2.1.11]. In future, improvement of the measurement system such as equipping a cold trap to avoid the specimen surface contamination will be carried out.

RIC of Al_2O_3 has been measured by in-situ measurements using X-ray, gamma-ray, electron, proton and fission neutron irradiation [2.1.2, 2.1.3, 2.1.7, 2.1.12-14]. Fig. 2.1.4 shows a comparison of the relationships between the electrical conductivity of Al_2O_3 under irradiation in the range 300 to 570 K and ionization dose rates in the present study with those in the similar temperature range in some of the other studies mentioned above. The values which are

obtained by extrapolating the present results in the range 300 to 570 K to higher dose rate region are in good agreement with those of 0.004 wt% Cr_2O_3 doped Linde Al_2O_3 single crystal specimens irradiated with electrons [2.1.7]. On the other hand, the extrapolated values are smaller than those of undoped Linde single crystal specimens, and larger than 0.03 wt% Cr_2O_3 doped Linde single crystal specimens [2.1.7]. The RIC at does rates around 10^0 Gy s^{-1} in the present study are larger than that in the Vitox Al_2O_3 polycrystal specimens irradiated at 300 K with X-ray [2.1.12].

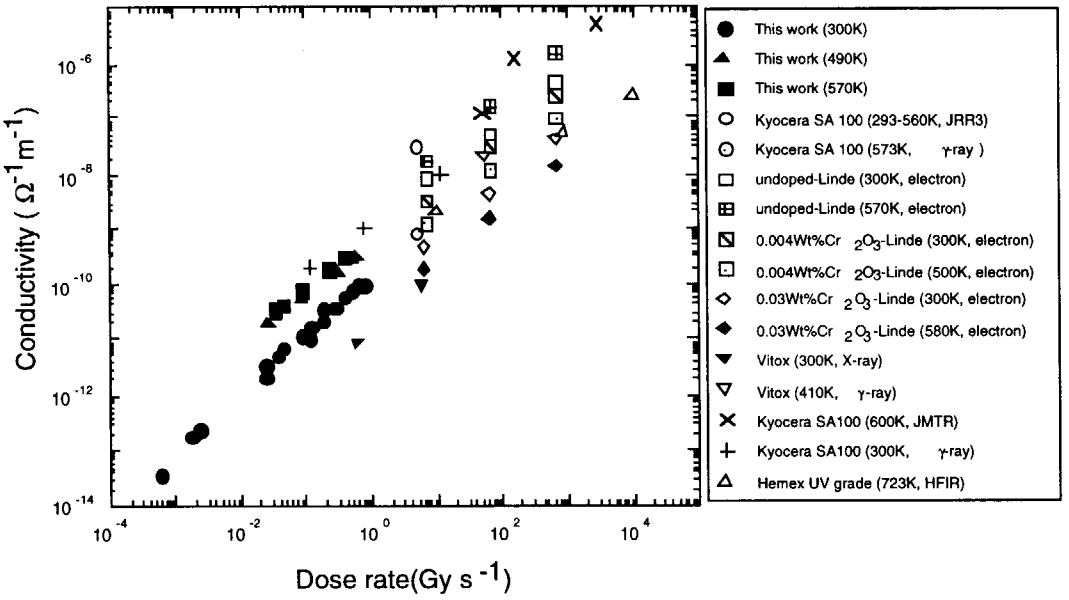

Fig. 2.1.4 Comparison of relationship between electrical conductivity of Al_2O_3 single crystals under 14 MeV neutron irradiation and ionization dose rate in the present study with those for various Al_2O_3 specimens under X ray, gamma-ray, electron, proton, fission neutron irradiation in other studies.

RIC depends on impurity levels and radiation damage levels; RIC decreases with concentration of impurities and radiation damage in general [2.1.2, 2.1.3]. The impurities levels of 0.004 wt% Cr_2O_3 doped Linde Al_2O_3 single crystal specimens are considered to be similar to those in the present study. The impurity levels of the specimens in the present study is higher than those of the undoped Linde single crystals, while lower than those in 0.03 wt% Cr_2O_3 doped Linde single crystals. In the temperature range 300 to 570 K, the electrical conductivity of Al_2O_3 under irradiation is predominantly contributed by RIC, except very low dose rate levels, when RIED does not occur. The RIC decreases with impurities levels in general, as mentioned previously. From this standpoint, the experimental results on RIC in the present study in which the damage levels are negligible small are considered to be quite reasonable.

A typical dose rate due to neutrons and gamma-ray for ceramic insulator materials at the first wall in ITER is expected to be about $2X10^3$ $Gy.s^{-1}$ [2.1.15]. Operation temperatures for most of the ceramic insulators are supposed to be 570 K or below in ITER, although the temperature also depends on the design strongly. The RIC of Al_2O_3 at the first wall of ITER, where the irradiation condition was severer than the other regions, was evaluated by extrapolating data of RIC due to 14 MeV neutrons at 570 K in the present study and of RIC due to gamma-ray (Kyocera SA 100) in the previous work [2.1.14]. The values of RIC extrapolated to the dose rate levels of 10^3 to 10^4 $Gy.s^{-1}$ using the above-mentioned two data sets are almost identical, and the RIC at the first wall of ITER (dose rate level: $2X10^3$ $Gy.s^{-1}$) is evaluated to be about $8X10^{-7}\Omega^{-1}m^{-1}$, if such extrapolation is appropriate for the evaluation. The neutron irradiation produces irradiation damage which decreases the RIC in general [2.1.2], and therefore, the RIC at high fluence levels may be smaller than $8X10^{-7}\Omega^{-1}m^{-1}$.

For prototype or demonstration fusion reactors, the irradiation environments will be severer than that of ITER. The highest dose rate of about 10^4 $Gy.s^{-1}$ (total of dose rates due to neutrons and gamma-ray) will be attained for Al_2O_3 at the first wall in SSTR which was designed as a prototype fusion reactor at JAERI [2.1.16]. The RIC level at the region near the first wall in the SSTR is evaluated to be about $4X10^{-6}\Omega^{-1}m^{-1}$ in the same manner as the evaluation for ITER.

For most ceramic insulator applications, the electrical conductivity during irradiation should be less than $10^{-4}\Omega^{-1}m^{-1}$ in order to prevent dielectric breakdown due to excessive Joule heating. However, even for low power applications typical for many diagnostic components, it is desirable to keep the conductivity $\sigma < 10^{-4}\Omega^{-1}m^{-1}$ to prevent instrument decalibration due to spurious currents [2.1.2]. From this standpoint, the electrical conductivity in Al_2O_3 under operation condition of the fusion reactors is not considered to provide any significant problems for ceramic insulator components, if only RIC is taken into account for electrical degradation in the irradiation field. It is, however, possible that the very low conductivity levels ($<10^{-6}\Omega^{-1}m^{-1}$) is desirable for the better accuracy of measurements in some diagnostic components. In such cases, the RIC level at the first wall of ITER (i.e., the highest dose rate level in ITER) may be evaluated to meet this criterion, while that for SSTR may not. Consequently, the RIC level for insulators of diagnostic components for the prototype fusion reactor has to be decreased to the desired level by moving the position of the components from the region near the first wall to the outer region of the blanket.

RIED was observed for irradiation with an electrical field in the temperature range 470 to 870 K even for small damage level of 10^{-5} to 0.1 dpa in several studies [2.1.2, 2.1.3, 2.1.4-6], while RIED as a bulk effect was not in some recent studies [2.1.3, 2.1.11, 2.1.13, 2.1.8-10, 2.1.17]. The observed RIED phenomena were very complicated and depended on the applied electric field, temperatures, dose rates, fluence levels, impurities levels, sorts of radiation, irradiation atmosphere, etc., and the mechanism of RIED is still unclear [2.1.17]. However,

the fusion ceramic materials community has reached consensus of the following view for RIED: RIED is not serious issue for use of particular alumina in the ITER level irradiation condition [2.1.17]. From this standpoint, the RIC dominates degradation of electrical insulation performance of alumina as a typical insulator ceramics in the ITER condition, and this led importance of accurate RIC data for ITER design.

In the present study, the RIC due to 14 MeV neutrons for the Al_2O_3 single crystals was evaluated in the limited temperature range, i.e., 300 to 570 K. Alunima other than the Al_2O_3 single crystal and the various ceramic insulators will be used in fusion reactors, and use of ceramic insulators at the higher temperatures is also expected. Thus, further studies to evaluate RIC due to 14 MeV neutrons with sufficient accuracy level are needed to obtain the RIC data of various ceramic materials in the wider temperature range for fusion reactor designs.

2.1.5 Conclusion

The radiation induced conductivity (RIC) due to 14 MeV neutrons for Al_2O_3 in the temperature range 300 to 570 K was measured in the neutron dose rate range 10^{-2} to 10^{0} $Gy.s^{-1}$ using the Fusion Neutronics Source (FNS) at the Japan Atomic Energy Research Institute. The RIC of Al_2O_3 was estimated for the severest irradiation environment in ITER and a prototype fusion reactor (SSTR) by extrapolating the data due to 14 MeV neutrons in the present study and those due to gamma-ray in the other study. It was considered from the measured RIC data extrapolated to the higher dose rate level that the electrical degradation of alumina due to the RIC was allowable level for electrical insulator materials and diagnostic materials for ITER. Further studies to evaluate RIC due to 14 MeV neutrons with sufficient accuracy level are needed to obtain the RIC data of various ceramic materials in the wider temperature range for fusion reactor designs.

2.1.6 Remaining issues and future plan:

In-situ measurement of electrical resistivity of sintered Al_2O_3, Cr-doped Al_2O_3, etc. in the temperature range 300 to 570 K and at much higher temperatures.
Improvement of the system for appropriate measurements at the higher temperatures.

References

[2.1.1] K. Noda, T. Nakazawa, Y. Oyama, H. Maekawa, J. Kaneda and C. Kinoshita, Fusion Eng. Des. **29** (1995) 448.
[2.1.2] J. Zinkle and E.R. Hodgson, J. Nucl. Mater. **191-194** (1992) 58.
[2.1.3] L.W. Hobbs., F.W. Clinard, Jr., S.J. Zinkle, R.C. Ewing, J. Nucl. Mater.

216 (1994) 291.
[2.1.4] E.R. Hodgson, J. Nucl. Mater. **179-181** (1991) 383.
[2.1.5] G.P. Pells, J. Nucl. Mater. **184** (1991) 177.
[2.1.6] T. Shikama, M. Narui, Y. Endo, T. Sagawa and H. Kayano, J .Nucl. Mater.**191-194** (1992) 575.
[2.1.7] R.W. Klaffky, B.H. Rose, A.N. Goland and G.J. Dienes, Phys. Rev. **B 21** (1980) 3610.
[2.1.8] E.H. Farnum, T. Shikama, M. Narui, T. Sagawa and K. Scaborough, J. Nucl. Mater. **228** (1996) 117.
[2.1.9] S.J. Zinkle, D.P. White, L.L. Snead, W.S. Eatherly, A.L. Qualls, D.W. Heatherly, R.G. Sitterson, R.L. Wallace, D.G. Raby, M.T. Hurst, E.H. Farnum, K. Scaborough, T. Shikama, M. Narui, and K. Shiiyama, F usion Material Semiann. Prog. Report for the period ending, June 30 (1996), DOE/ER-0313/20 p.257.
[2.1.10] T. Tnanifuji, Y. Katano, T. Nakazawa and K. Noda, J. Nucl. Mater. in press.
[2.1.11] W. Kesternich, F. Scheuermann and S.J. Zinkle, J. Nucl. Mater. **219** (1995) 190.
[2.1.12] G.P. Pells, Radiat. Eff. 97 (1986) 199.
[2.1.13] E.R. Hodgson and S. Clement, J. Nucl. Mater. **155-157** (1988) 357.
[2.1.14] T. Shikama, M. Narui,, Y. Endo, A. Ochiai and H. Kayano, J. Nucl. Mater. **191-194** (1992) 544.
[2.1.15] L.L. Snead, D.P. White and S.J. Zinkle, J. Nucl. Mater. in press.
[2.1.16] Y. Seki, et al. , JAERI-M 91-081 (1991).
[2.1.17] Proceeding of the 9th IEA workshop on Radiation Effects in Ceramic Insulators, Cincinnati, May 8-9, 1997, compiled by S.J. Zinkle and G.L. Burn, ORNL/M-6068.

2.2 Data Evaluation of Radiation Effects of Ceramics

Tatsuo Shikama

2.2.1 Electrical properties

Electrical properties of ceramic insulators are affected by impurities, inclusions, precipitates along grain boundaries, preferred orientation, grain size, etc.. Recent advancement of quality control of manufacturing processes of fine ceramics has been resulting in relatively reliable and reproducible database of electrical properties of ceramic insulators without irradiation. Especially, alumina(Al_2O_3), which is a principle electrical insulator in the contemporary industry, has an extensive database of electrical properties without irradiation. However, recently revealing discrepancies and disagreements among results of irradiation experiments are strongly implying that not-well-evaluated material properties, which resulted from not-yet-well controlled manufacturing processes, would affects radiation effects on electrical properties, as well as on other properties.

Each home team is carrying out its irradiation tests on its own ceramics in general, such as the USA on Wesgo, the EU on Vitox, Russia on her own, and Japan on Kyocera in the case of alumina. Recent international round-robin tests of electrical conductivity on the Wesgo high grade polycrystal alumina has qualified reproducibility of each measurement, and the HFIR-TRIST-ER [2.2.1] experiment (In-situ Electrical Resistivity measurements in Temperature Regulated In-Situ Test facility in High Flux Isotope Reactor in Oak Ridge National Laboratory) in the US/Japan collaborative venture called JUPITER program clarified dependence of electrical conductivity on materials.

Figure 1 shows results of in-situ electrical measurements under the 14 MeV fusion neutron irradiation in Fusion Neutron Source in Tokai Research Establishment of JAERI, whose details were described in the previous section, in comparison with other reported data. Figure 2 shows results of the HFIR-TRIST-ER experiment. These results clearly show that obtained results concerning the phenomenon called radiation induced conductivity (RIC) agreed well quantitatively with each other, regardless of irradiation sources used in each experiment. The results indicate that the applied measuring technique, so-called three electrode guarded configuration, has been established well and it yielded reliable quantitative data of electrical conductivity under irradiation. It could be concluded that the increase of electrical conductivity due to the phenomenon of RIC will not be a problem for the plasma diagnostics in ITER, namely the electrical conductivity of alumina will be smaller than 10^{-6} S/m at the electronic excitation rate of 10^4Gy/s.

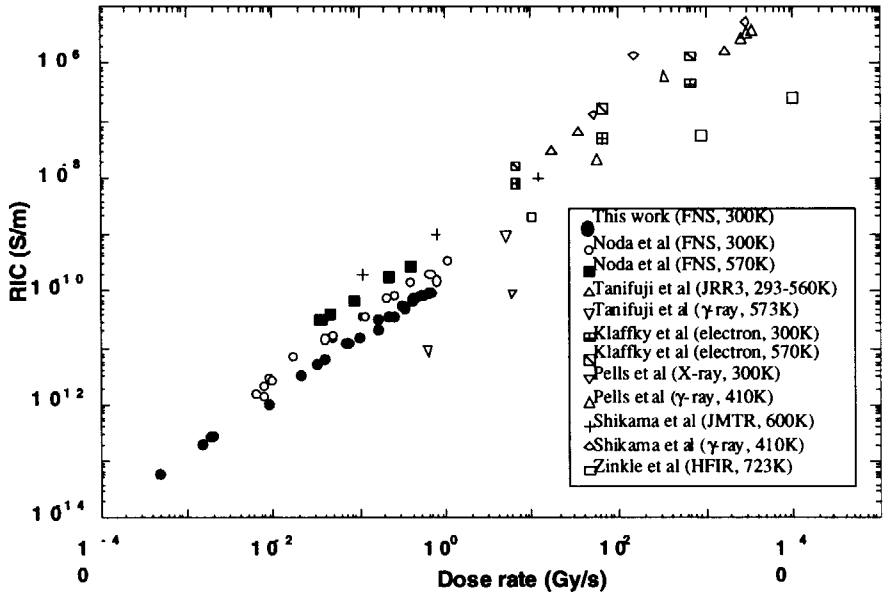

Fig.2.2.1 Comparison of dose rate dependence of conductivity calculated from center current in FNS data for Al_2O_3 specimen in this work with the other RIC data.

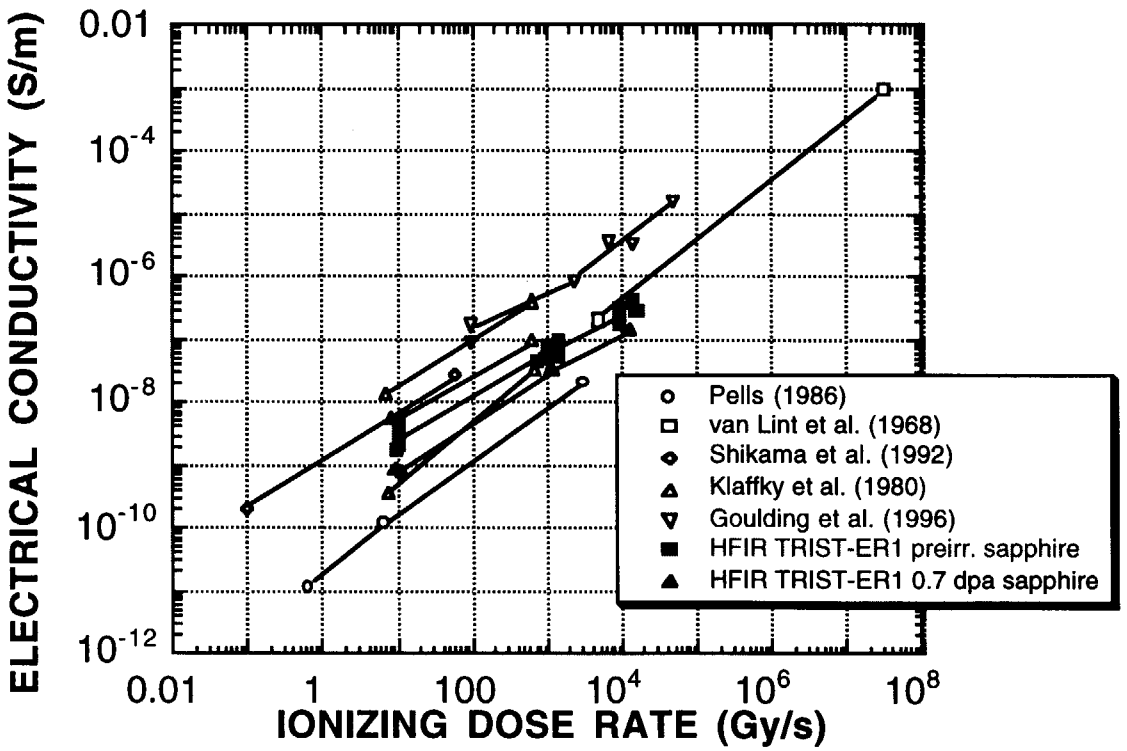

Fig. 2.2.2 Comparison of values of RIC.

However, there are some statistical data scatters in the compiled data shown in Figs.2.2. 1&2.2.2. Namely, the more recently measured data showed the less value of RIC for alumina. The 14 MeV neutron irradiation data in Fig. 2.2.1 clearly showed it. These results imply strongly that the older results might have been affected by unexpected leakage current and have estimated bulk electrical conductivity larger than true value.

The results, that the 14 MeV neutron irradiation gave about the same value of RIC as those obtained in gamma-ray irradiation in Fig. 2.2.1, should not be overlooked. The 14 MeV neutron irradiation in the facility, FNS described in the previous section, had a very marginal intensity of associated gamma-ray. Its electronic excitation is mainly caused by energetic knocked-on atoms in the displacement cascade that is generated by the incident 14 MeV neutron. The displacement cascade is isolated in space and in time with each other. The results, that the 14 MeV irradiation agrees with other irradiation such as gamma ray irradiation, should imply that an effective mean path of excited conduction electron should be large enough to contribute bulk electrical conduction. Also, the electronic excitation rate in the displacement cascade caused by the 14 MeV neutron would exceed more than 10^6Gy/s. Then, the results also imply that the phenomenon of RIC would not show saturation behavior below the electronic excitation dose rate of 106Gy/s.

The HFIR-TRIST-ER results showed dependence of RIC on the grade of alumina, up to the electronic excitation rate of 10^3Gy/s, as shown in the following order;

Normal-grade-polycrystal → High-grade-polycrystal → doped sapphire (Ruby) → normal grade sapphire → UV-grade sapphire

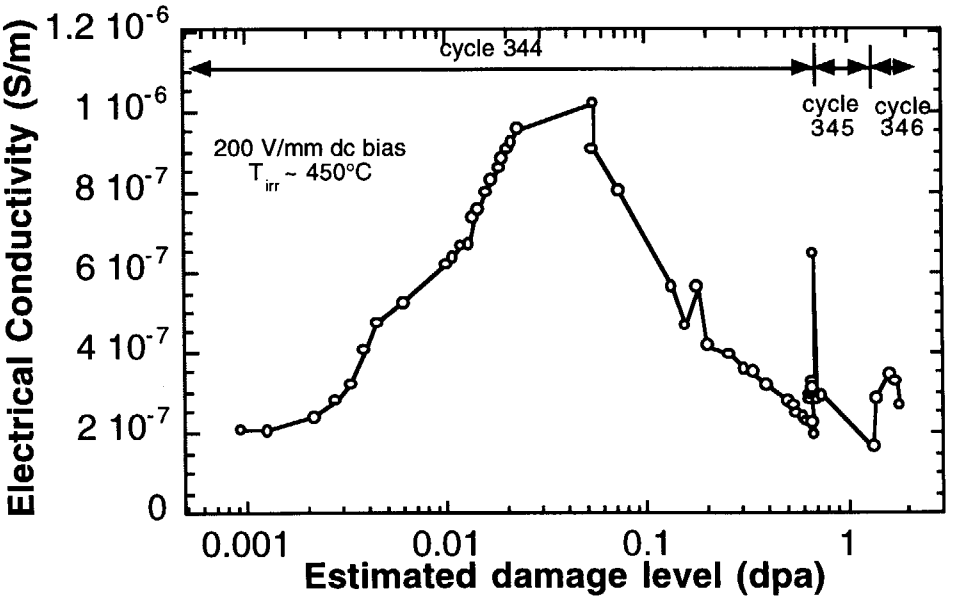

Fig. 2.2.3 Behavior of electrical conductivity under HFIR reactor irradiation.

However, the dependence becomes weak at he ionizing dose rate above 10^3Gy/s. At about 10^4Gy/s, all of the examined alumina showed a value of RIC of about $2x10^{-7}$S/m. Moderate increase of RIC was observed in the initial stage of irradiation. The values of RIC attained their maximum value of about $1x10^{-6}$S/m at about 0.05-0.1 dpa (displacement per atom), then began to decrease continuously to the end of 3dpa irradiation (Fig. 2.2.3) [2.2.1,2.2.2]. The accumulated results indicate confidently that RIC would not be a problem in general but the observed gradual increase of RIC might impose a technological problem in ITER, whose severest demand is 10^{-6}S/m at about 10^4G/s in a magnetic probe at present.

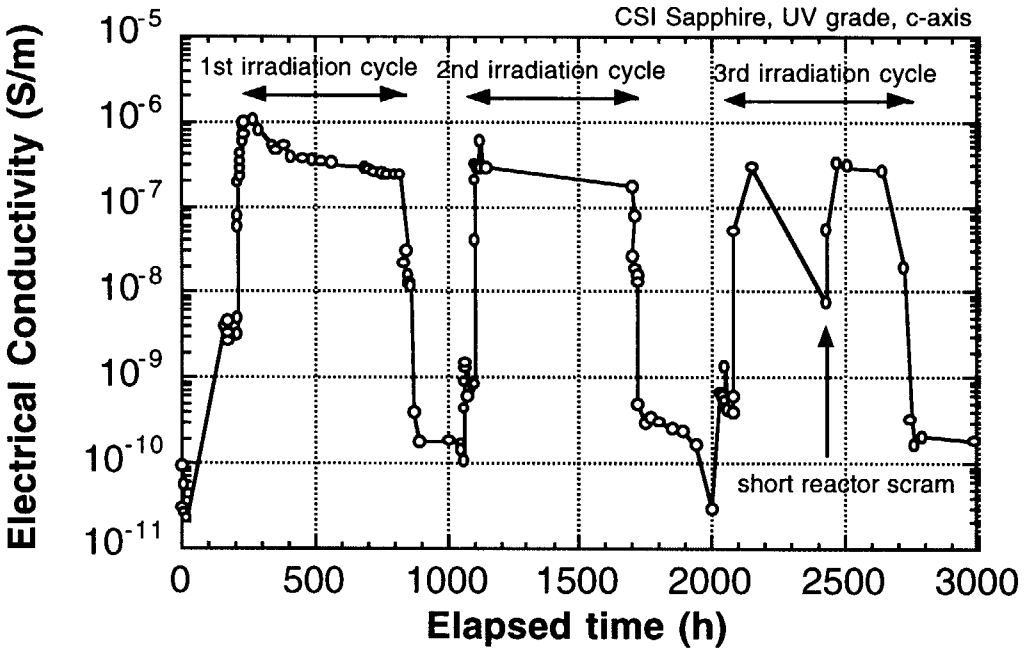

Fig. 2.2.4 No detection of RIED on sapphire in HFIR irradiation up to 3dpa.

The HFIR-TRIST-ER experiment [2.2.1] did not confirm long term and permanent increase of electrical conductivity in the alumina, which is called as the radiation induced electrical degradation (RIED). Figure 2.2.4 shows electrical conductivity of sapphire (single crystal alumina) in the course of the HFIR 3 cycles irradiation, up to 3 dpa. The value of 3 dpa exceeds the expected dose level of the atomic displacement in the ITER diagnostics. The HFIR-TRIST-ER experiment adopted the well-qualified and standardized measuring technique, which was recommended in the IEA workshop on radiation effects in ceramic insulators at Stresa in Italy in 1993. The technique has been improved for application to the high flux reactor irradiation by preliminary reactor experiments. The results indicate that the phenomenon of RIED of alumina

would not be a problem in the plasma diagnostics in ITER. It should be noted, however, it is assumed that environmental effects are not important for RIED. The TRIST-ER experiment adopted helium environment, in the meantime the environment for plasma diagnostics will be reductive, namely a high vacuum containing hydrogen isotopes. The planned reactor irradiation by the EU home team will reveal environment effects. Also, chromium doped sapphire showed substantial increase of electrical conductivity exceeding 10^{-4}S/m. Impurities may play a role in the electrical degradation in alumina and choice of appropriate alumina would be important in the development of ITER.

The long term increase of electrical conductivity was sometimes reported and sometimes was not reported on insulators in mineral insulated (MI) cables. The Japanese, Russian, and the US home team have extensive irradiation data on the MI-cables, some of which were not reported yet. Specification of the MI-cables for ITER diagnostics is important to be done. To do so, disclosure of irradiation data and detailed discussions should be needed.

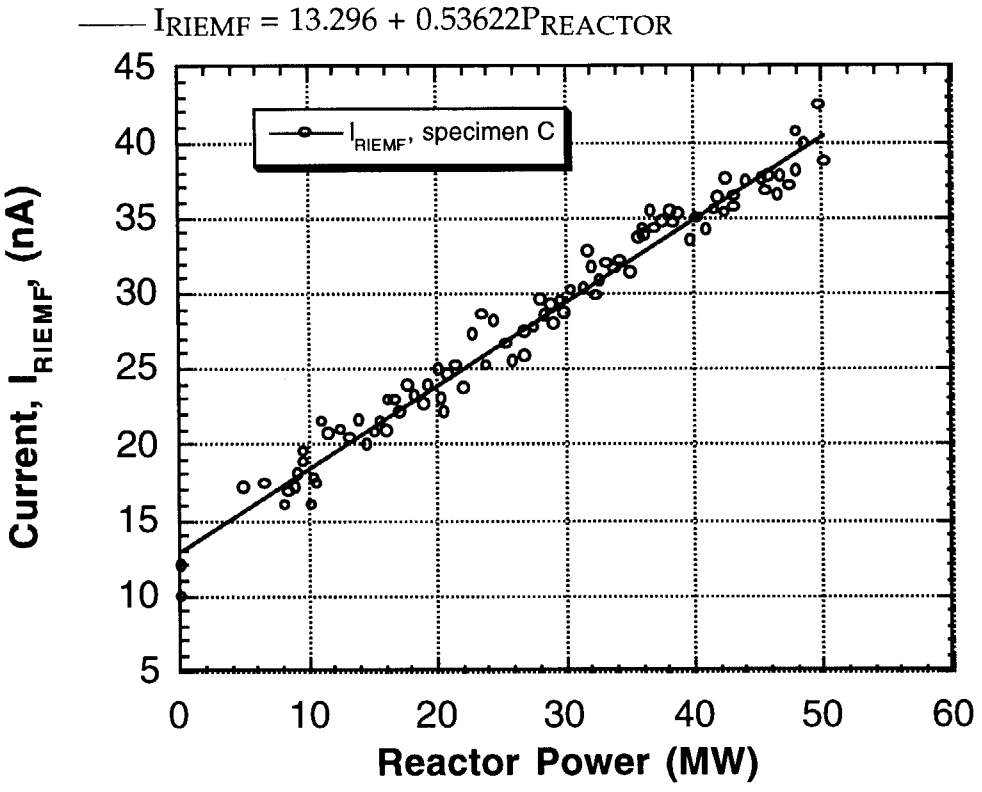

Fig. 2.2.5 Electrical motiveforce induced in MI-cable under JMTR irradiation.

Radiation induced electrical current and/or voltage were sometimes observed in in-situ experiments with metal/ceramic complex systems, and they were called as radiation induced electromotive force (RIEMF). A typical example

is an electrical voltage generated between a center lead and an outer sheath of the MI-cables under reactor irradiation. Figure 2.2.5 shows the RIEMF observed in about 1 m long and 1.6mm diameter MI-cable in the Japan Materials Testing Reactor (JMTR), as a function of reactor power [2.2.3]. In general, the observed RIEMF is current-driven, and the generated current and voltage are in the range of namo amperes and micro volts, respectively. Such radiation induced electrical current and voltage have been observed in fission reactor dosimetry and they were interpreted due to charge-redistribution among materials having different electron densities under electronic excitation irradiation. In the HFIR-TRIST-ER experiment, radiation induced electrical current of a few to a few tens micro amperes was observed, and its cause is not understood well yet [2.2.1, 2.2.2]. Their transient behavior as well as their magnitude will be important to say definitely whether radiation induced electrical current and/or voltage will cause problems in plasma diagnostics in ITER.

2.2.2. Optical properties

Studies of radiation effects on optical properties of dielectric ceramics have a long history, but they have been limited to fundamental research fields until recently. The concerned ITER research activity is accumulating engineering and quantitative results. The data-comparison among reported values by each home team shows good agreement in general. The Japanese home team produced valuable irradiation database concerning sapphire windows and silica core optical fibers. They will be described in details in following sections. Those data were examined in comparison with data reported by other home teams and showed good agreements, especially in the case of sapphire windows. Concerning optical fibers, only the Japanese home team has yielded heavy irradiation database using JMTR. Behavior of radioluminescence (radiation induced luminescence) and radiation induced absorption would be different between electronic-excitation-dominant-low-dose-rate irradiation (gamma ray irradiation) and atomic-displacement-accompanying-high-dose-rate irradiation (high flux fission reactor irradiation). One typical example is effects of so-called hydrogen-treatment on radiation induced absorption peak at about 600-650nm, which is interpreted to be caused by non-bridging oxygen hole centers (NBOHC). The hydrogen treatment was reported to be effective to suppress the NBOHC absorption band in the case of gamma-ray irradiation, meanwhile it was not effective under neutron associated irradiation.

The 14 MeV irradiation in the FNS reported interesting results concerning fundamental aspects of radiation effects on optical properties of sapphire as shown in Fig. 6. There, radioluminescence of Kyocera sapphire, normal grade sapphire of t-direction, under the 14MeV neutron irradiation is shown in comparison with that under the gamma-ray and with the data reported by the EU home team on a similar sapphire under electron irradiation. The gamma-ray irradiation showed good agreement with the electron irradiation but it was found more effective than the 14 MeV neutron irradiation, when they were compared at the same electronic excitation rate. The results indicate that saturation of radioluminescence caused by electrons in specific energy states took

place in the case of 14 MeV neutron irradiation. As described above, the electronic excitation takes place densely in localized area of displacement cascade in the 14 MeV irradiation.

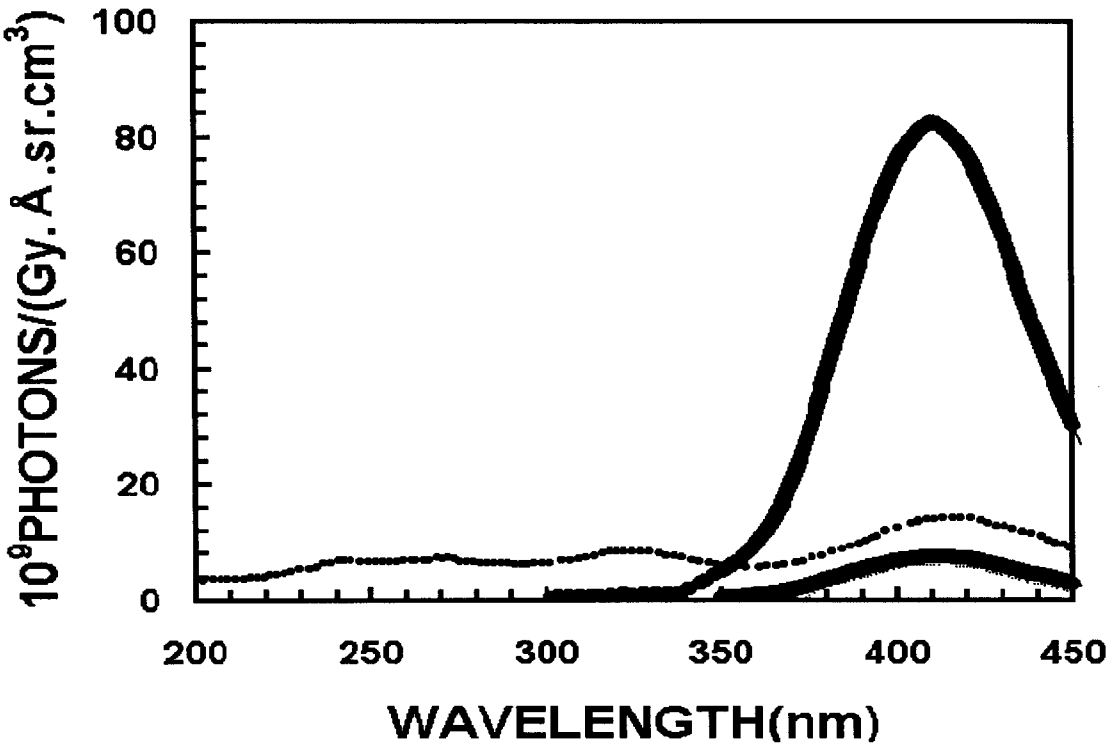

Fig. 2.2.6 Comparison of photon emission spectra for sapphire irradiated with ^{60}Co gamma-rays, 14 MeV neutrons (JAERI-FNS) and 1.8 MeV electrons (EU,Hodgson).

Optical ceramics are considered to be used in weak irradiation (low dose rate) environments in the present design of ITER. However, it is probable that optical ceramics such as optical fibers and windows should be used nearer to the plasma, as the design evaluation proceed. The FNS and the JMTR will be invaluable irradiation sources to evaluate radiation effects of optical ceramics for the ITER diagnostics.

2.2.3. Characterization and specification of candidate materials

Irradiation effects on properties of ceramic materials depend on detailed characteristics of ceramic materials, as partly described above. Detailed characterizations of materials are needed to establish qualified and quantified database of ceramic materials for the ITER diagnostics. It will not be an easy work and international collaboration will be essential. Founding on reliable

characterizations, primary candidate materials should be recommended with detailed specifications. There, it will be very important that the specifications cover not only fundamental materials-parameters, such as purity, grain size, etc., but also manufacturing-parameters, such as details of sintering processes, and details of drawing procedures for optical fibers and MI-cables.

References

[2.2.1] S.J.Zinkle, T.Shikama, et al., in Fusion Materials Semiannual Progress Report for the Period Ending June 30, DOE/ER-0313/20 (1995) 257; also submitted to J. Nucl. Mater..
[2.2.2] T. Shikama and S.J.Zinkle, Presented in the 8th Int. Conf. Fusion Reactor Materials, Sendai 1997.
[2.2.3] T. Shikama, et al., Nucl. Instrm. Methods in Phys. Res. B122 (1997) 650.

3. Windows

3.1 Light Emission from Window Materials for Irradiations by 14 MeV Neutrons and ^{60}Co Gamma-rays

Yukio Oyama, Fuminobu Sato and Toshiyuki Iida

3.1.1 Objectives

Examination of light emission from optical window materials under 14 MeV neutron irradiation is a crucial issue for design of diagnostic systems in ITER. For this purpose, an absolute efficiency of light emission in unit mass and unit dose is essential to apply such data to the ITER design. Therefore, in this study most of efforts were devoted to calibration for obtaining an absolute value.

3.1.2 Specimen

(1) Materials

Test materials are selected for two sapphire samples (Kyocera and rare metal), pure quarts, Ge-doped quarts, single crystal quarts(KU-quartz distributed by Russia), CaF_2, NE102A plastic scintillator for calibration of light emission efficiency and measuring system. Table 3.1.1 shows impurities of sapphire-1 and KU-quartz.

Table. 3.1.1 Impurities of sapphire-1 and KU-quartz

Impurity in a-sapphire (SA-100)

Impurity	Si	S	Fe	Na	K	Ca	Ti	Y	Zr	Cr	Total
(ppm)	10	4	2	1	1	1	<1	<1	<1	<1	<28

Impurity in KU-1 quartz

Impurity	OH	Fe	K	Na	Ca	Al	Mg	Cu	Mn	Ti
(ppm)	821	1.6	1.4	1.0	1.0	0.4	0.4	0.1	0.02	0.01

(2) Sample dimension

The disk samples are used mostly for test specimens, though fiber samples are used for pure and Ge-doped quarts specimens. The fiber samples are used to get high efficiency of light collection. The samples and sizes are summarized in Table 3.1.2 together with the measurements performed.

Table 3.1.2 Samples and sizes together with the measurements performed.

Sample		Size (mm)	Polychro-mator system	Photon Counting Spectrometer	Integrating Photon Counting System
Sapphire-1	Kyocera (SA-100)	25.4φ × 5	○	○	
Sapphire-2	Rare Metal	10φ × 2	○●		○
High pure silica glass	Mitubishi Cable	1.2φ × 30	○●		○
Ge doped silics glass	Mitubishi Cable	1.2φ × 30	○●		○
Quartz	KU-1	16φ × 8	○	○	
Calcium fluoride	Oriel	25.4φ × 6.4	○●		○
Plastic scintillator-1	NE (NE102A)	25.4φ × 2-6.4	○●	○	○●
Plastic scintillator-2	NE (NE102A)	1.2φ × 30	○●		○●

(○:14 MeV neutron, ●:^{60}Co gamma-ray)

3.1.3 Experimental Condition

(1) Irradiation facility

14 MeV neutrons

An irradiation by 14 MeV neutrons was performed at Fusion Neutronics Source (FNS) in Japan Atomic Energy Research Institute (JAERI). The FNS generates neutrons by D-T reactions using a 350 keV deuteron accelerator. The accelerated beam current is up to 25mA and bombarded at 37 TBq of tritium-titanium target. The neutron production yield is 3 x 10^{12} n/s. The target is located inside a room of 5 m cubic surrounded by thick concrete shield wall.

60-Co Gamma-rays

The 60-Co Irradiation Facility at JAERI is used for gamma-ray irradiation. The source produces both 1.17 and 1.33 MeV gamma-ray peaks. The facility has a 1.17 PBq of ^{60}Co source and able to irradiate a sample in the exposure dose rate of 10-1.55 x 10^2 C/kg/h. The exposure dose rate is changed by moving the source from the sample.

(2) Irradiation condition

14 MeV neutrons

A test sample is placed at a distance of 1cm from the D-T reaction point, where the 14 MeV neutron flux of 3 x 10^{11} n/cm^2/s can be obtained at maximum. The experimental set-up is shown in Figs. 3.1.1 and 2. The irradiation condition at a sample position is estimated by calculation using a Monte Carlo neutron transport code, MCNP. The calculation includes energy deposition by recoils and charged particle emissions by neutron nuclear reaction. The calculated absorbed dose distribution is shown in Fig. 3.1.3 for SiO_2.

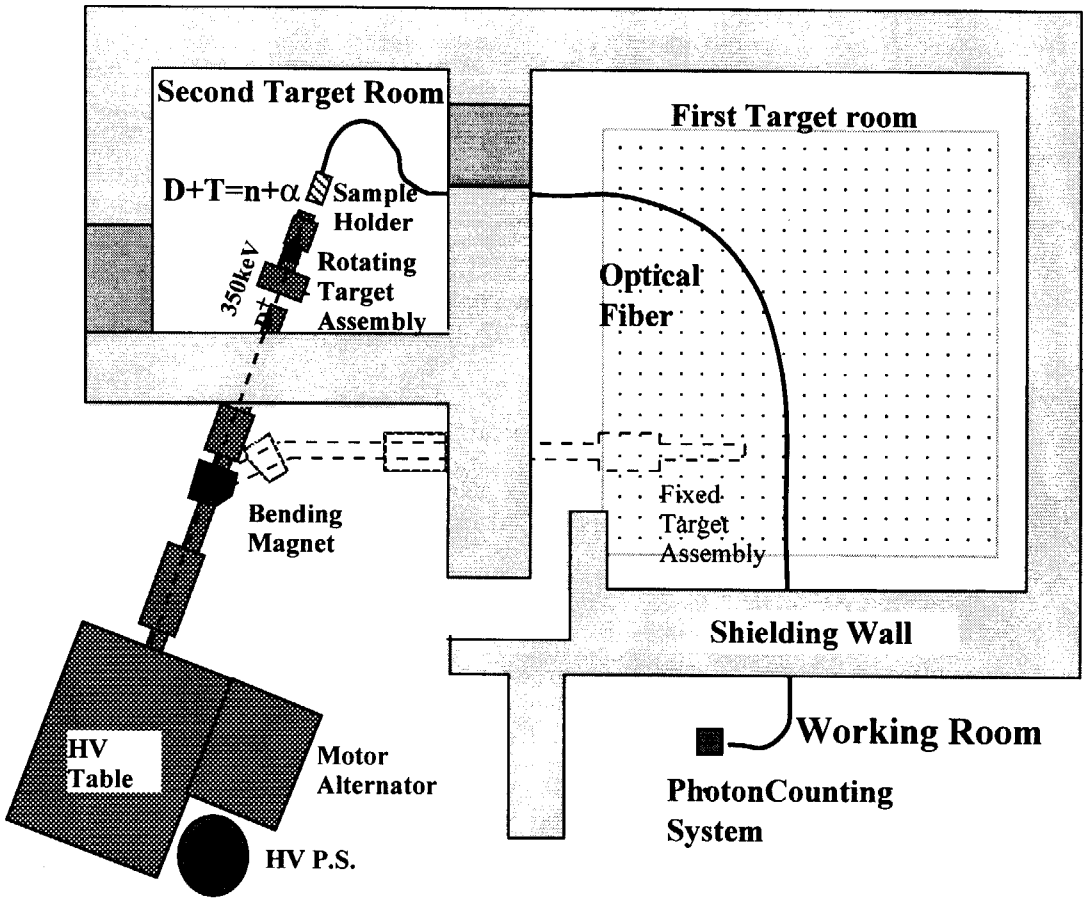

Fig.3.1.1 Schematic layout of the experiment to measure photons emitted from window materials by neutron irradiation at FNS.

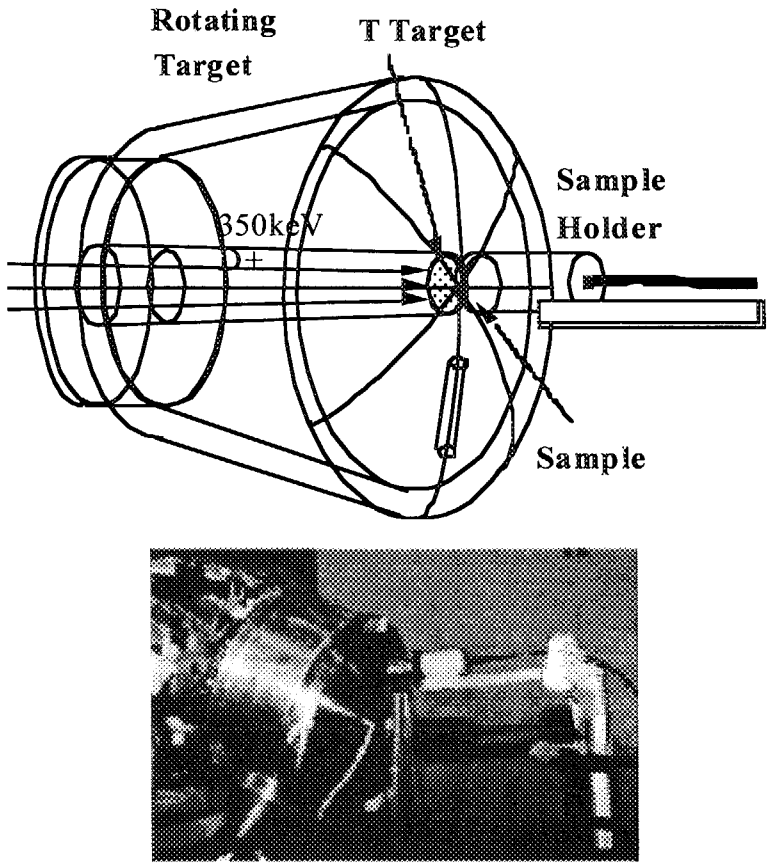

Fig.3.1.2 Arrangement of a sample holder and 14 MeV neutron target of FNS.

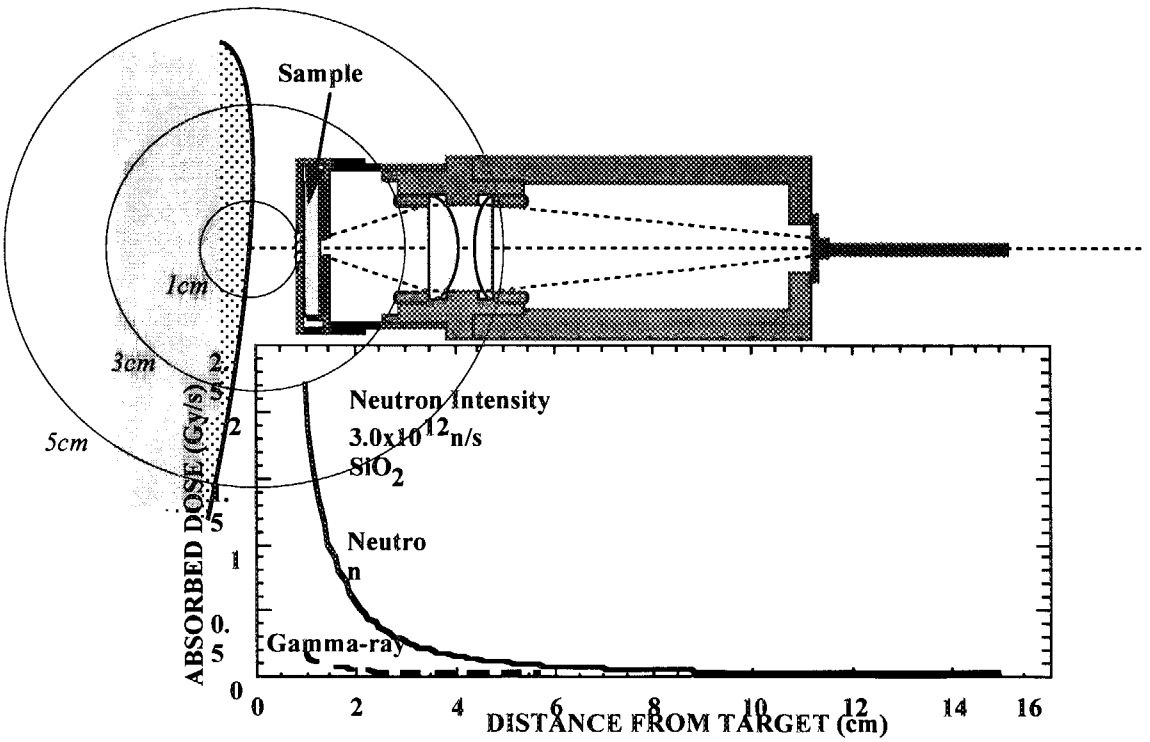

Fig. 3.1.3 Absorbed dose distribution by neutrons from FNS.

Co-60 gamma-rays

The exposure dose distribution used in the facility is shown in Fig. 3.1.4 and the absorbed dose distribution calculated for SiO_2 is shown in Fig. 3.1.5.

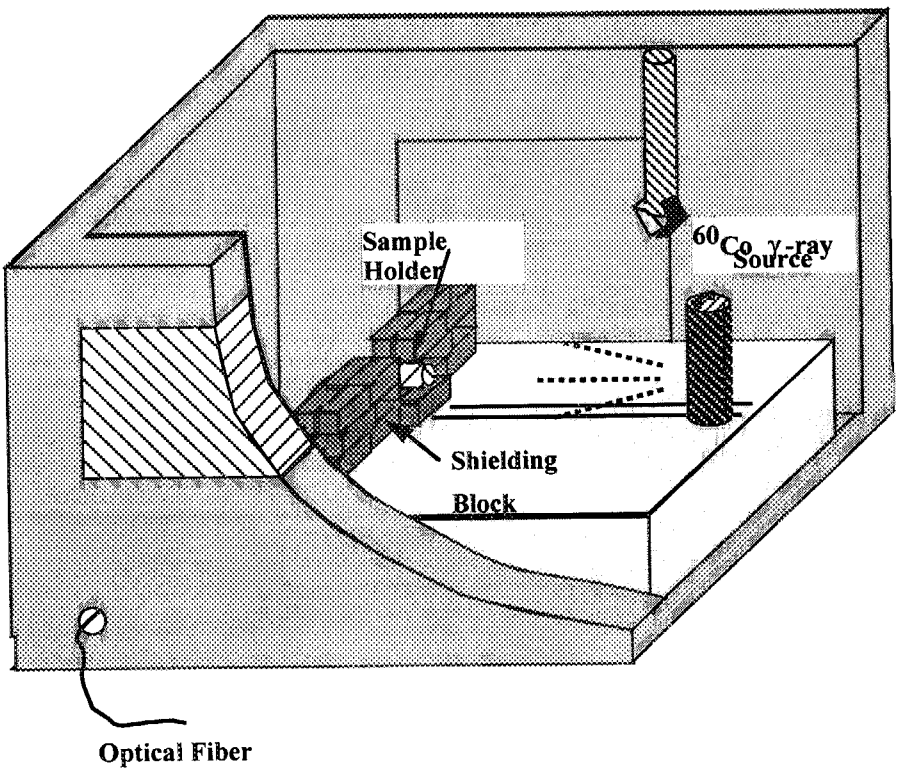

Fig.3.1.4 Schematic layout of the experiment to measure photons emitted from window materials by gamma irradiation at Co-60 facility.

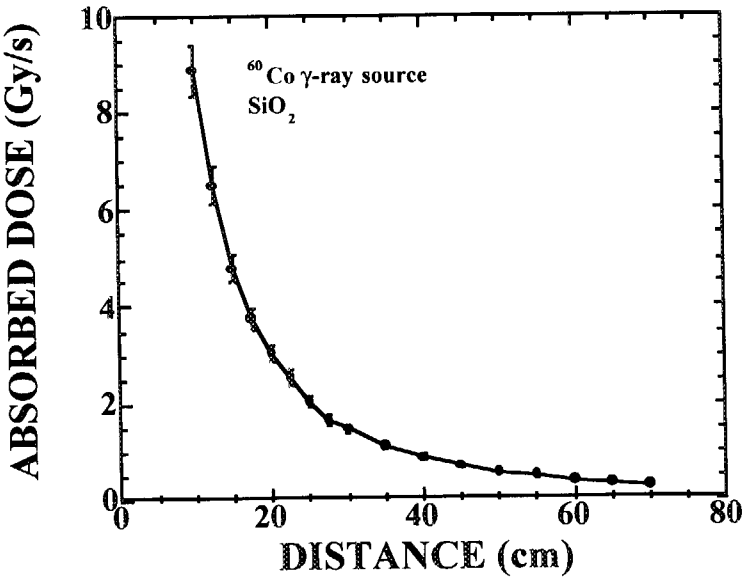

Fig.3.1.5 Gamma-ray dose distribution of Co-60 irradiation calculated by MCNP.

(3) Experimental devices

The test sample is mounted in a cylindrical chamber and the emitted light is collected by two focusing lens to introduce into a single core quarts optical fiber with 1.2 mm in diameter (Mitsubishi Densen, ST 1200I-SY). The sample chamber is shown in Fig.3.1.6. The light introduced in the fiber is transmitted to photon measuring system at 30m distance from the sample.

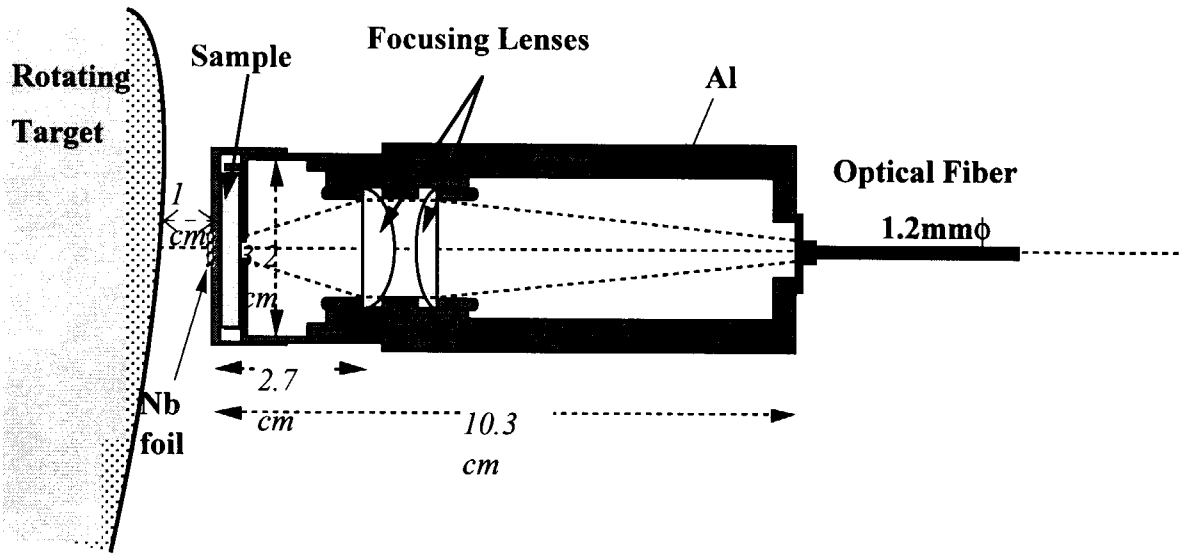

Fig.3.1.6 Sample holder with light collecting lenses.

Three kinds of measuring systems were used in the experiment. Those systems are polychrometer with image intensifier (Hamamatsu Photonics, M5098 and PMA-10), photon counting system with scanning monochrometer (Shimazu, SPG-100 and Hamamatsu, R928P) and wave length integrated photon counting system (Hamamatsu, R1635P). The former two system are used for spectrometric measurement and the latter one is used for high sensitivity measurement of weak light emission. The covered wave length range by those measuring systems are summarized in Fig. 3.1.7 with sensitivity profile.

The typical measuring system is shown in Fig. 3.1.8. The neutron flux is monitored by the associated alpha detection and the gamma flux is controlled by irradiation time. The data taking is controlled by the computer.

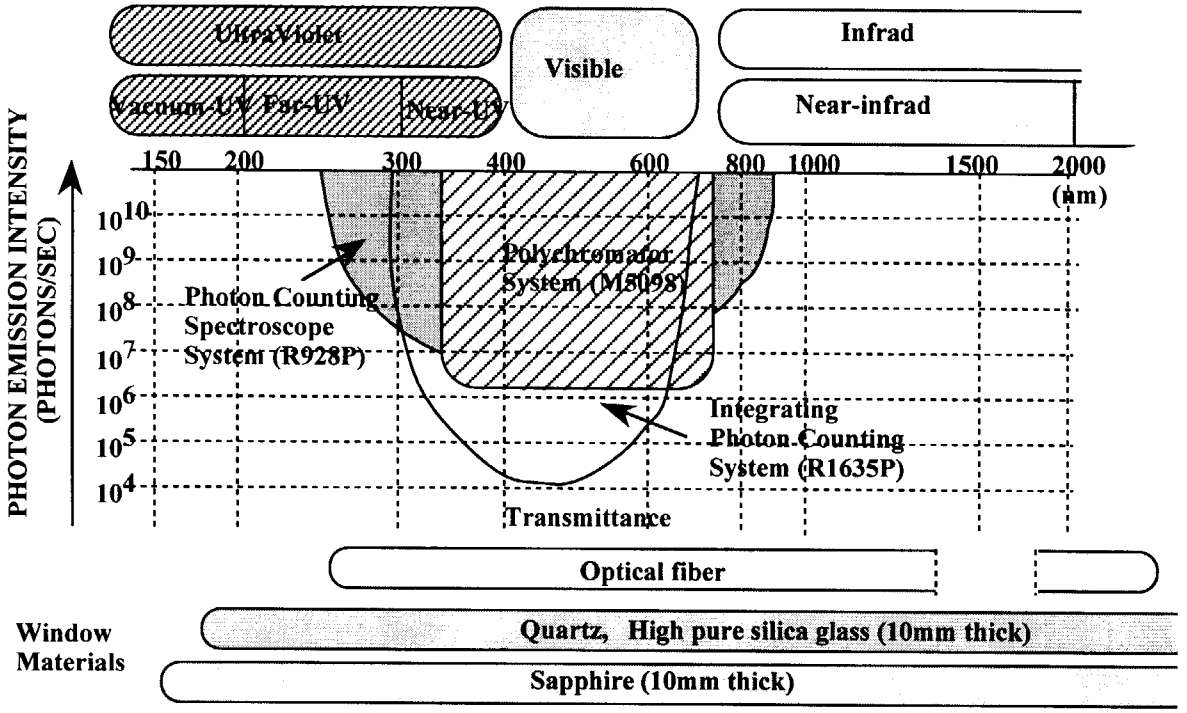

Fig. 3.1.7 Comparison of performance of photon measurement system used in this experiment.

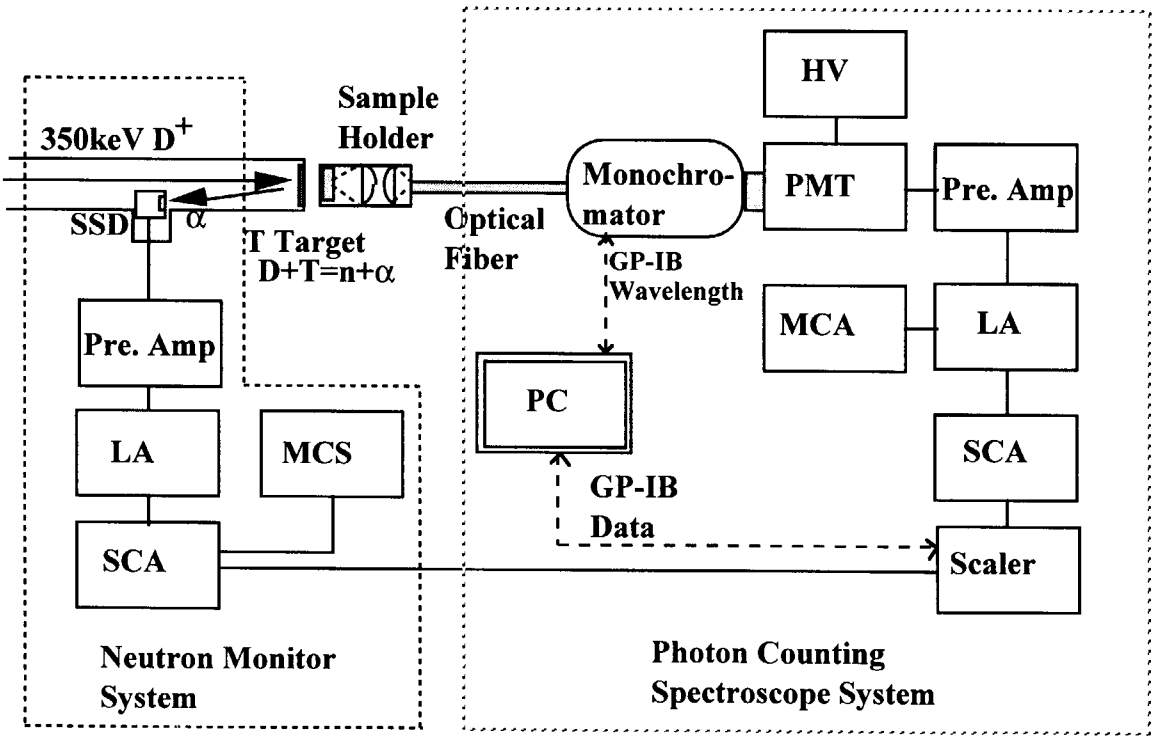

Fig. 3.18 Schematic diagram of typical photon measurement system used this experiment.

(4) Measurement

System calibration

The absolute light emission efficiency was defined as follows:

$$N_{abs}(\lambda) = \frac{N_C(\lambda) - N_B(\lambda)}{\eta_F(\lambda)\,\eta_L \Delta\lambda_M \eta_M(\lambda)\,\eta_Q(\lambda)} \quad \text{(Photon/nm)},$$

where $N_C(\lambda)$: counts in foreground run,
$N_B(\lambda)$: counts in background run without sample,
fÉ : wave length,
$\eta_F(\lambda)$: transmission efficiency of optical fiber,
η_L : light collection efficiency from the effective measured volume of sample,
$\Delta\lambda_M$: wave length resolution of spectrometer=10 nm,
$\eta_M(\lambda)$: diffraction efficiency of grating of spectrometer,
$\eta_Q(\lambda)$: quantum efficiency of photomultiplier.

The light emission efficiency per absorption energy is :

$$Y(\lambda) = \frac{N_{abs}(\lambda)}{\rho\, V_{eff} D} \quad \text{(photon/nm/MeV)},$$

where ρ : mass density of sample
V_{eff} : effective measured volume of sample
D : energy absorption dose at sample position (Gy).

To obtain these efficiencies, several calibrations were performed by the following procedures.

a) transmission efficiency of optical fiber, $\eta_F(\lambda)$

Using a LED and standard light sources, the transmission efficiency was obtained in the wave length range of 300 to 800 nm. Figure 3.1.9 shows the measured efficiency.

b) light collection efficiency from the effective measured volume of sample, η_L

This was calculated from geometrical relation between emission angle at the position of the effective measured volume and incident angle at the fiber entrance. It was assumed that the emission probability is isotropic. The acceptance of fiber is larger than focusing cone. The calculation was also compared to the measurement by replacing by a plastic scintillator which has well-known light emission efficiency as shown in Fig. 3.1.10.

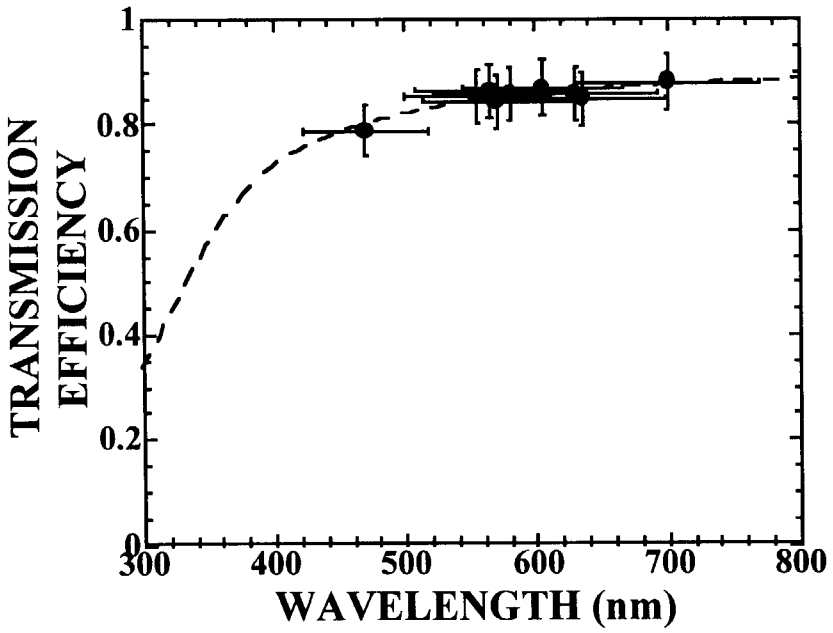

Fig. 3.1.9 Measured transmission efficiency of the optical fiber.

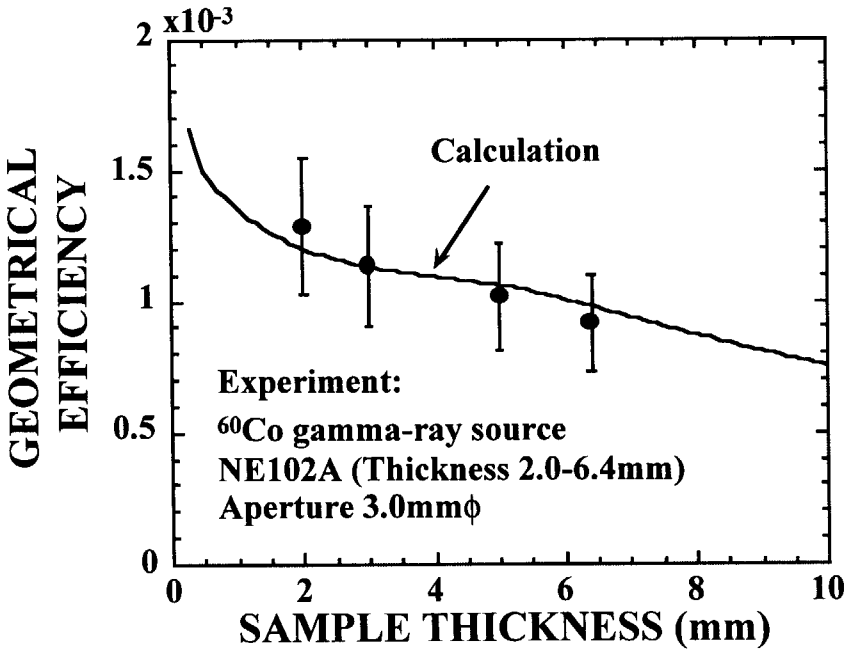

Fig. 3.1.10 Comparison of measured and calculated light collection efficiency(geometrical).

c) spectrometer, wave length, and diffraction efficiency of grating,$\eta_M(\lambda)$

The wave length axis of spectrometer was calibrated by using standard peaks from mercury lamp. The diffraction efficiency was obtained from the ratio of intensity of a calibrated standard light source(Labsphere, USS-600) to the output from the spectrometer as shown in Fig. 3.1.11. The obtained diffraction efficiency is shown in Fig. 3.1.12.

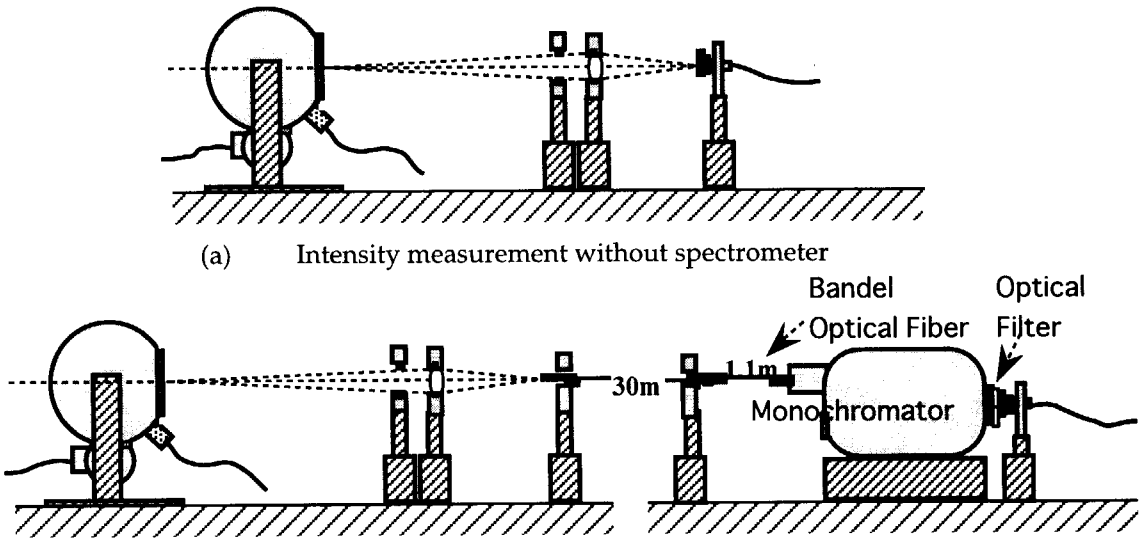

Fig.3.1.11 Schematic illustration of calibration setup for diffraction efficiency of photon counting spectrometer. (a) spectrum without spectrometer, (b) spectrum through spectrometer.

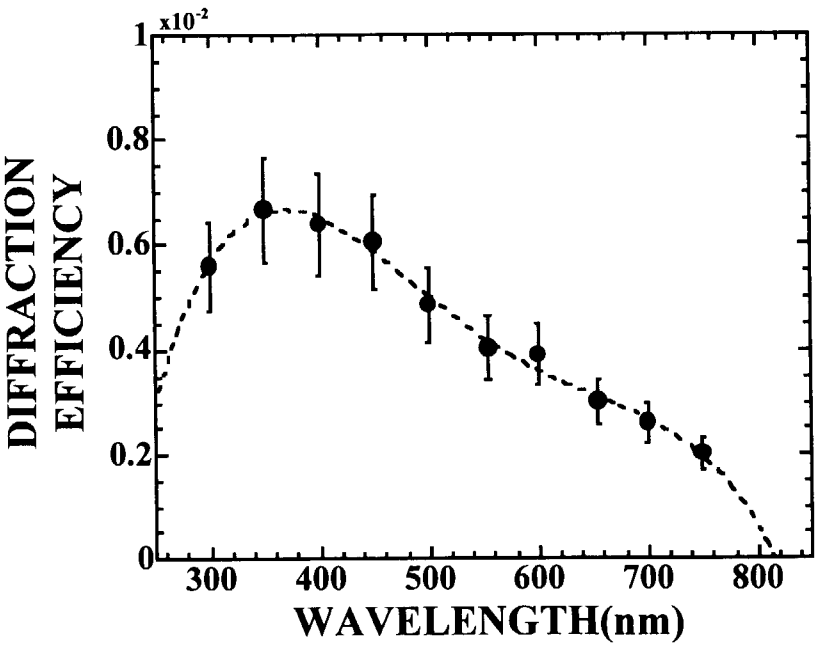

Fig. 3.1.12 Measured diffraction efficiency of photon counting spectrometer.

d)quantum efficiency of photomultiplier, $\eta_Q(\lambda)$

This value is taken from the data given by Hamamatsu photonics as shown in Figs. 3.1.13.

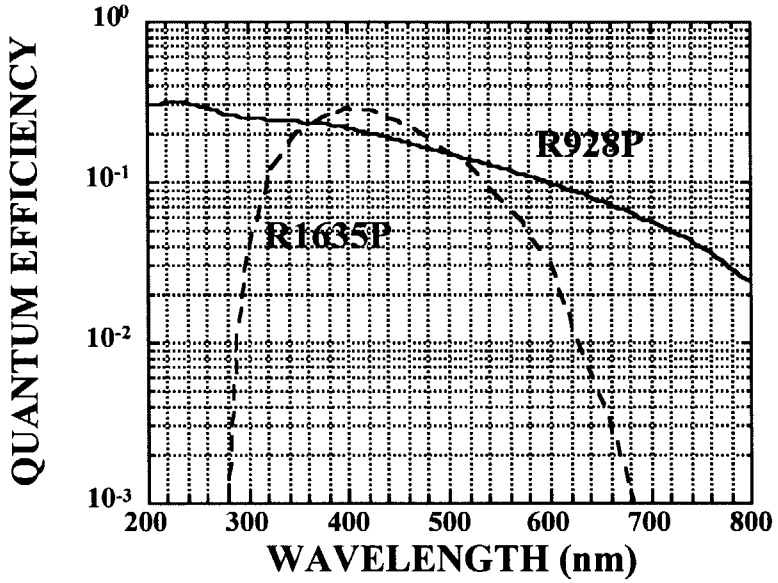

Fig. 3.1.13 Quantum efficiency of photo-multiplier tube.

e) effective measured volume of sample, V_{eff}

This value is a volume of cylinder defined by an aperture and sample thickness.

14 MeV irradiation

The sample chamber was placed at 1cm distance from the neutron target surface. The beam current was changed in 10^6 to 10^{11} n/cm^2/s to see the linearity of light output with neutron flux. The polychrometer measurement was normalized to scanning monochrometer measurement. The calculated neutron and gamma-ray fluxes at the sample position are shown in Table 3.1.3 and the dose rates for sample materials are summarized in Table 3.1.4.

Table 3.1.3 Calculated neutron and gamma-ray fluxes at the sample position.

Distance from target (mm)	Neutron flux (n/cm^2/s)	Gamma-ray flux (Photon/cm^2/s)
15	7.5×10^{10}	9.0×10^9
30	2.3×10^{10}	2.8×10^9
45	1.1×10^{10}	1.3×10^9

(DT neutron intensity: 3.0×10^{12} n/s

Table 3.1.4 Calculated dose rate at samples.

Sample	Neutron dose (Gy/s)	Gamma dose (Gy/s)	Total dose (Gy/s)
Sapphire	0.92	0.10	1.0
High pure silica glass	1.0	0.12	1.1
Ge doped silics	1.0	0.11	1.1
Calcium fluoride	1.3	0.06	1.4
Plastic scintillator	5.8	0.15	6.0

(DT neutron intensity:3.0×10^{12} n/s, 25.4 mmϕ × 4 mm^t sample was plased 12 mm from target.)

Co-60 gamma-ray irradiation

The gamma-ray intensity was changed by changing the distance of 15 to 70 cm. This also showed good linearity of the output.

Table 3.1.5. Estimated error of this experiment.

	Factor	Uncertainty		Uncertainty
Random Error	Photon counting	<10%	Statistical error	<10%
	Absorbed dose for neutron and Secondary gamma-ray	<13%	4π DT neutron intensity	<3%
			Sample position	<12%
			Dose calculation	<5%
	Absorbed dose for ^{60}Co gamma-ray	<6%	Dose measurement	5%
			Dose calculation	<3%
System Error	Quantum efficiency of PMT	10%	Uneven quality	10%
	Transmission Efficiency of Optical fiber	6%	Uniform light source system	6%
	Diffraction efficiency	14%	Uniform light source system	6%
			Quantum efficiency of photodiode	10%
	Geometrical efficiency	19%	Uncertainty in calibration	17%
			Maximum difference between calculation and experimental efficiencies	9%
Total	Random error + System error	<31%		

Experimental error

From errors originating in calibration and monitor, the experimental error was estimated as Table 3.1.5. The error of quantum efficiency was assumed to be 10%.

3.1.4 Experimental results

Light emission spectrum from pure silica (quartz) is shown in Fig. 3.1.14 and its dependence on neutron flux in Fig. 3.1.15. The strong peak of 450nm is seen in the figure. The Ge-doped quartz result is shown in Fig. 3.1.16, but its peak is at around 390 nm and its intensity is 10 times larger than the pure silica. The results of KU-quartz is shown in Fig. 3.1.17. This round robin sample indicates very different spectrum that two weak peaks are found at 420 and 640 nm. The results for gamma-ray irradiation are shown in Figs. 3.1.18 and 19 for pure and Ge-doped quartz samples.

For sapphires, the results of Kyocera single crystal (sapphire-1) and Rare Metal (sapphire-2) are shown in Figs. 3.1.20 and 21. The [1102] surface of sapphire-1 sample was measured. The peaks of 330, 410 and 690 nm were found.

Figures 3.1.22 and 23 shows light emission spectra from CaF_2 and NE102A plastic scintillator. The peaks of 550 nm and 420 nm are found respectively. The results integrated over 350 to 650 nm are summarized in Table 3.1.6.

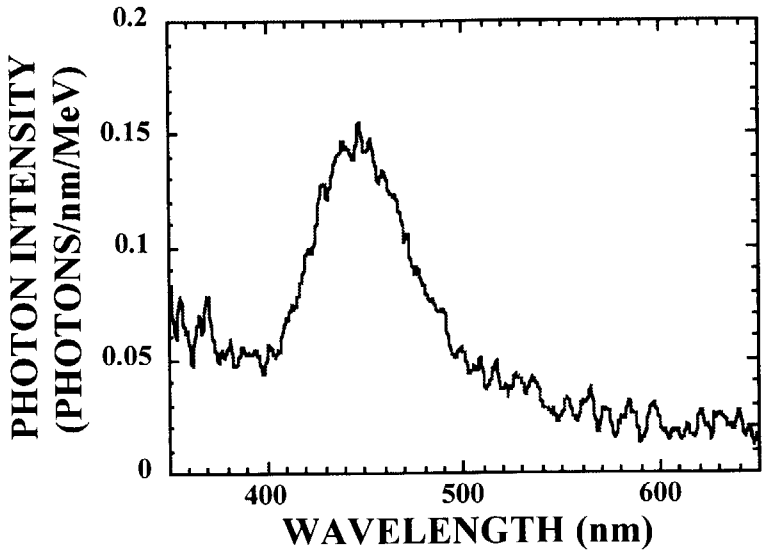

Fig.3.1.14 Photon spectrum emitted from high purity quartz glass for 14 MeV neutron irradiation

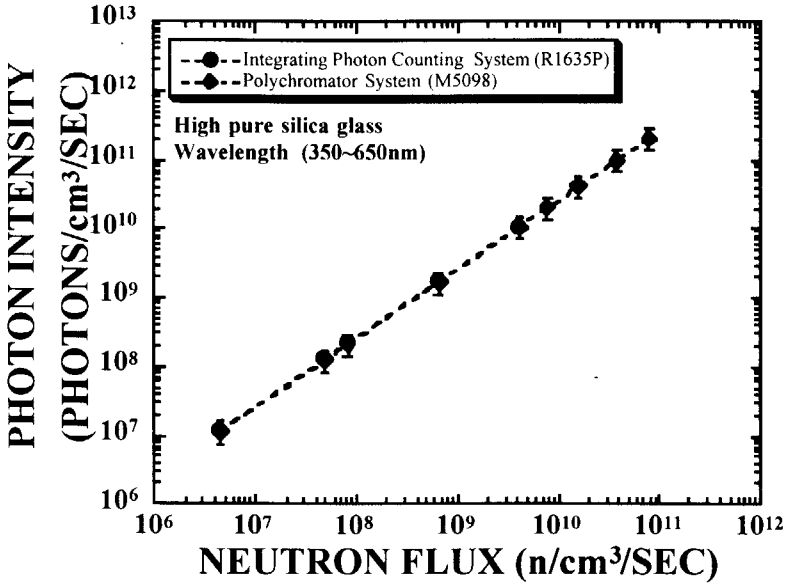

Fig.3.1.15 Neutron flux dependence of photon emission.

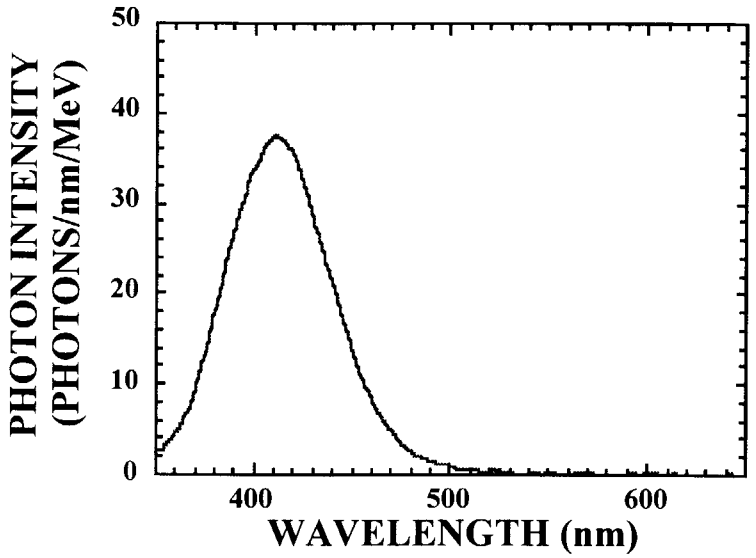

Fig.3.1.16 Photon spectrum emitted from Ge-doped quartz glass for 14 MeV neutron irradiation.

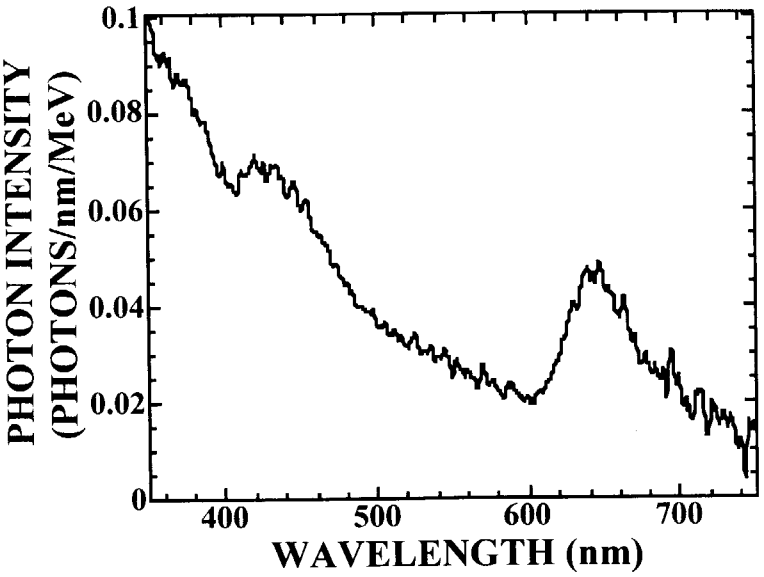

Fig.3.1.17 Photon spectrum emitted from KU quartz (single crystal) for 14 MeV neutron irradiation.

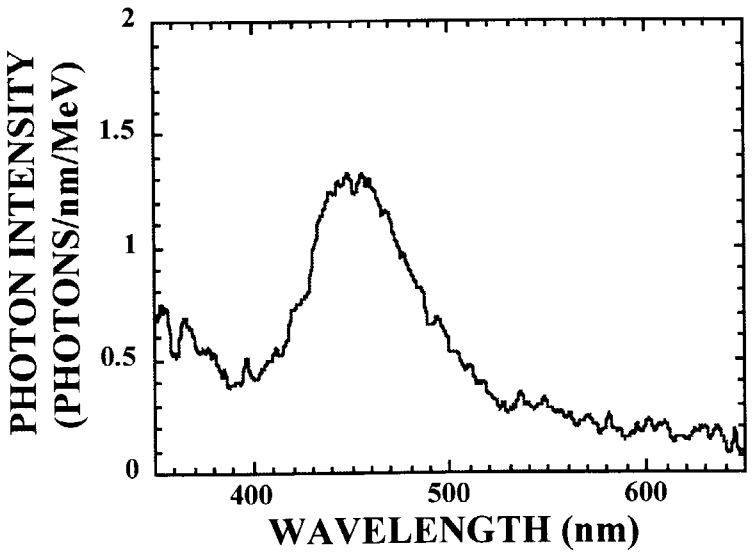

Fig. 3.1.18 Photon spectrum emitted from high purity quartz glass for ^{60}Co gamma-ray irradiation.

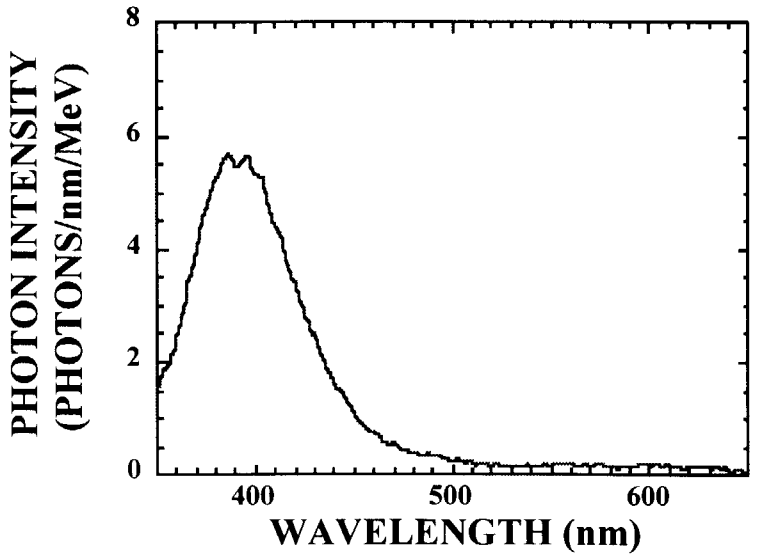

Fig.3.1.19 Photon spectrum emitted from Ge-doped quartz glass for Co-60 gamma-ray irradiation

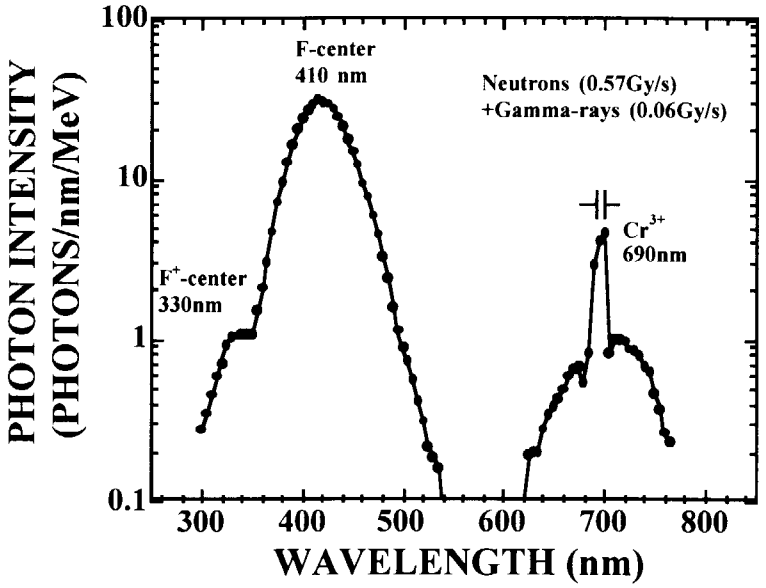

Fig.3.1.20 Photon spectrum emitted from sapphire-1 (Kyocera) for 14 MeV neutron irradiation.

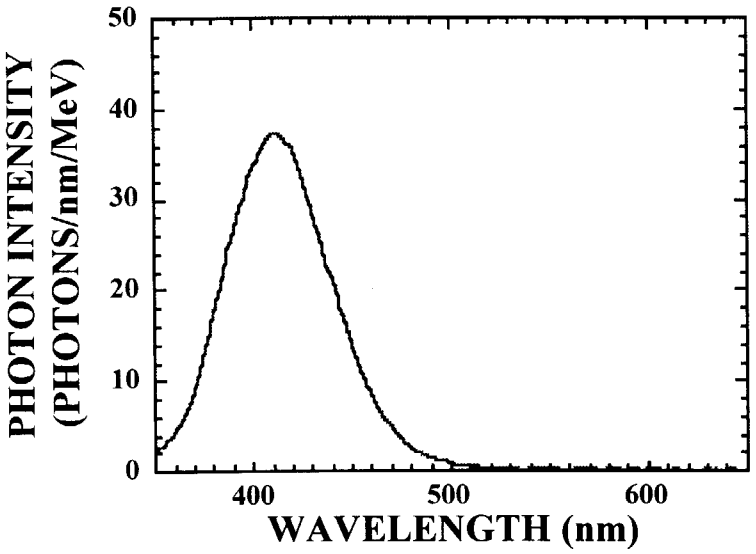

Fig.3.1.21 Photon spectrum emitted from sapphire-2 (Rare Metal) for 14 MeV neutron irradiation.

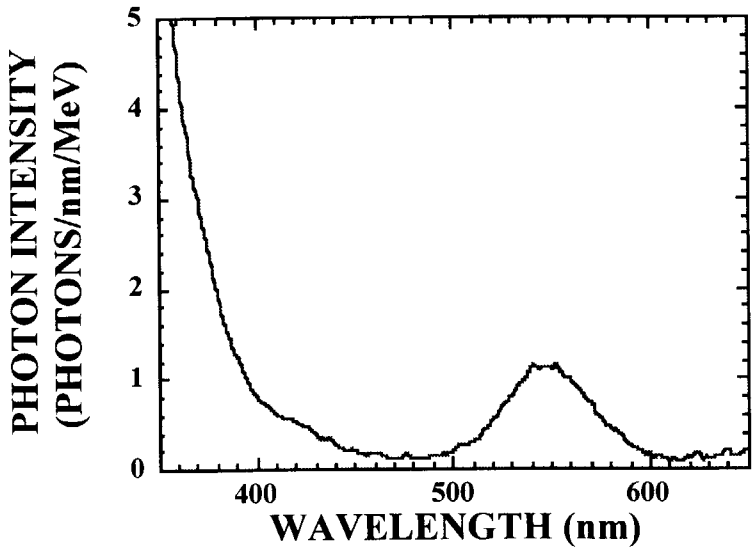

Fig.3.1.22 Photon spectrum emitted from NE102A plastic scintillator for 14 MeV neutron irradiation.

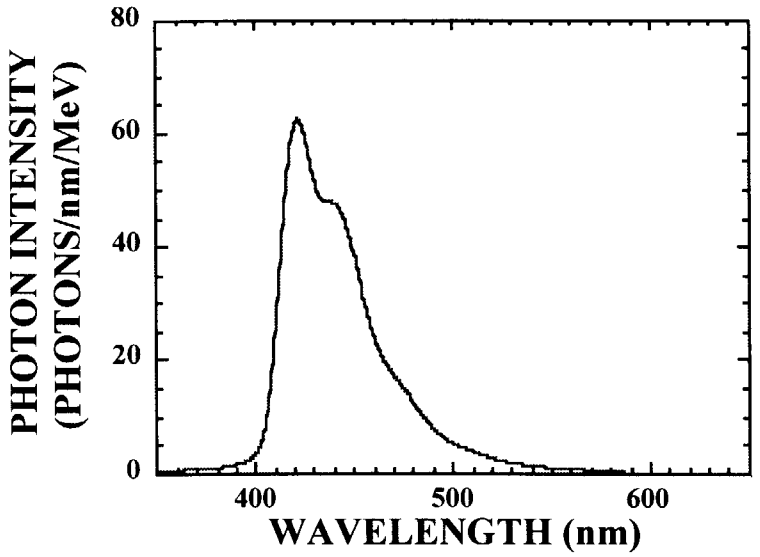

Fig.3.1.23 Photon spectrum emitted from NE102A plastic scintillator for 14 MeV neutron irradiation.

Table 3.1.6 Number of emitted photons per unit absorbed energy.

Sample	Peak wavelength (nm)	14 MeV neutrons +induced gammas (photons/MeV)	^{60}Co gamma-rays (photons/MeV)
Sapphire-1	410	2200±700	
Sapphire-2	410	2500±800	27000±8000
High pure silica glass	450	17±5	170±50
Ge doped silics glass	390	83±30	410±130
Quartz	450, 650	14±4(350-750 nm)	
Calcium fluoride	<350, 550	270±80	1300±400
Plastic scintillator	422	3000±900	11000±3000 Ref. 10300±710

3.1.5 Discussions

(1) Quartz (SiO_2)

For pure-quartz, this non-crystal has an impurity less than 1 ppm. The peak of 450 nm is due to intrinsic emission by exciton of electron hole of oxygen. This peak energy and intensity will be changed by impurity and defect. The continuous emission spectrum part is caused by Cerenkov radiation. The neutron induced Cerenkov radiation contribution is separated by calculation using electron spectrum induced from gamma-ray radiation at the sample. This Cerenkov radiation strength is proportional to neutron flux in the range of 10^6-10^{11} $n/cm^2/s$. However, there is no observation of fluence dependence in the range of below 10^{13} n/cm^2.

For Ge-doped quarts (3-8% Ge doped), a small peak around 390 nm is seen. This emission is more than 10 times stronger than a 450 nm peak observed in the pure quartz. Thus there could not be seen the 450 nm peak. For KU-quarts, there is a peak of 650 nm. Because this sample has large amount of OH-base , i.e., 821 ppm, the 650 nm peak can be explained by chemical luminescence by ozone from O_2 molecule. This is caused by absorption of 300 nm by ozone created by irradiation.

In comparison of neutron induced emission with gamma-ray induced one, a light emission efficiency of neutron is two order smaller than that of gamma-ray. After subtraction of Cerenkov contribution, those efficiencies are 135±50 photons/MeV for gamma-ray and 5±3 photons/MeV for neutron, respectively. This fact suggests that a light emission efficiency by heavy ion is smaller than electron and is very similar to a scintillation efficiency.

(2) Sapphire

For the single crystal sapphire (sapphire-1), there are peaks of 410 nm, 330 nm and around 690 nm, and these peaks are corresponded to F-center, F^+-center and Cr^{3+}, respectively. The F^+-center emission is two order smaller than F-center one, in contrast to the case of irradiation by ion an electron. The intensity of Cr^+ peak seems to be larger than expected in such low content less than 1 ppm. On the other hand, the pure alumina (Rare Metal sample) has no Cr^{3+} peak observed. In comparison to EU electron results, F-center peak efficiency was very close to our neutron data but 4-5 times smaller than γ ray data as shown in Fig. 3.1.24.

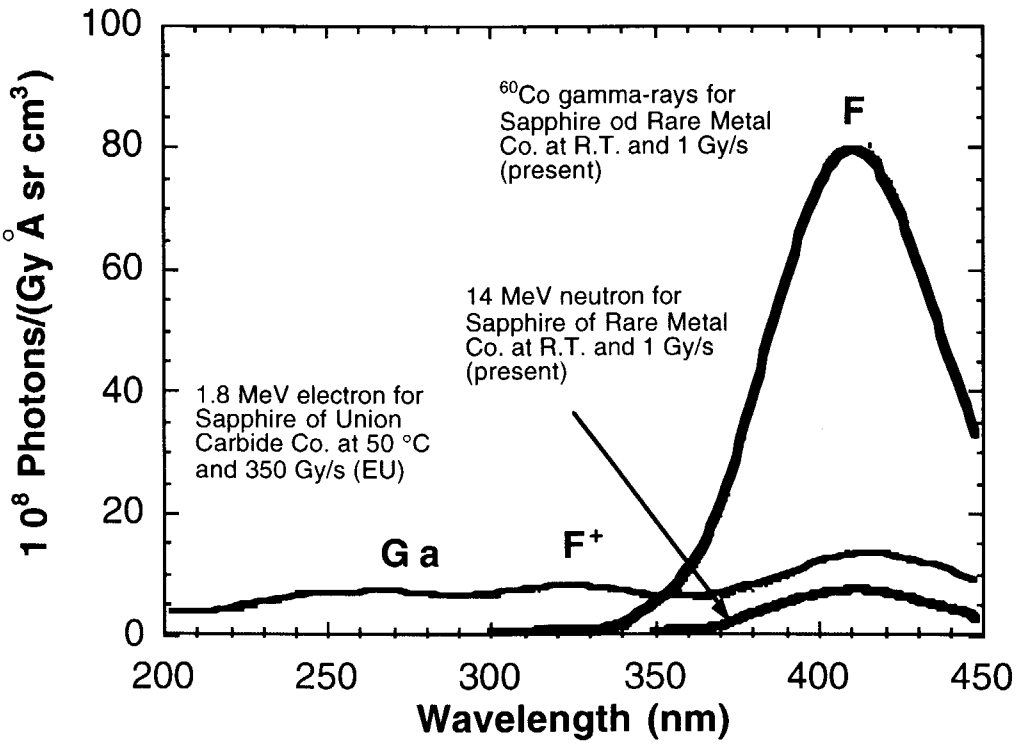

Fig. 3.1.24 Comparison of photon emission spectra for sapphires irradiated with ^{60}Co gamma-rays, 14 MeV neutrons (JAERI-FNS) and 1.8 MeV electrons (EU,Hodgson).

There is no observation of fluence dependence in the range less than 10^{13} n/cm^2, while the emission should be originated from F-center created by irradiation. This can be explained if the number of F-center of the sample before irradiation is larger than the number created by the present fluence. According to the report of transmission experiment, the transmission decreases by 10^{16} n/cm^2. Therefore, a fluence dependence might be appeared from the range of 10^{14}-10^{16} n/cm^2.

(3) CaF2

A strong peak below 350 nm and a weak peak at 550 nm were observed. The light emission is rather small compared to sapphire.

(4) NE102A

The observed light emission efficiency by gamma-ray is 11000±3000 photons/MeV and very closed to the value found in the literature [3.1.4], which

is 10300±710. It shows an excellent agreement within 7%. Therefore, the present calibration is approved with good confidence.

3.1.6 Conclusion

Sample materials with well known composition were used. The measurement devices were calibrated by an absolute method. Gamma-ray contribution in D-T irradiation was evaluated by Co-60 irradiation data. Those contributions for quartz glass were 29%,53%,18% due to n, γ, Cerenkov for DT, and 79%, 21% due to γ, Cerenkov for Co-60 source. In a result, the ratio of the emission efficiency of neutron to that of Co-60 γ ray was 0.037.

By correcting contributions of Cerenkov radiation and neutron induced gamma-ray radiation, the absolute efficiencies of 14 MeV neutron induced luminescence were obtained with respect to absorbed dose rate. These data can be extended to estimate light emission levels in window materials at any locations in a fusion reactor through dose rate.

3.1.7 Remaining issues and future plan

For the further studies necessary to add the present work, the followings can be pointed out.

1) Temperature dependence

The emission efficiency might have temperature dependence. So the data with respect to material temperature is necessary.

2) Relation to light absorption property

Light emission is strongly related to absorption structure which represents electron-hole levels inside materials and can characterize materials. Because even in the same materials these structure might be different, we should clarify the sample condition.

3) Damage effect (Fluence effect)

In the present work, no fluence effect was observed because of low fluence level due to the present DT source ability.

4) Impact of produced radioactivity

When an irradiation with larger fluence is applied, material itself is activated by neutron reaction. This radioactivity creates self irradiation field in the material. This effect might be important for heavy irradiation condition.

At the present, we have no future plan, because the above remaining issues requires more complicate device and specially the latter two cases are more than the ability of our facility.

References

[3.1.1] F. Sato, Y. Oyama, T. Iida, F. Maekawa, J. Datemichi, A. Takahashi and Y. Ikeda, Fusion Technology 1996 (1997) 857.

[3.1.2] F. Sato, Y. Oyama and T. Iida, " 14 MeV Neutron Irradiation Experiment on Window Materials for Fusion Experimental Reactor," JAERI-Research 97-042 (May 1997) (In Japanese).

[3.1.3] F.Sato, Y.Oyama, T. Iida, F. Maekawa and Y. Ikeda, "Experiment of D-T Neutron Induced Luminescence on Window Matarials," Proc. of Int. Symp. on Fusion Nuclear Technology ISFNT-4 , April 6-11, Tokyo (1997).

[3.1.4] D. Clark, Nucl. Instr. Meth., 117 (1974) 295 (NE102A light output effficiency)

3.2 Off-line Irradiation Tests of Windows in JMTR

Etsuo Ishitsuka, Hisashi Sagawa and Hiroshi Kawamura

3.2.1 Experimental object

Optical properties of window materials for the neutron irradiation and irradiation temperature is important as diagnostic design because these effects will be caused to the some measurement error. As a first step, off-line irradiation tests were carried out to summarize these effects. Change of transmission spectrum by neutron irradiation on the different fluence and temperature were measured as a Post Irradiation Examination (PIE) test.

3.2.2 Specimen

(1) Material

Neutron irradiated specimens were sapphire (Al_2O_3, 99.9 %) which produced by Kyosera Co..

(2) Sample dimension

Specimens number were 15 pieces. Dimension and weight of the sapphire sample is about ϕ13×^{t}1.1mm, 580 mg.

3.2.3 Experimental Condition

(1) Irradiation facility

JMTR (Japan Materials Testing Reactor)

(2) Irradiation conditions

General irradiation conditions is shown in Table 3.2.1.

Table 3.2.1 General irradiation conditions

-Irradiation period	:Mar., 1995 - Jul. 1995
-Irradiation hole	:E-6
-Size of the hole	:ϕ42×750 mm
-Irradiation temperature	:300, 400 and 500 °C
-Irradiation environment	:He gas

Five set samples were installed in the three inner capsule for neutron irradiation, and each inner capsule were controlled at 300°C (No.1~5), 400°C (No.11~15) and 500 °C (No.6~10) by the heater. Neutron fluence (E>1MeV) for each inner capsule were as follows.

300 °C , 2×10^{20} n/cm^2
400 °C , 3×10^{20} n/cm^2
500 °C , 4×10^{20} n/cm^2

(3) Experimental devices

Inner capsule for neutron irradiation is shown in Fig. 3.2.1. Each inner capsule were controlled at 300, 400 and 500 °C by the heater.

(4) Measurement

Transmission spectrum of neutron irradiated sapphire specimens were measured by UV-3100 (Shimadzu Co.) in the wavelength of 200~3200 nm.

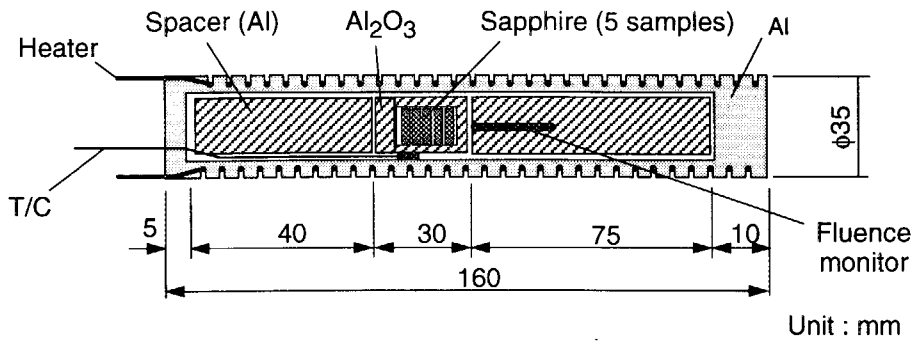

Fig. 3.2.1 Inner capsule for neutron irradiation.

3.2.4 Experimental results

Photograph of neutron irradiated sapphire specimens is shown in Fig. 3.2.2. The color of neutron irradiated sapphire specimens were change to green or brown. Un-irradiated and low fluence (old task : JB-IVA-2: 250 °C , 5×10^{19} n/cm^2) sapphire also shown in same figures.

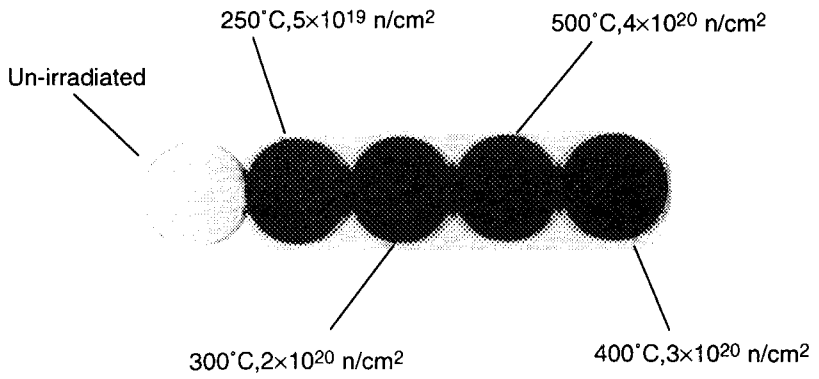

Fig. 3.2.2 Photograph of neutron irradiated sapphire specimens.

Transmission spectrum of neutron irradiated sapphire for wide range and narrow range are shown in Fig. 3.2.3 and 3.2.4. In the range of wavelength 800-5000 nm, neutron irradiation did not affect to transmission spectrum (see JA W-T28-01-P). Transmission rate of neutron irradiated sapphire in the wavelength of 200-800 nm decreased by defects of neutron irradiation (250~400°C). Spectrum of 500°C shows recover even in high neutron fluence.

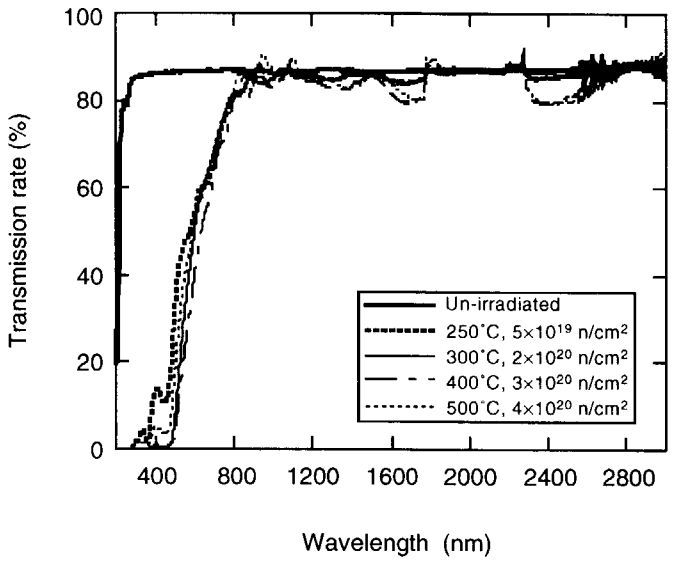

Fig. 3.2.3 Transmission spectrum for wide range.

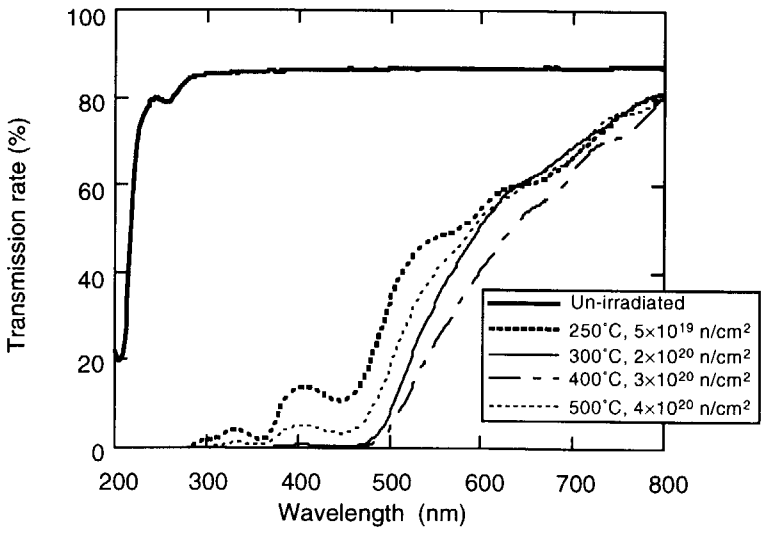

Fig. 3.2.4 Transmission spectrum for narrow range.

3.2.5 Discussions

In the range of wavelength 200-800 nm, decreasing of the transmission rate depended on neutron fluence and irradiation temperature. We can recognized the annealing effect under high temperature irradiation [3.2.1].

Umeda [3.2.2] reported that the optical properties of neutron irradiated sapphire (1.2×10^{17} n/cm^2) recovered by heating of 650°C and 5 min at the after irradiation (as PIE). However, the recovery of the transmission rate at 500°C was a little in this test, so we could not expect the annealing effect so much in visible range.

As the second step, in-situ irradiation tests discussed in the session of 3.3 to clear the behavior of optical properties of sapphire in details.

3.2.6 Conclusion

In the range of wavelength 200-800 nm for neutron irradiated sapphire, decreasing of the transmission rate is unavoidable, and could not expect the annealing effect by heating. We found that there was not significant change of the transmission in the range of wavelength 800-5000 nm, which shows that the sapphire window may be utilized in IR-FIR region on ITER.

3.2.7 Remaining issues and future plan

None

References

[3.2.1] T.Nishitani, E.Ishitsuka et al., Japanese Contribution to ITER Task of Irradiation Test on Diagnostic Components, Fourth International Symposium on Fusion Nuclear Technology, Apr. 6-11, Tokyo, Japan (1997)
[3.2.2] Umeda, Journal of the atomic energy society of Japan ,Vol.35, No.6 (1993) 543.

3.3 In-situ Irradiation Tests of Windows in JMTR

Etsuo Ishitsuka, Tatsuo Sugie, Takeo Nishitani, Satoshi Kasai and
Hiroshi Kawamura

3.3.1 Experimental object

Change of the transmission spectrum for sapphire and KU-quarts by neutron irradiation on the different temperature were measured as a in-situ transmission spectrum measurement by the special irradiation capsule.

3.3.2 Specimen

(1) Material

Two specimens of sapphire and two specimens of KU-quarts were irradiated. Impurities contents of each specimens is shown as follows, and unirradiated transmission spectrum is shown in Fig. 3.3.1.

(a) Sapphire
Al_2O_3:99.99 %

(b) KU-quarts
Results of chemical spectroscopic analysis is shown in Table 3.3.1.

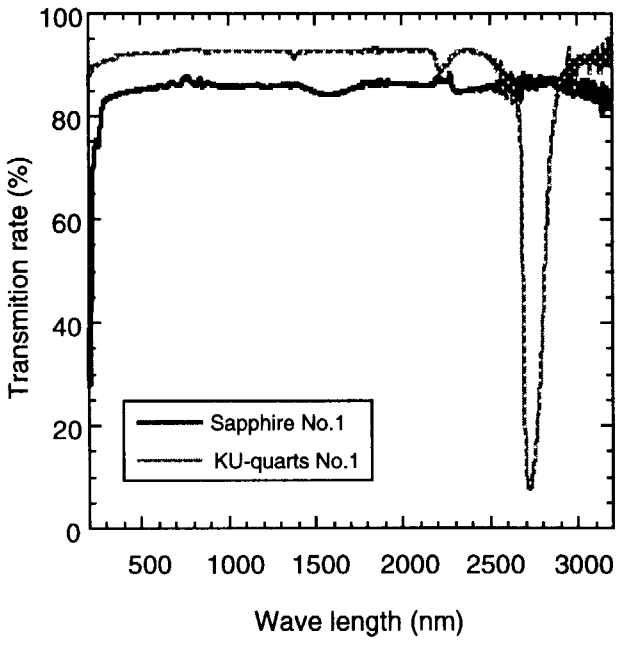

Fig. 3.3.1 Unirradiated transmission spectrum.

Table 3.3.1 Impurities contents (ppm)

Al	Ca	Cu	Fe	Mg	Mn	Ti	Na	K	OH
0.4	1.0	0.1	1.6	0.4	0.02	0.01	1.0	1.7	821

(2) Sample dimension
$\phi 11 \times t1$ mm

3.3.3 Experimental Condition

(1) Irradiation facility
JMTR (Japan Materials Testing Reactor)

(2) Irradiation conditions

General irradiation conditions is shown in Table 3.3.2.

Table 3.3.2 General irradiation conditions

-Irradiation period	:Nov., 1997 - Dec. 1997
-Irradiation hole	:G-4
-Size of the hole	:ϕ65×750 mm
-Irradiation environment	:He gas

Sapphire and KU-quarts were set on two sample stage, and each sample stage were controlled by the heater. Neutron flux, fluence (E>1MeV) and temperature for each sample stage were as follows.

Upper sample stage : Sapphire (S1) and KU-quarts (KU1)
: 4×10^{12} n/cm^2/s, 300 °C
1×10^{19} n/cm^2
Lower sample stage : Sapphire (S2) and KU-quarts (KU2)
: 7×10^{12} n/cm^2/s, 400 °C
2×10^{19} n/cm^2

(3) Experimental devices
Special irradiation capsule were developed for this measurement, so called in-situ transmission spectrum measurement capsule. Outline of in-situ transmission spectrum measurement capsule is shown in Fig. 3.3.2.

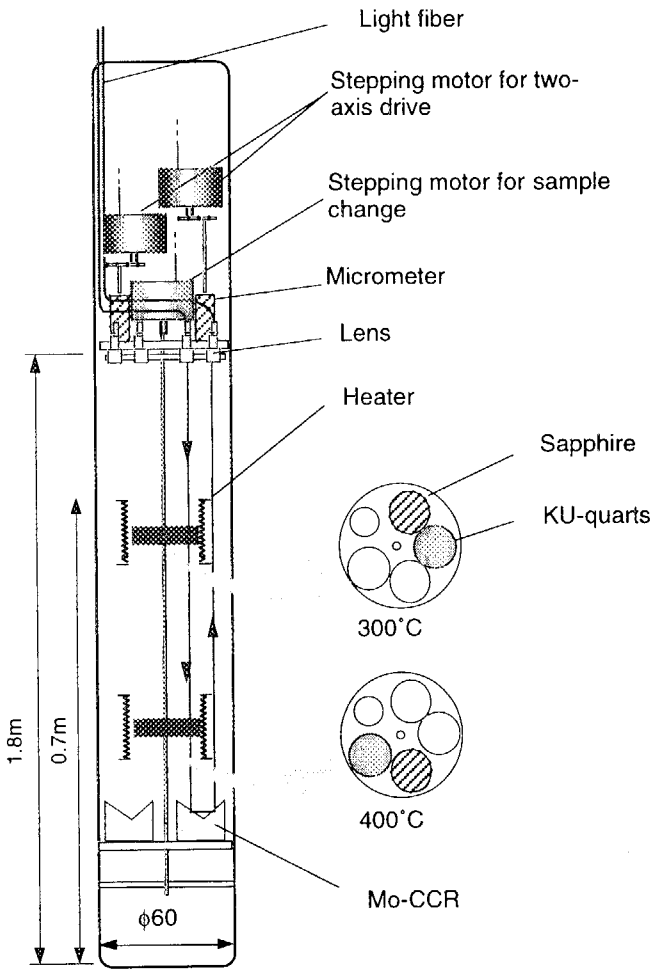

Fig. 3.3.2 In-situ transmission spectrum measurement capsule

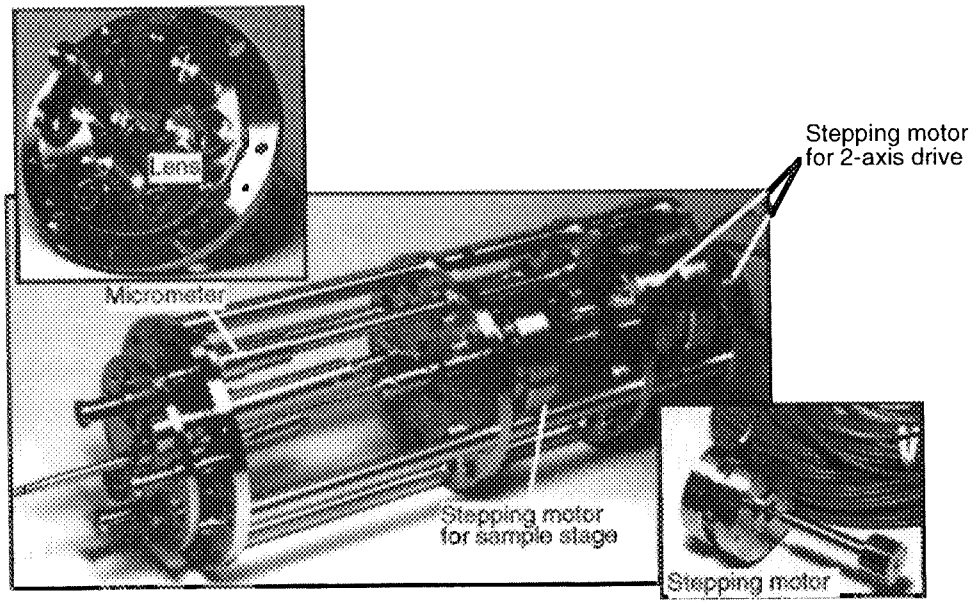

Fig. 3.3.3 Photographs of 2 axis driving system and stepping motor for sample stage rotation.

Capsule consist of 2 axis driving system, sample stage, Mo-CCR and heater. Light axises have two, one of light axis is used as spear for any accident. Two light axis adjust by 2 axis driving system, and stepping motor for sample stage rotation role as a sample changer (see Fig. 3.3.3).

(4) Measurement

Sapphire and KU-quarts of the each sample stage is possible to distinguish by small hole (see Fig. 3.3.4), and this small hole was always used as reference of air (Blank). This measurement procedure is possible to remove the attenuation of transmission light of fiber, lens and etc., by the γ-ray or neutron irradiation effects.

White light source (AQ-4303B, Ando Electric CO., LTD.) and optical spectrum analyzer (AQ-6315, Ando Electric CO., LTD.) were used as measurement equipment.

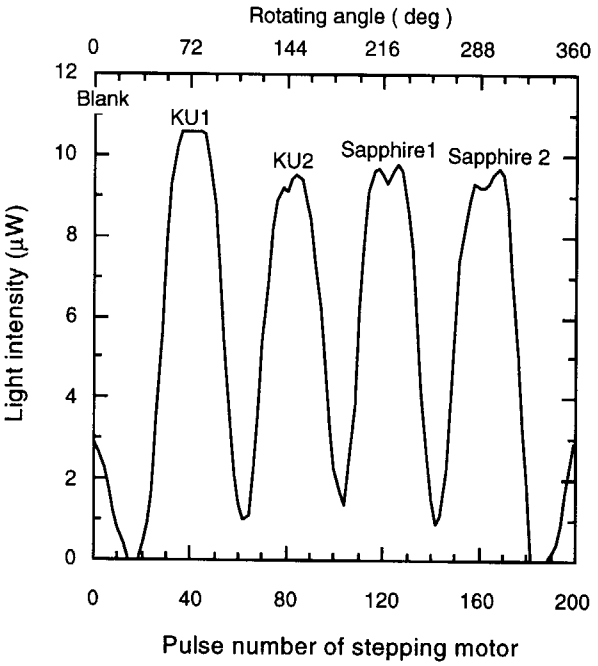

Fig. 3.3.4 Result of sample stage rotation test.

3.3.4 Experimental results

Effects of transmission spectrum by the neutron fluence and irradiation temperature were examined by special irradiation capsule. Reactor thermal power and irradiation temperature of the each specimens is shown in Fig. 3.3.5. In-situ heating up to 700°C was attempted to clear the annealing effects under the neutron irradiation condition.

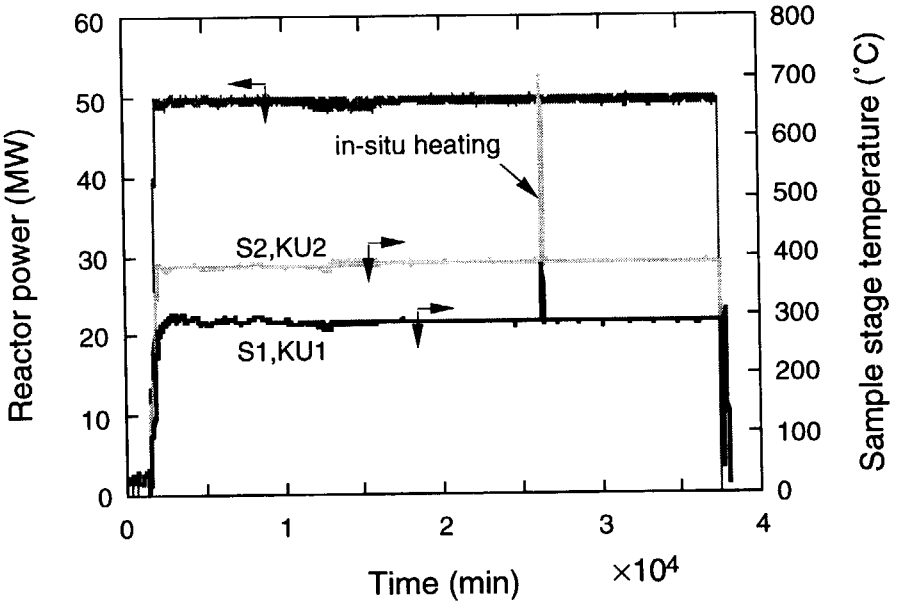

Fig. 3.3.5 Reactor power and irradiation temperature of the each specimens.

Measurement of the short wavelength side (<550nm) could not carried out due to induced loss of fiber. Induced loss on the long wavelength side (>1000nm) did not change (see session 3.2). In addition, the absolute values of measured induced losses have errors of around 1 dB, because of the low signal to noise ratio.

Induced loss of transmission spectrum at reactor power up is shown in Fig. 3.3.6. Transmission spectrum of sapphire and KU-quarts were affected by low temperature neutron irradiation even if low fluence, and KU-quarts was more sensitive than that of sapphire.

Induced loss of transmission spectrum at 50MW (full power) is shown in Fig. 3.3.7. Induced loss of each specimens increased with neutron fluence and decreased with higher irradiation temperature, and KU-quarts was smaller than that of sapphire. Transmission spectrum of each specimens became a constant at about 10 days irradiation (Total irradiation day was 25 days).

Also, induced loss of each specimens on the reactor shut down increased as remarkable. Reactor power and irradiation temperature at the reactor shut down is shown in Fig. 3.3.8. This results showed that low temperature irradiation was significantly affected on transmission spectrum .

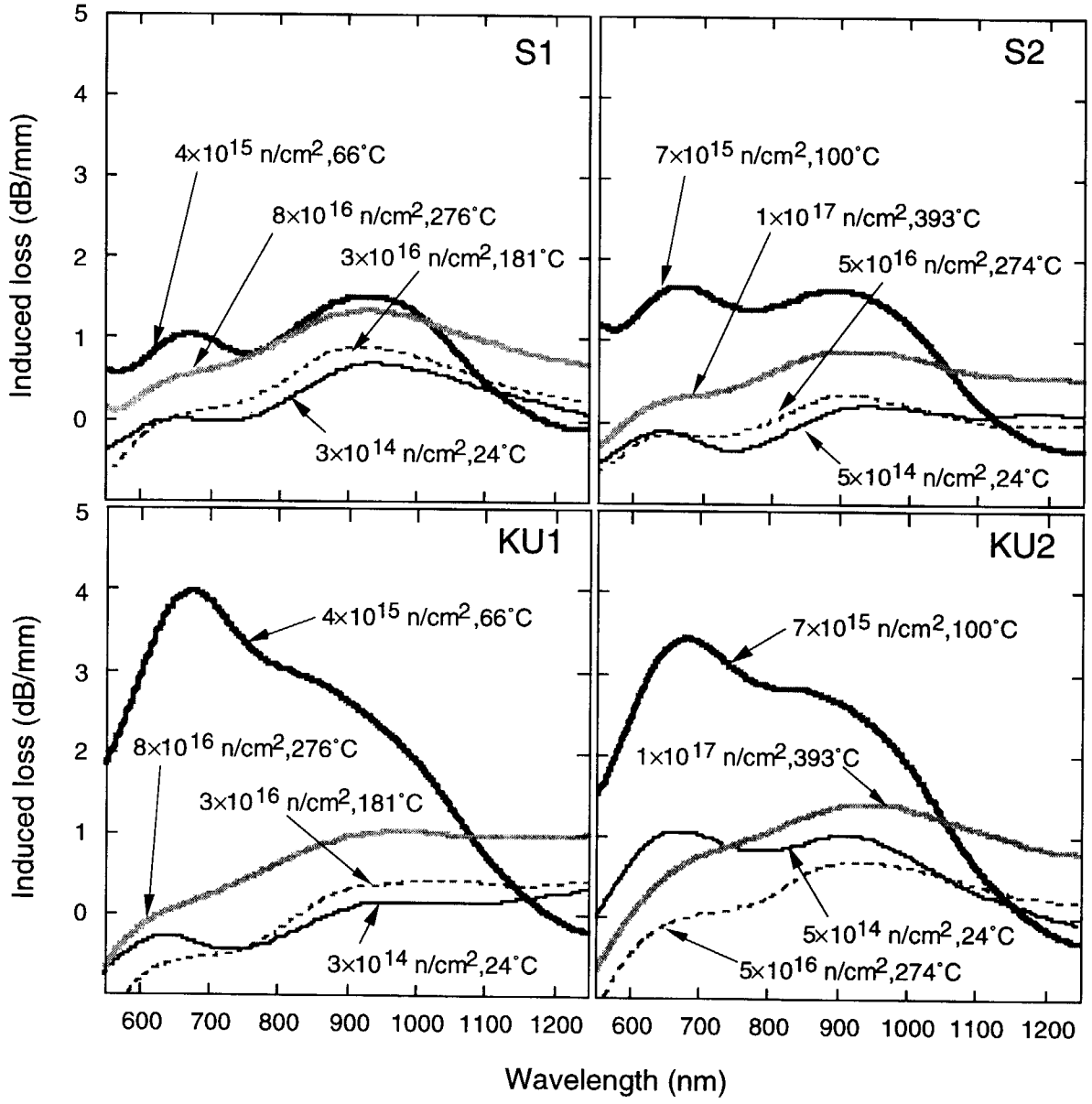

Fig. 3.3.6 Induced loss of transmission spectrum at reactor power up.

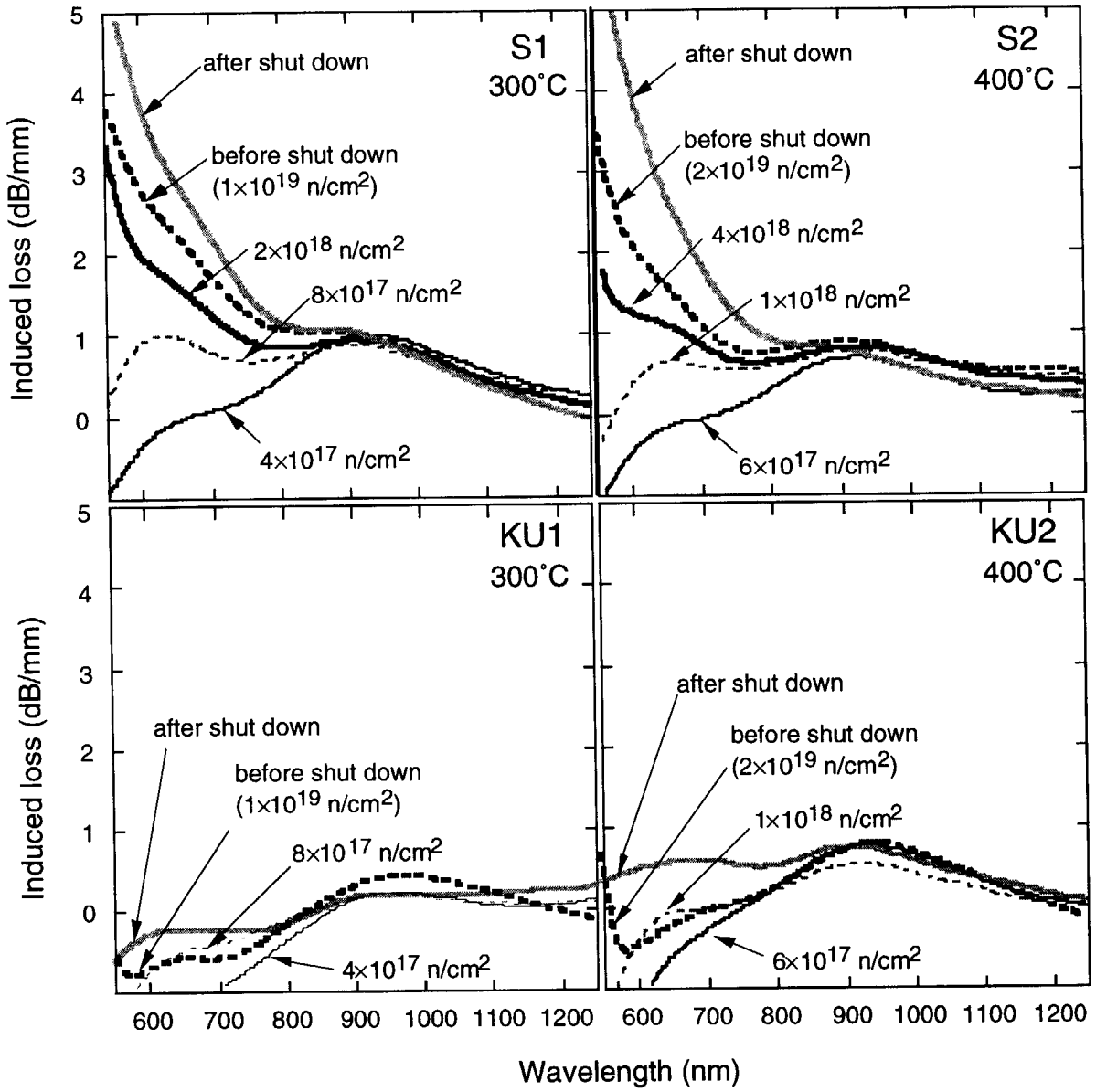

Fig. 3.3.7 Induced loss of transmission spectrum at 50MW.

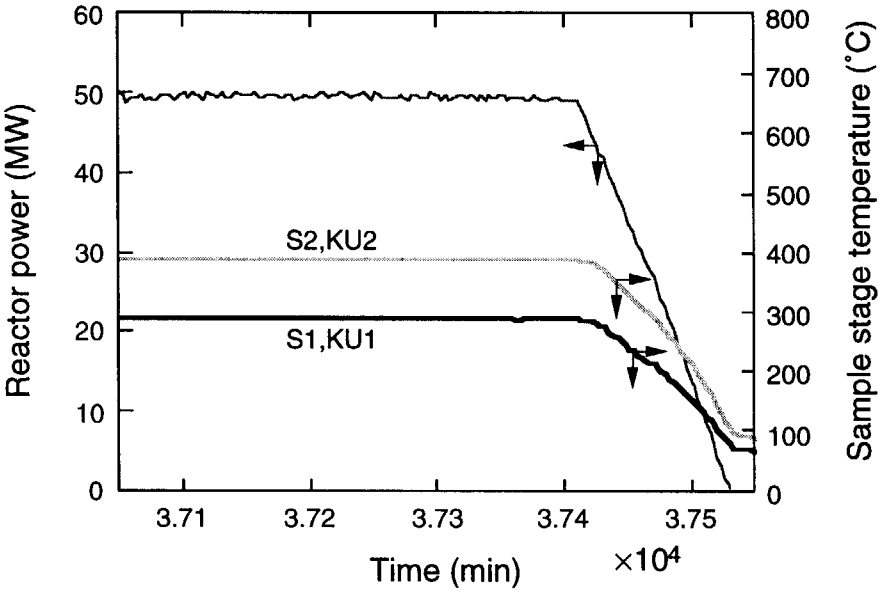

Fig. 3.3.8 Reactor power and irradiation temperature at the reactor shut down

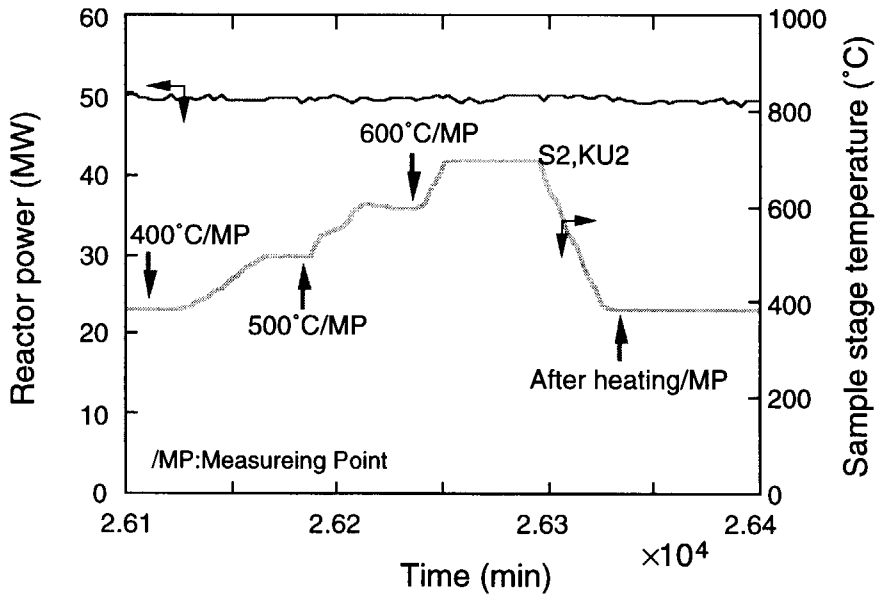

Fig. 3.3.9 Change of irradiation temperature on in-situ heating

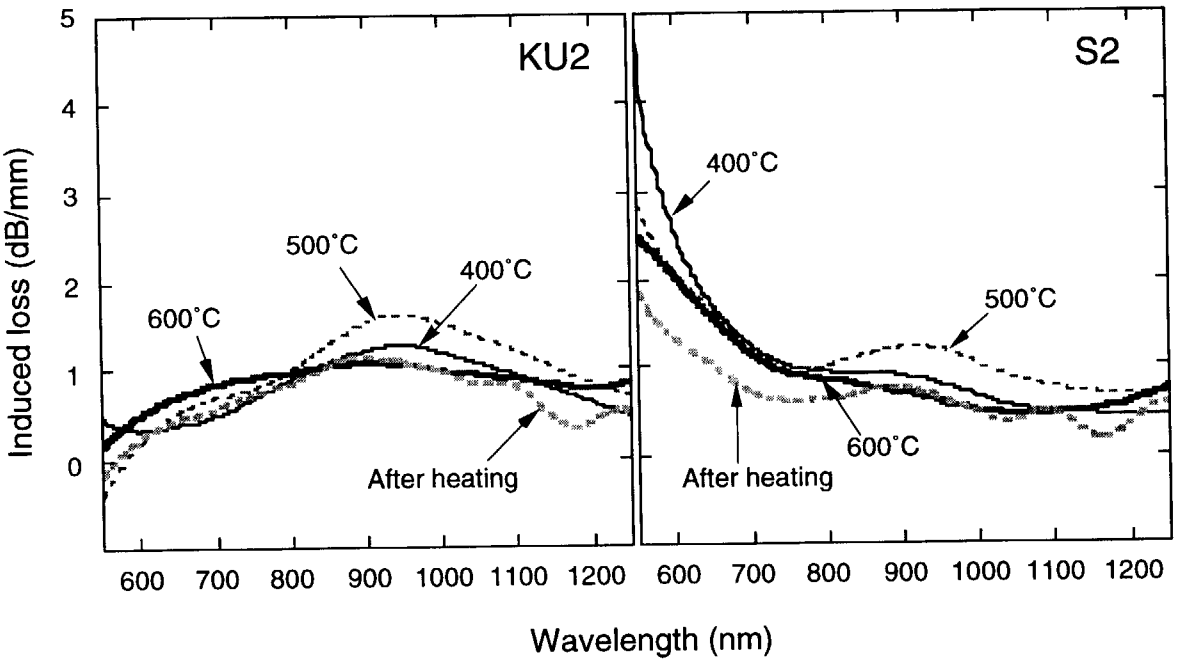

Fig. 3.3.10 Results of in-situ heating for S2 and KU2.

In-situ heating up to 700°C for S2 and KU2 was attempted to clear the annealing effects under the neutron irradiation. Change of irradiation temperature on in-situ heating is shown in Fig. 3.3.9. In this figure, arrows shows measuring points. Measurement at 700°C could not carried out because of the trouble of sample stage rotation (sample stage rotation maybe obstructed by thermal expansion). Results of each measuring points for S2 and KU2 is shown in Fig. 3.3.10. Higher irradiation temperature cause decreasing of induced loss. Some data [3.3.1-3.3.2] showed the perfect recover the transmission spectrum by the heating (up to 700°C) on the post irradiation examination (PIE) , however, the perfect recover did not observed on the in-situ heating.

3.3.5 Discussions

Induced loss of the transmission spectrum maybe settle to the valance point of increasing speed of defects (neutron flux) and recover speed of defects (irradiation temperature). Therefore, these data could not used directly because fluence of the window materials for recent design is very low (~10^{17} n/m^2). Experiments of low neutron flux should be carried out by some critical facilities.

3.3.6 Conclusion

Induced loss of each specimens increased with neutron fluence and decreased with higher irradiation temperature, and KU-quarts was smaller than that of sapphire. Utilization of KU-quarts in the short wavelength range is suitable. However, low temperature irradiation was significantly affected on transmission spectrum, and we should be caution for design.

We should not be expect the perfect recover of transmission spectrum by in-situ heating on the high neutron flux, and the monitoring of transmission spectrum of windows must be consider for the design of plasma diagnostic components.

3.3.7 Remaing issues and future plan

None.

References

[3.3.1] S.Yamamoto, Design Description Document, Radiation effect (WBS 5.5.M), ITER JCT (1997) 55.

[3.3.2] Umeda, Journal of the atomic energy society of Japan ,Vol.35, No.6 (1993) 543.

4. Optical Fibers

Several kinds of optical fibers were examined on their dynamic optical phenomena during irradiation in a medium power fission reactor JMTR, a ^{60}Co gamma-ray irradiation facility, and a 14 MeV fusion neutron irradiation facility FNS.

4.1 Irradiation Tests on Polymer Jacketed Fibers in JMTR

Tsunemi Kakuta and Etsuo Ishitsuka

4.1.1 Experimental objective

To investigate the radiation-resistant characteristics of polymer jacketed conventional type optical fibers, step-index type multimode fibers (SI), single-mode type fibers (SM), and single polarization fibers (PANDA), were irradiated in a medium power fission reactor JMTR.

4.1.2 Experimental conditions

(1) Material

Polymer jacketed conventional type optical fibers used for this experiments are listed in Table 4. 1. 1. Two types of SI fibers with low-OH contained SiO_2 core, two types of SM fibers with pure SiO_2 core, and two types of PANDA fibers, were used for this experiments.

Table 4. 1. 1 Polymer Jacketed Conventional Type Optical Fibers Used for JMTR Irradiation

Types of Fibers	Core		Cladding	Nylon Jacket	Supplier
	Composition	Diameter	Diameter	Diameter	
Step-Index (SI)	SiO_2	200μm	250μm	0.9mm	Fujikura Ltd.
	SiO_2	200μm	250μm	0.9mm	Mitsubishi Cable Co.
Singel-Mode (SM)	SiO_2	10μm	125μm	0.9mm	Fujikura Ltd.
	SiO_2	10μm	125μm	0.9mm	Mitsubishi Cable Co.
Single Polarization (PANDA)	SiO_2	10μm	125μm	0.9mm	Fujikura Ltd.
	SiO_2	10μm	125μm	0.9mm	Mitsubishi Cable Co.

(2) Irradiation facility
JMTR in JAERI Oarai.

(3) Irradiation condition
Fluxes 3.1 × 10^{13}/cm^2s (E>1MeV), Fluence 1.3 × 10^{20} n/cm^2, Temperature 130°C, Irradiated fiber length about 20cm.

(4) Experimental devices (incl. capsule)
Special capsule was used in the core region of reactor to irradiate the optical fibers. Total length of optical fibers was 50 meters, and centered 20 cm was irradiated in the special capsule. Figure 4. 1. 1 shows accommodation of optical fibers in the capsule. To measure the optical transmissivity and radio-luminescence characteristics, one end of fiber was connected to AQ-4303B xenon-lamp white light source and other end was connected to AQ-6315A optical spectrum analyzer. The fibers were irradiated up to the fast neutron(E>1MeV) fluence of 1.3 x 10^{20} n/cm^2 under fast neutron fluxes of 3.1 x 10^{13} n/cm^2·s with gamma-ray dose-rates of about 10^3 Gy/s. Temperature of optical fibers during irradiation was about 130 °C.

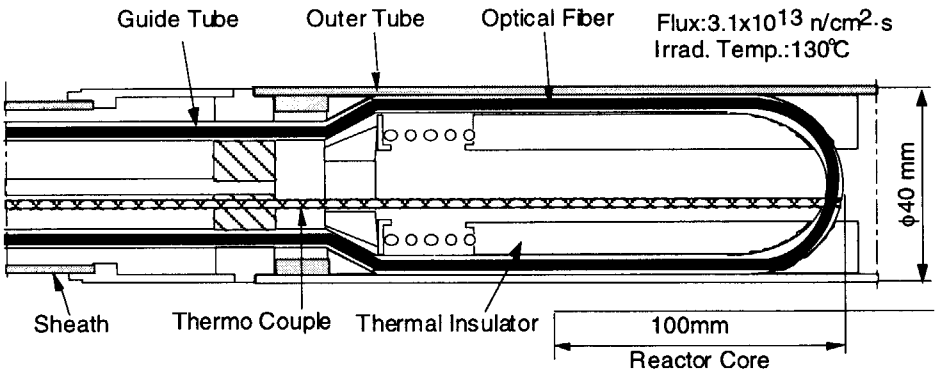

Fig. 4. 1. 1 Accommodation of Optical Fibers in Special Capsule of JMTR

(5) Measurement
In-situ measurement for optical transparency and fluorescence phenomena.
i) Step-index fiber (SI) : Wavelength region from 350 nm to 1750 nm.
ii) Single-mode fiber (SM) : Wavelength region from 800 nm to 1750 nm.
iii) Single polarization fiber (PANDA) : Wavelength region from 800 nm to 1750 nm.

4.1.3 Experimental results

One of serious problems optical fibers is the increase in transmission loss due to the radiation-induced defects and the formation of the color centers. Induced loss spectra in polymer jacketed conventional type SI and SM fibers during irradiation are shown in Fig. 4. 1. 2 and Fig. 4. 1. 3.

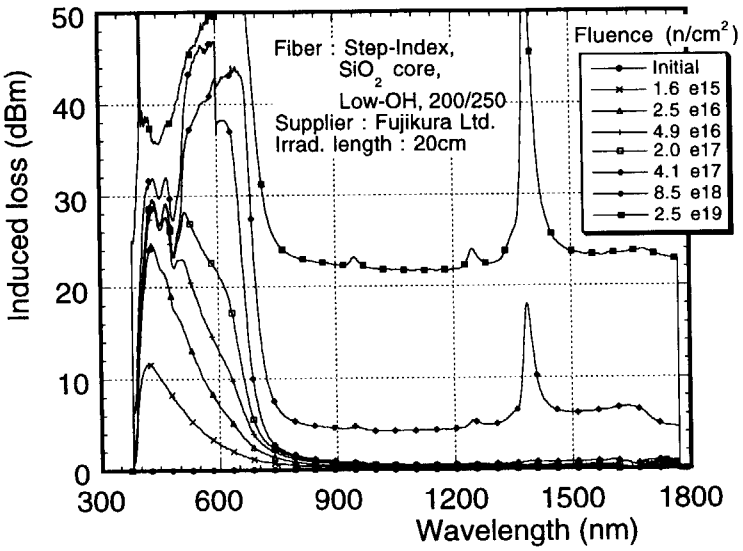

Fig. 4. 1. 2 Observed Induced Loss in Polymer Jacketed Conventional Type SI Fiber During Irradiation with JMTR

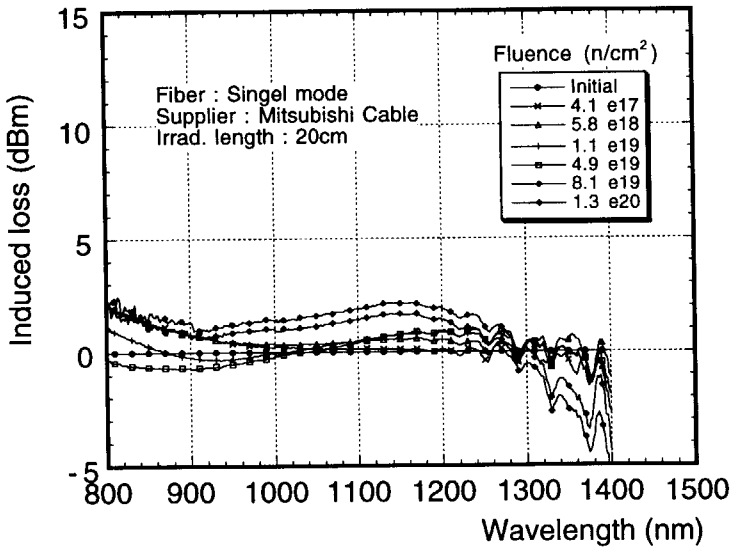

Fig. 4. 1. 3 Observed Induced Loss in Polymer Jacketed Conventional Type SM Fiber During Irradiation with JMTR

In case of SI fibers, large absorption loss in the wavelength shorter than 700 nm by means of E'-center and non bridging oxygen hole center(NBOHC), were observed. OH absorption peak at the wavelength of 1390 nm was observed irradiation larger up to 8.5 x 10^{18} n/cm^2. However, the conventional (not radiation hardened) type SI fibers were survived irradiation up to about 1 x 10^{18} n/cm^2 in the

wavelength region from 700 to 1700 nm. Figure 4. 1. 3 shows an example of induced loss spectra in SM fiber. SM type fibers were appeared good radiation resistance in the wavelength region from 800 nm to 1400 nm. The absorption loss of conventional type SM fiber was less than 5 dBm at the irradiation up about 1 x 10^{20} n/cm^2. PANDA fibers which a kind of SM fiber also appeared good radiation resistance in the wavelength region from 800 to 1300 nm.

Another significant optical phenomena, optical emission in the fibers through a fluorescence process was observed[4.1.1-4,8]. The optical emission of SI fibers whose wavelength ranged from 400 to 1700 nm with a sharp peak intensity at about 1270 nm was observed. The optical intensity distribution is approximately inversely proportional to the cube of the wavelength in the range from 700 to 1700 nm. This optical distribution was considered as fluorescence of Cerenkov radiation by gamma-ray[4.1.1].

Fission neutron irradiation on polymer jacketed conventional type optical fibers in JMTR, following characteristics were pointed out. SM type (incl. PANDA) fibers appeared good radiation resistance in the wavelength region from 800 to 1300 nm. All conventional type SM fibers survived irradiation up to about 1 x 10^{20} n/cm^2.

References

[4.1.1] T. Shikama, M. Narui, T. Kakuta, et al.,"Study of optical radiation from SiO_2 during reactor irradiation", Nucl. Instrum. Methds, **B-91**, 342-345 (1994).

[4.1.2] P. D. Morgan, Proc. 17th Symp. Fusion Technol, Rome, 14-18 Sept. (1992).

[4.1.3] T. Tanabe, "Photon Emission Induced by Neutron and Ions", Dynamic Effects of Irradiation in ceramics, A U.S. / Japan Workshop, Santa Fe, New Mexico, pp231-256 (1992).

[4.1.4] T. tanabe, S. Tanaka, et al., "Neutron Induced Luminescence of Ceramics", Journal of Nucl, Mater., **212-215**, 1050-1055 (1994)

4.2 ^{60}Co Gamma-ray Irradiation Tests on Polymer Jacketed Fiber

Tsunemi Kakuta and Tatsuo Shikama

4.2.1 Experimental objective

To investigate the radiation-resistant characteristics of polymer jacketed conventional type optical fibers, step-index type multimode fibers (SI), single-mode type fibers (SM), and single polarization fibers (PANDA), were irradiated in ^{60}Co gamma-rays.

4.2.2 Experimental conditions

(1) Material

Polymer Jacketed conventional type optical fiber, low-OH SiO_2 core with fluorine doped SiO_2 clad step-index (SI) fiber was irradiated by the ^{60}Co gamma-ray source. The irradiated fiber was same as the sample of JMTR irradiation which supplied by Fujikura Ltd. The diameter of the core and cladding are 200μm and 250μm, respectively. Outer diameter of nylon-jacket is 0.9 mm. Total length of fiber used for experiment was 30 meter and centered 10 meter was exposed to the ^{60}Co gamma-ray source. (See Section 4.1.1 (1))

(2) Irradiation facility

^{60}Co irradiation facility in JAERI Tokai.

(3) Irradiation condition

Dose rate 5.0 Gy/s, , Total dose 1.2×10^6 Gy, Room-temperature

(4) Measurement

In-situ measurement for transmissivity at the wavelength region from 350 nm to 1750 nm was conducted by means of white light source and optical spectrum analyzer. One end of fiber was connected to AQ-4303B xenon-lamp white light source and other end was connected to AQ-6315A optical spectrum analyzer. The fiber was irradiated up to 1.2×10^6 Gy under the dose-rate of 5.0 Gy/s. Temperature of optical fiber during irradiation was about 20 °C.

4.2.3 Experimental results

Figure 4. 2. 1 .shows the induced transmission loss spectra in polymer jacketed conventional type optical fiber during irradiation with ^{60}Co gamma-ray under the dose-rate of 5.0 Gy/s. During irradiation, the absorption loss by means of E'-center and NBOHC increased and distributed to the wavelength of 900 nm, but after irradiation, the absorption loss recovered rapidly.

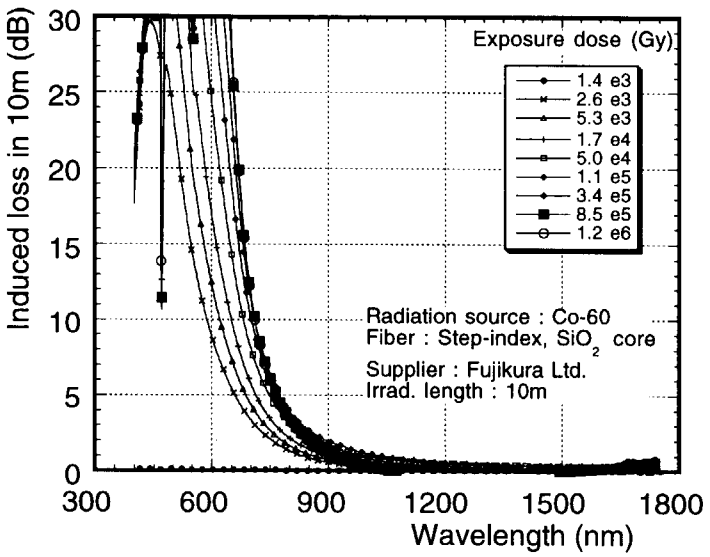

Fig. 4. 2. 1 Observed Induced Loss in Polymer Jacketed Conventional Type SI Fiber During Irradiation with ^{60}Co Gamma-Ray.

Temperature effects on absorption characteristics was also measured[5]. The irradiation temperature ranged from R.T. to 300 °C. Material composition of core and cladding are same as above SI fibers expected nylon jacket. Figure 4. 2. 2 shows the temperature dependence of the absorption spectra on the SiO_2 core fiber.

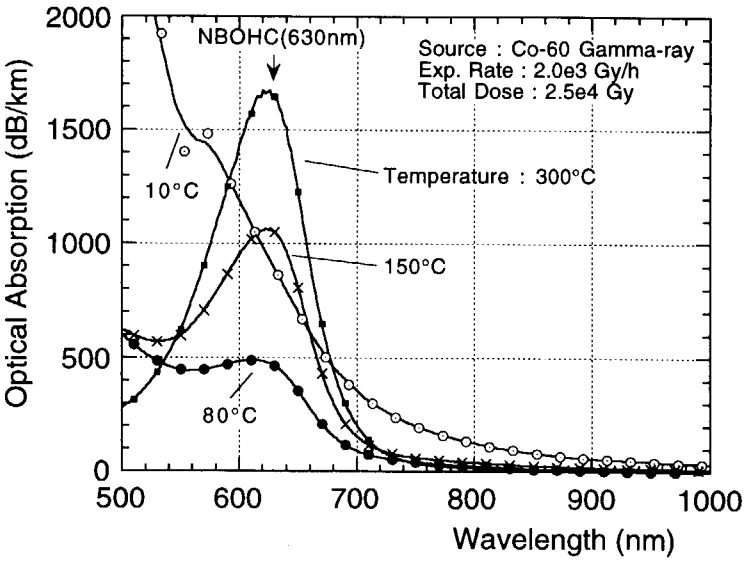

Fig. 4. 2. 2 Observed Absorption Spectra in SiO2 Core Fiber as Function of Temperature.

When the temperature rise up, absorption of the UV band decreased sharply because of recombination of electron-hole pairs. By contrast, the absorption of 630 nm band increased with the temperature. The increase in 630 nm band would be a effect of diffused oxygen in the fiber. At the high temperature, combination of the activated oxygen creates the new proxy radicals (620 nm) and/or NBOHC (630 nm)[4.2.1-2].

References

[4.2.1] T. Kakuta, T. Shikama, et al., "Temperature Dependence of Irradition Effects onOptical Fibers", 1997 Fall Mtg., AESJ, Oct. 14-17, C16, Ginowan Okinawa (1997).

[4.2.2] D. L. Griscom, "Gamma and fission reactor radiation effects on the visible-range transparency of aluminum-jacketed, all-silica optical fibers", J. Appl. Phys., **80** 2143-2155 (1996).

4. 3 Irradiation Tests on Aluminum Jacketed Fiber in JMTR

Tsunemi Kakuta and Tatsuo Shikama

4.3.1 Experimental objective

To investigate the fission neutron irradiation effects and radiation-resistance characteristics of Aluminum-jacketed fiber optics which are ITER relavant.

4.3.2 Experimental conditions

(1) Material

Several kinds of radiation-resistant optical fibers have been fabricated and fission neutron irradiation tests were carried out in the JMTR. A list of radiation-resistant optical fibers is shown in Table 4. 3. 1. Five kinds of SiO_2 based optical fibers, fibers Nos. 1, 2 and 5 of OH free pure SiO_2 core, Nos. 3 and 4 of pure silica with F-doped core, were used for this experiments. All five kinds of fibers consist of F-doped SiO_2 cladding and 300μm diameter Aluminum jacket. The contents of fluorine in the core and cladding of fiber Nos. 3 and 4 were, 1.6 wt% and 5.6 wt%, respectively.

Table 4. 3. 1 Aluminum Jacketed Fibers Used for Experiments

Fibers		Core		Cladding		Jacket	Supplier
No.	Types of Fibers	Composition	Dia.	Composition	Dia.	Dia.	
1	Step-Index pure-Silica	SiO_2	200μm	SiO_2-F F:4.0wt%	250μm	300μm Al	Fujikura Ltd.
2							Mitsubishi Cable Co.
3	Step-Index F-dope	SiO_2-F F:1.6wt%	200μm	SiO_2-F F:5.6wt%	250μm	300μm Al	Fujikura Ltd.
4							Mitsubishi Cable Co.
5	Step-Index pure-Silica	SiO_2	200μm	—	250μm	300μm Al	U S Fiber Guide

(2) Irradiation facility

JMTR in JAERI Oarai.

(3) Irradiation condition

Experiments were carried out in the JMTR fission reactor at JAERI. A special capsule in the core region of the reactor was used to irradiate the optical fibers. The

irradiated length of the optical fibers was about 1 meter. The optical fibers were irradiated up to a fast neutron(E>1MeV) fluence of 2 x 10^{20} n/cm^2 under a fluxes of 4 x 10^{13} n/cm^2·s, with a gamma-ray dose of 5 x 10^9 Gy. Irradiation temperature was about 220-230 °C.

(4) Experimental devices (incl. capsule)

Irradiation capsule is same as in Fig.4.1.1. The radiation-induced optical absorption and radio-luminescence in the optical fibers was measured with an optical spectrum analyzer (Ando AQ-6315A) in the wavelength range of 350 - 1800 nm. The AQ-6315A optical spectrum analyzer is measuring the optical power density and its sensitivity is about -80dBm(10^{-11}W). One end of the optical fiber was connected to the xenon-lamp white-light-source (Ando AQ-4303B) and the other end to the optical spectrum analyzer.

4.3.3 Experimental results

An example of the observed optical transmission spectra of the aluminum-jacketed fibers by fission neutron irradiation, is shown in Fig. 4. 3. 1. The figure shows the induced optical absorption of pure-SiO_2 core fiber and F-doped core fiber at the irradiation up to 4.3 x 10^{18} n/cm^2.

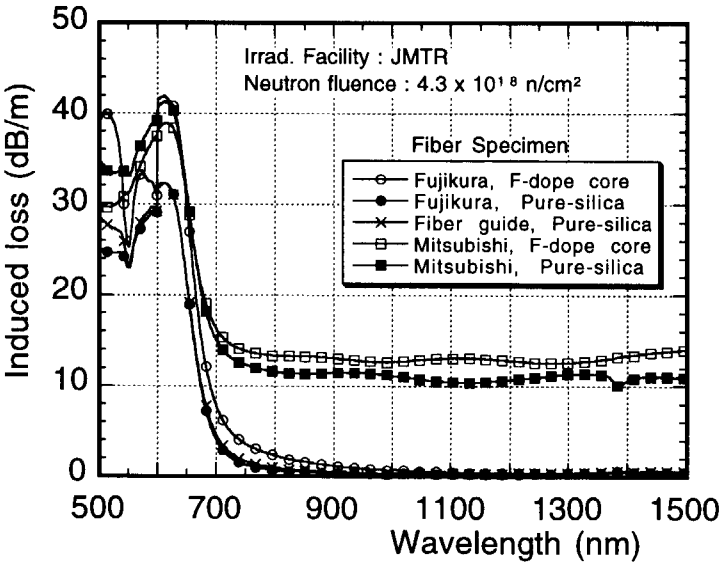

Fig. 4. 3. 1 Observed Induced Loss Spectra in Aluminum Jacketed Fibers

As the results of fission neutron irradiation, the following characteristics have become clear. The absorption induced by heavy neutrons can be concentrated in the UV to visible wavelength region. Also, the optical absorption in the UV to visible wavelength was previously reported[4.3.1-2]. Large and permanent absorption losses at wavelengths of less than 700 nm by means of E' center and NBOHC was

observed. By contrast, the increase in absorption of the all five aluminum jacketed fibers were quite low in the wavelength range from 700 to 1500 nm. Figure 4. 3. 2 shows an increase in monochromatic optical transmission for the aluminum jacketed fibers. The increase in transmission-loss at the end of irradiation period was less than 10 dB/m in the IR wavelength region. All five types of aluminum jacketed fibers survived fast neutron irradiation up to about 2 x 10^{20} n/cm^2, concurrent with gamma-ray doses of 5 x 10^9 Gy. In this observation by the fission neutron irradiation, the absorption of F-doped core fiber is quite similar to that of pure-SiO_2 core fiber. In the previous investigation of medium-dose gamma-ray irradiation, the absorption of F-doped core fiber was quite low as compared with pure-SiO_2 core fiber[9,10]. Furthermore, large and comparatively rapid recovery of absorption was observed after irradiation.

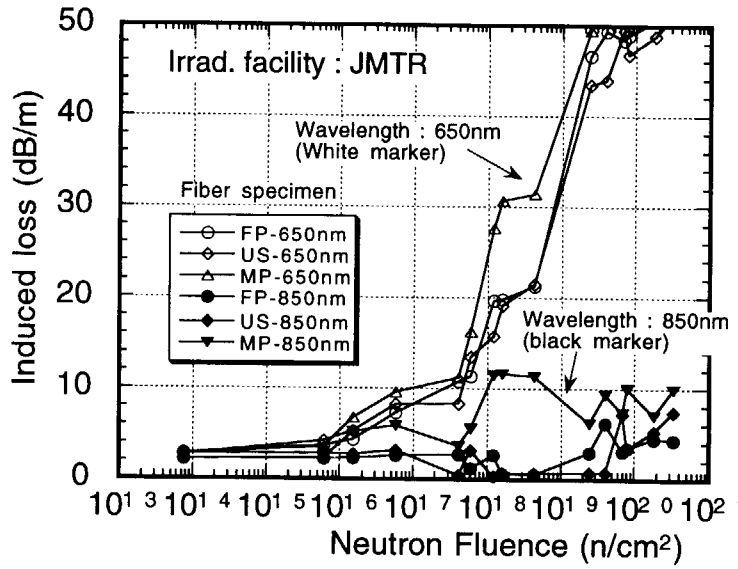

Fig. 4. 3. 2 Increase in Monochromatic Transmission-Loss for Aluminum Jacketed Fibers

One of the main reasons for the permanent absorption by the heavy neutron irradiation would be the influence of atomic displacement. The rapid recovered optical absorption by gamma-ray irradiation is influenced to the ionization. The result of absorption measurements showed that effects of the irradiation associated with fission neutron would be different from effects of the ionizing irradiation.

Another significant effect, namely the optical emission in the fibers through a fluorescence process was observed[4.1.1-4, 4.3.2]. An example of the spectral optical emission, in the Aluminum Jacketed fibers is shown in Fig. 4. 3. 3. The optical emission which wavelength ranged from 400 nm to 1400 nm with a sharp peak intensity at about 1270 nm was observed. Also, the broad band optical emission peak at 450 nm was observe[4.1.3-4, 4.3.5]. The optical intensity distribution is approximately inversely proportional to the cube of the wavelength in the range from 700 to 1400 nm. The optical distribution in the wavelength range from 700 to

1400 nm was considered as fluorescence of Cerenkov radiation by gamma-ray[4.1.1]. The peak values of 1270 nm is directly proportional to the reactor power[4.3.2, 4.3.4].

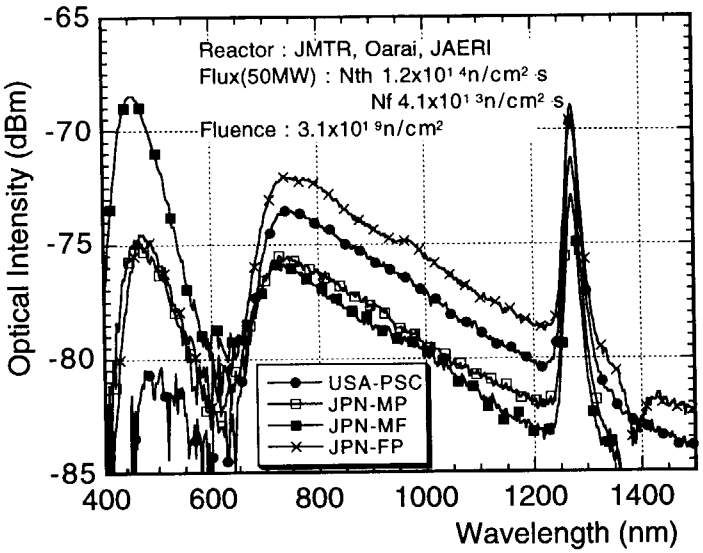

Fig. 4. 3. 3 Observed Radio-Luminescence in Aluminum Jacketed Fibers

During fission neutron irradiation, the absorption of aluminum jacketed fibers were quite low in the wavelengths range from 750 to 1500 nm. The fluorescence signal in the wavelength range 750 to 1400 nm is not affected by the absorption of optical fibers. The result suggests the possibility of using radiation-resistant optical fibers as a new optical diagnostics for the fusion reactor[4.3.4].

References

[4.3.1] T. Shikama, T. Kakuta, et al., "Optical Properties in Fibers During Irradiation in a Fission Reactor", Journal of Nucl. Mater., **225** (1995) 324-327.

[4.3.2] T. Kakuta T. Shikama, et al., "Development of In-Core Monitoring System using Radiation Resistant Optical Fibers", 1994 IEEE Conference Record, NSS11-11, 371 (1994).

[4.3.3] T. Kakuta, K. Ara, N. Shamoto, et al., "Radiation resistance characteristics of fluorine doped silica core fiber", The Fujikura Giho, No.86, pp 50-54 (1994).

[4.3.4] T. Kakuta, T. Shikama, et al., "Behavior of Optical Fibers under Heavy Irradiation", 4th International Symp. on Fusion Nuclear Technol., MR-P36, Tokyo, 6-11 April (1997).

[4.3.5] K. Tanimura et al., "Creation of Quasistable defects by electron excitation in SiO_2", Phys. Rev. Lett. **54**. 1650 (1983).

4.4 ^{60}Co-Gamma Irradiation Tests on Aluminum Jacketed Fibers

Tsunemi Kakuta and Tatsuo Shikama

4.2.1 Experimental objective

To investigate the gamma irradiation effects and radiation-resistance characteristics of Aluminum-jacketed fiber optics which are ITER relevant.

4.2.2 Experimental conditions

(1) Material

Silica(SiO_2) based aluminum-jacketed SI type optical fibers were tested with ^{60}Co gamma-ray source. Three kinds of pure SiO_2 core fiber and a Fluorine-doped SiO_2 core fiber, shown in Table 4. 3. 1, were irradiated in the gamma-ray. Total length of fiber used for experiment was 30 meter and centered 10 meter was exposed to the ^{60}Co gamma-ray source.

(2) Irradiation facility

60Co irradiation facility at JAERI

(3) Irradiation condition

The fiber was irradiated up to 1.6x 10^6 Gy under the dose-rate of 2.78 Gy/s. Temperature of optical fiber during irradiation was about 20 °C.

(4) Measurements

In-situ measurement for transmissivity at the wavelength region from 350 nm to 1750 nm was conducted by means of white light source and optical spectrum analyzer. One end of fiber was connected to AQ-4303B xenon-lamp white light source and other end was connected to AQ-6315A optical spectrum analyzer.

4.2.3 Experimental results

Figure 4. 4. 1 .shows the induced transmission loss spectra in aluminum jacketed type optical fibers with comparison between pure-SiO_2 core fibers and a F-doped core fiber. Observed transmission loss characteristics were quite different in comparison with specimens. The absorption band in three kinds of pure SiO_2 core fibers were distributed to the wavelength ranged from UV to 800 nm by means of E'-center and NBOHC. By contrast, the F-doped core fiber appeared UV-tail by means of E'-center and sharp absorption peak at 630 nm by means of NBOHC. Increase in transmission loss were quite low in comparison with SiO_2 core fibers. Figure 4. 4. 2 shows the absorption loss spectra in the F-doped core fiber.

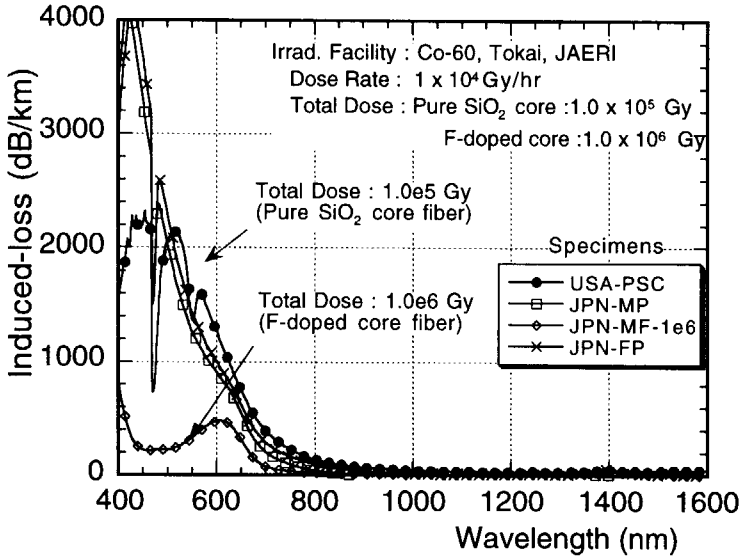

Fig. 4. 4. 1 Observed Induced Loss Spectra in Aluminum Jacketed Fibers

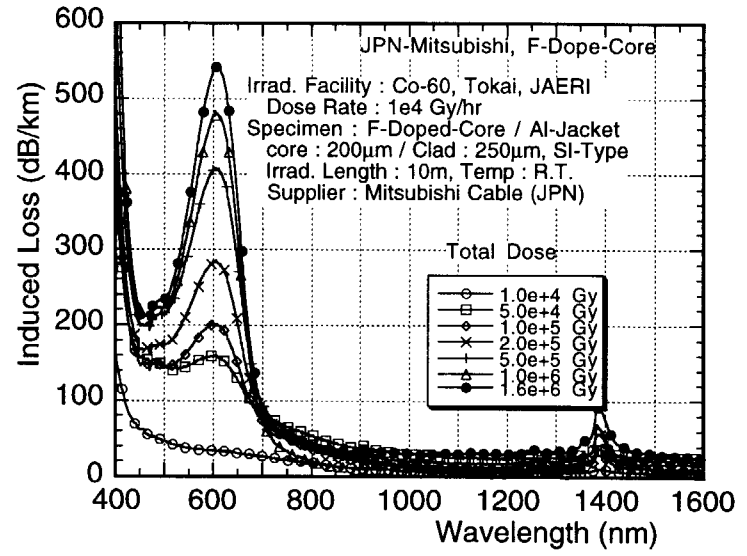

Fig. 4. 4. 2 Observed Induced Loss Spectra in Fluorine Doped Core Fiber

In this observation of ^{60}Co gamma-ray irradiation for aluminum jacketed fibers, the F-doped core fiber showed the good radiation resistivity in comparison with pure SiO_2 core fibers. The optical absorption loss of all kinds of fibers also recovered rapidly after gamma-ray irradiation. The rapid recovered optical absorption by gamma-ray irradiation would be the influence of ionization in silica defects.

4.5 14 MeV Fusion Neutron Irradiation Tests on Aluminum Jacketed Fibers

Tsunemi Kakuta and Tatsuo Shikama

4.5.1 Experimental objective

To investigate the 14 MeV neutron irradiation effects and radiation-resistance characteristics of Aluminum-jacketed fiber optics which are ITER relevant.

4.5.2 Experimental conditions

(1) Material
Two kinds of Fluorine doped core fibers and a Pure SiO_2 core fiber , shown in Table 4. 3. 1, were used for 14 MeV fusion neutron irradiation tests. Two kinds of F-doped core fibers were supplied by Fujikura Ltd. and Mitsubishi Cable Inc. and a pure SiO2 core fiber was supplied by US Fiber Guide. The length of 50 meters for Fujikura fiber and 20 meters for Mitsubishi and US Fiber Guide were irradiated, and the optical transmission loss spectrum during irradiation was measured. Total length of three kinds of fibers were 100 meters.

(2) Irradiation facility
FNS in JAERI was used as a 14 MeV fusion neutron source.

(3) Irradiation condition
The optical fibers were irradiated about 10 hours/day under flux of 3.2×10^9 $n/cm^2 \cdot s$ with 14 MeV neutron beam, and irradiation was repeated 17 days. Total fluence of 14 MeV fusion neutron to the aluminum jacketed fibers were up to 2.0×10^{15} n/cm^2. Irradiation temperature was about 25 °C during irradiation period.

(4) Measurements
In-situ measurement for transmissivity at the wavelength region from 350 nm to 1750 nm was conducted by means of white light source and optical spectrum analyzer. One end of fiber was connected to AQ-4303B xenon-lamp white light source and other end was connected to AQ-6315A optical spectrum analyzer.

4.5.3 Experimental results

Examples of induced transmission loss spectra and monochromatic optical transmission loss for the aluminum jacketed optical fibers during irradiation with a 14 MeV fusion neutron flux of 3.2×10^9 $n/cm^2 \cdot s$, are shown in Fig. 4. 5. 1 and Fig. 4. 5. 2.

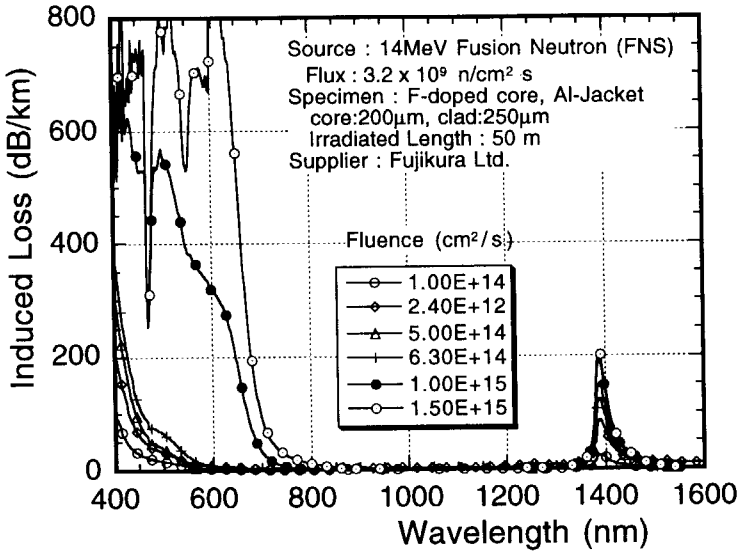

Fig. 4. 5. 1 Observed Loss Spectra in Aluminum Jacketed Fibers Measured with 14 MeV Fusion Neutron Source

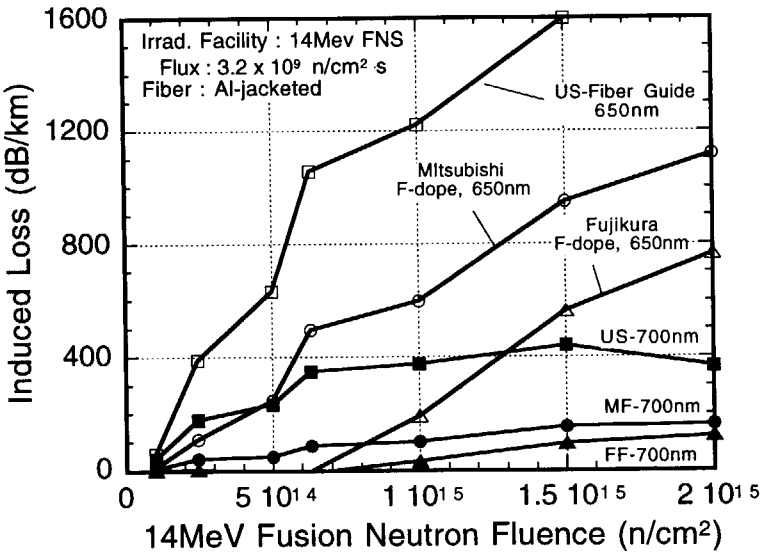

Fig. 4. 5. 2 Increase in Transmission Loss in Aluminum Jacketed Fibers Measured with 14 MeV Fusion Neutron Source

As the results of 14 MeV fusion neutron irradiation, the following characteristics have become clear. The absorption induced by 14 MeV fusion neutrons is quite similar to that of fission neutron irradiation. The absorption can be concentrated in the UV to visible wavelength region. Also the permanent losses at wavelength of less than 700 nm by means of atomic displacements, was observed. The F-doped core fibers showed the lower absorption loss than that of pure SiO_2 core fiber.

5. Mirror/Reflector

5. 1 Off-line Irradiation Tests of Molybdenum Reflector in JMTR

Etsuo Ishitsuka, Akira Nagashima, Tatsuo Sugie, Takeo Nishitani and Hiroshi Kawamura

5.1.1 Experimental object

Molybdenum is candidate material because it have low sputtering, easy polish and low activity. However, the change of mirror surface by neutron irradiation must be confirm by neutron irradiation test. Then, molybdenum reflectors Corner Cube Reflectors (Mo-CCR) were irradiated, and the surface condition was examined by an interferometric technique and the scanning electron microscope (SEM).

5.1.2 Specimen

(1) Material
Mo-CCR (Mo, 99.9%) were produced by Optic Mihara Co..

(2) Sample dimension
$\phi 13 \times {}^{h}15$ mm

5.1.3 Experimental Condition

(1) Irradiation facility
JMTR (Japan Materials Testing Reactor)

(2) Irradiation conditions
Irradiation conditions is shown in Table 5.1.1.

(3) Experimental devices
Mo-CCR was irradiated using by inner capsule shown as Fig. 5.1.1.

(4) Measurement
Interference measurement by interferometer of He-Ne laser and SEM observation were carried out to investigate the change of mirror surface by neutron irradiation. Interference measurement equipment and photograph of equipment are shown in Fig. 5.1.2 and 5.1.3. This equipment was set in lead cell to protect radioactivity.

Table 5.1.1 Irradiation conditions

-Irradiation period	:Mar., 1995 - Jul. 1995
-Irradiation hole	:E-6
-Size of the hole	:ϕ42×750 mm
-Irradiation temperature	:200 °C
-Irradiation environment	:He gas
-Neutron fluence (E>1MeV)	:1.4×10^{20} n/cm^2

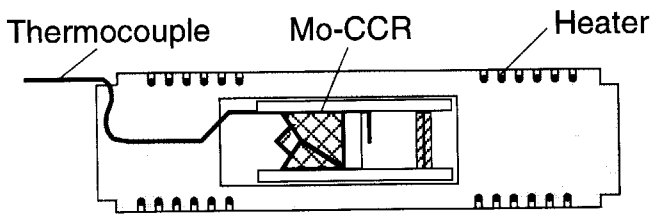

Fig. 5.1.1 Inner capsule for Mo-CCR.

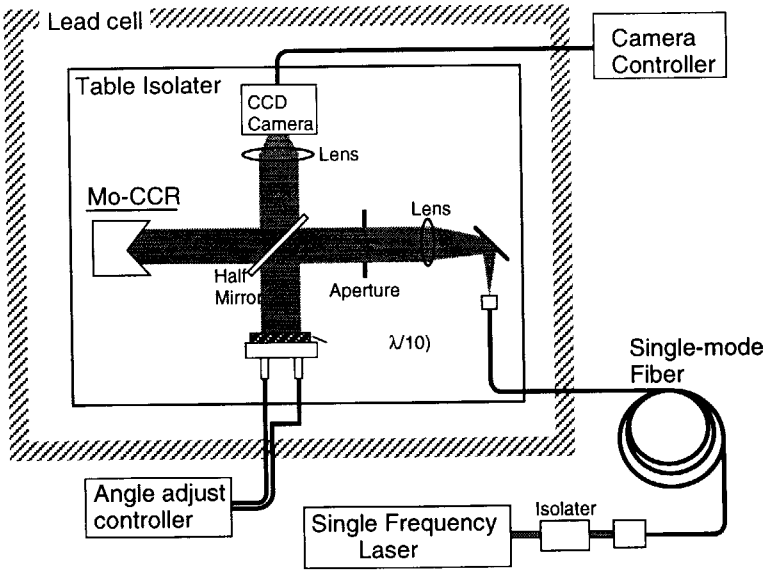

Fig. 5.1.2 Interference measurement equipment.

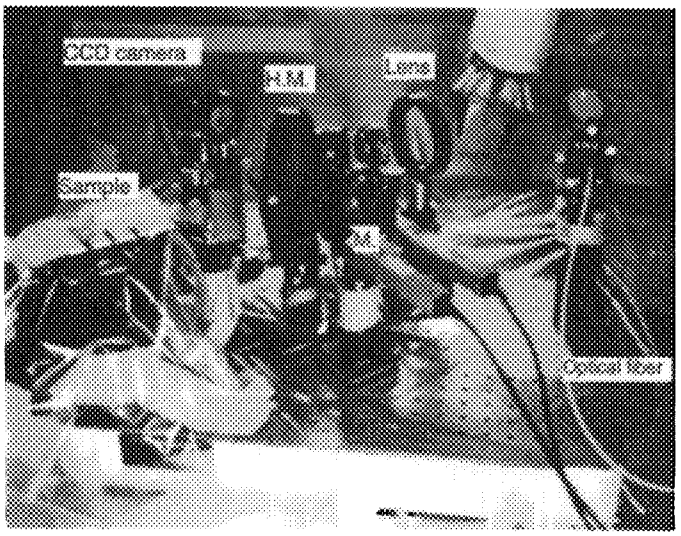

Fig. 5.1.3 Photograph of interference measurement equipment.

5.1.4 Experimental results

The results of interference measurement are shown in Fig. 5.1.4. White rectangular area were mirror surface area. The interference fringes of mirror surface are parallel, and the bad effects of neutron irradiation did not observed. The warp of interference fringes for left side of neutron irradiated Mo-CCR may occur by bolt for fix.

SEM observations were curried out on magnification of ×95-9500. The results of SEM observation are shown in Fig. 5.1.5 and 5.1.6. The surface of Mo-CCR was smooth and the effects of neutron irradiation could not observed.

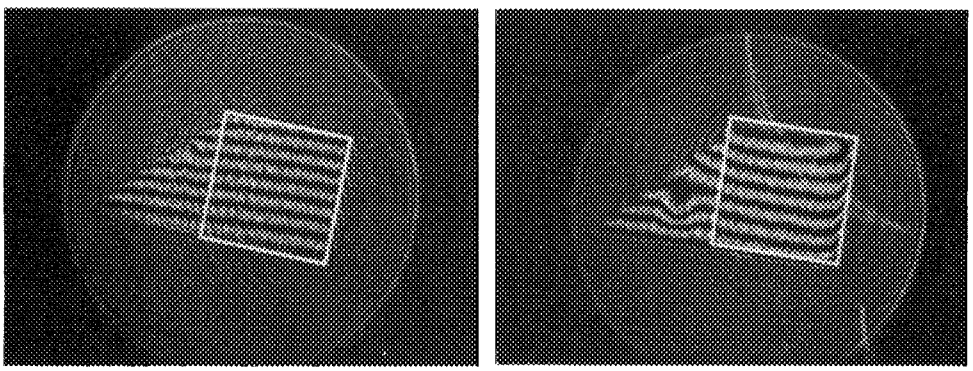

(a) Un-irradiated specimen (b) Neutron irradiated specimen

Fig. 5.1.4 Results of interference measurement.

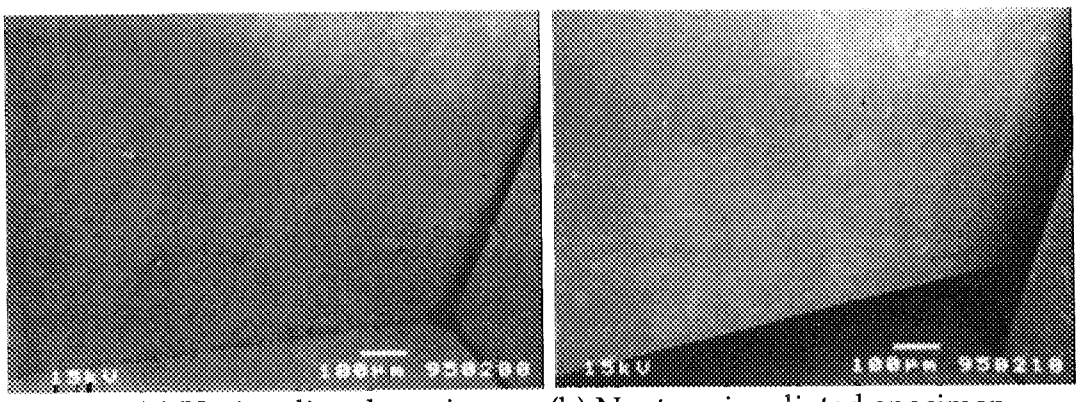

(a) Un-irradiated specimen (b) Neutron irradiated specimen

Fig. 5.1.5 Results of SEM observation (×95).

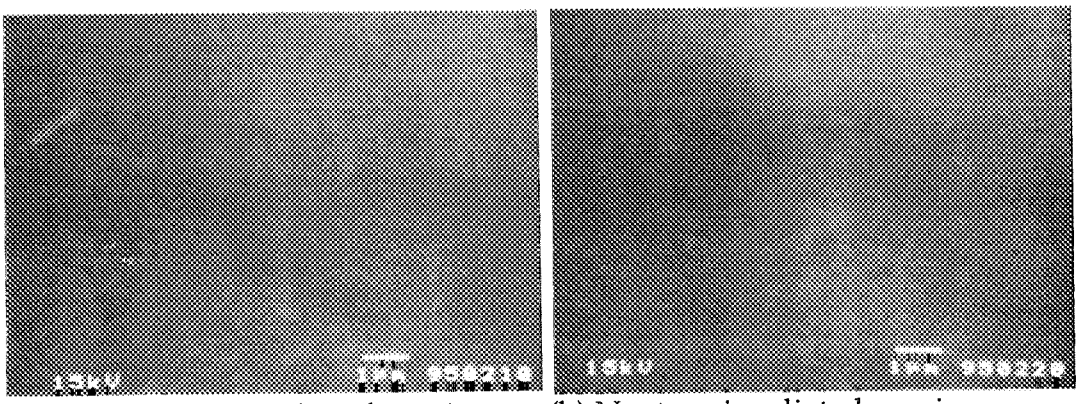

(a) Un-irradiated specimen (b) Neutron irradiated specimen

Fig. 5.1.6 Results of SEM observation (×9500).

5.1.5 Discussions

The results of interference measurement and SEM observations for Mo-CCR shows surface roughness did not change due to neutron irradiation. This results show no blistering or swelling for Mo-CCR.

5.1.6 Conclusion

No affects of neutron irradiation for the surface of Mo-CCR was observed. Thus we may use Mo-CCR as a plasma facing reflector in ITER.

5.1.7 Remaining issues and future plan

None

5. 2 Off-line Irradiation Tests of Gold Coated Mirror in JMTR

Etsuo Ishitsuka, Hisashi Sagawa and Hiroshi Kawamura

5.2.1 Experimental object

As a neutron irradiation test for the secondary mirror, the change of gold coated (Au-evaporated) mirror surface was investigated.

5.2.2 Specimen

(1) Material

Specimens of the structure for gold coated mirror is shown in Fig. 5.2.1. Gold was coated on the Cr under coating film which coated on the low expansion coefficient glass.

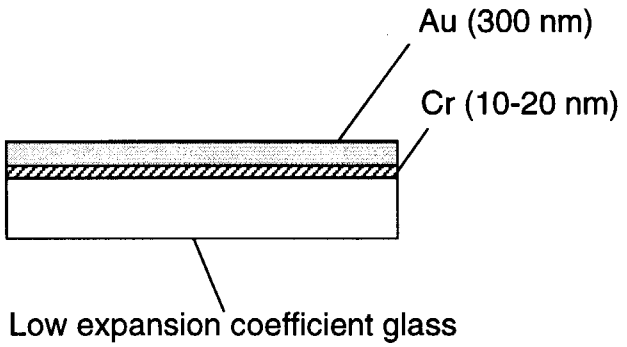

Fig. 5.2.1 Structure of gold coated mirror.

(2) Sample dimension

$\phi 15 \times t1$ mm

5.2.3 Experimental Condition

(1) Irradiation facility

JMTR (Japan Materials Testing Reactor)

(2) Irradiation conditions

Irradiation conditions is shown in Table 5.2.1.

(3) Experimental devices

Two gold coated mirror were irradiated using by inner capsule shown as Fig. 5.2.2.

Table 5.2.1 Irradiation conditions

-Irradiation period	:Mar., 1995 - Jul. 1995
-Irradiation hole	:E-6
-Size of the hole	:ϕ42×750 mm
-Irradiation temperature	:200 °C
-Irradiation environment	:He gas
-Neutron fluence (E>1MeV)	:1.4×10^{20} n/cm^2

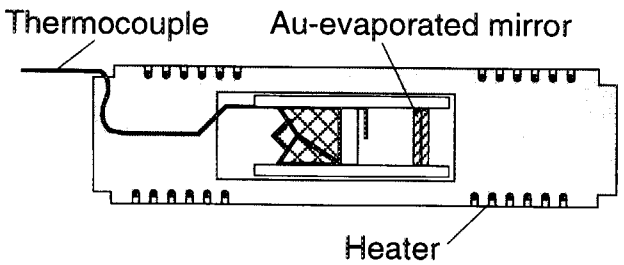

Fig. 5.2.2 Inner capsule for gold coated mirror.

(4) Measurement
Appearance observation was carried out by post irradiation examination.

5.2.4 Experimental results

Appearance photograph of gold coated mirrors are shown in Fig. 5.2.3. Surface of neutron irradiated gold coated mirror became dark.

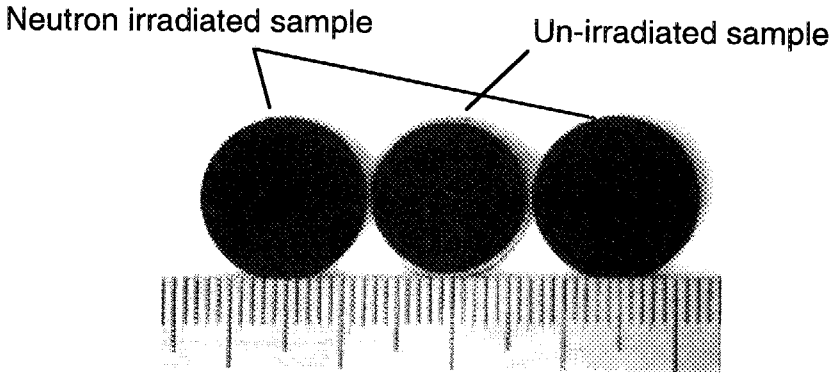

Fig. 5.2.3 Appearance photograph of gold coated mirrors.

5.2.5 Discussions

Surface of neutron irradiated gold coated mirror became dark. This reason was presumably caused by nuclear reaction as follows.

$^{197}Au\ (\ n_t,\ \gamma\ )\ ^{198}Au$ ---------> ^{198}Hg

σ=98.8 burn β^-, $T_{1/2}$=2.694 day

From above calculation, about 10 % Au changed to Hg, and Hg was presumably caused to change the darkened surface.

5.2.6 Conclusion

Some materials which have lager cross section of nuclear reaction should not be use under the neutron irradiated condition. Gold coated mirror is not suitable for the ITER conditions.

5.2.7 Remaining issues and future plan

None

5. 3 In-situ Irradiation Tests of Aluminum Mirror in JMTR

Etsuo Ishitsuka, Tatsuo Sugie, Satoshi Kasai and H. Kawamura

5.3.1 Experimental object

As a neutron irradiation test for the Aluminum secondary mirror, the change of reflectivity by neutron irradiation was investigated.

5.3.2 Specimen

(1) Material

Al-CCR mirror were produced by Optic Mihara Co..

Chemical composition of Aluminum (JIS H 4000) is shown in Table 5.3.1.

Table 5.3.1 Chemical composition of Al-CCR

(wt %)

Al	Mg	Fe	Cr	Si	Mn	Cu	Zn
96.8	2.47	0.26	0.20	0.12	0.08	0.03	0.01

(2) Sample dimension

Sample dimention is about $\phi 52 \times t 55.4$ mm (see Fig. 5.3.1).

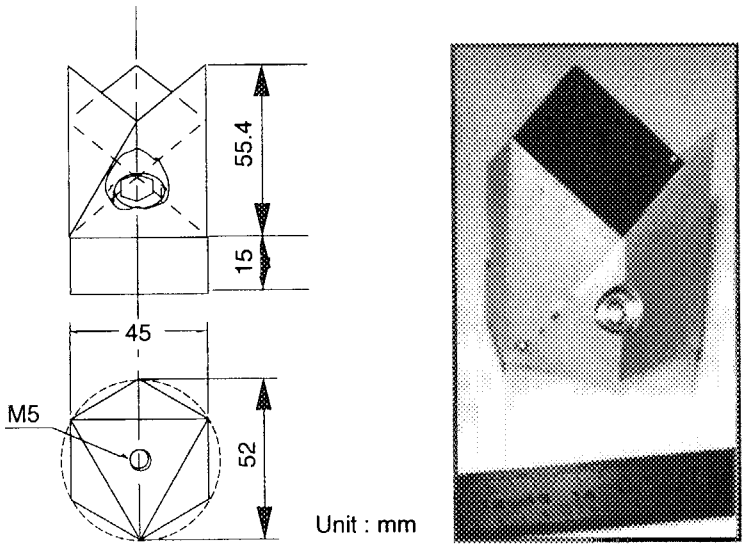

Fig. 5.3.1 Dimension and photograph of Al-CCR.

5.3.3 Experimental Condition

(1) Irradiation facility

JMTR (Japan Materials Testing Reactor)

(2) Irradiation conditions

Irradiation conditions is shown in Table 5.3.2.

Table 5.3.2 Irradiation conditions

-Irradiation period	:Apr., 1998 - May 1998
-Irradiation hole	:H-11
-Size of the hole	:ϕ65×750 mm
-Irradiation temperature	:200 °C
-Irradiation environment	:He gas
-Neutron fluence (E>1MeV)	:1×10^{20} n/cm^2

(3) Experimental devices

In-situ reflection spectrum measuring capsule with two-axis driving device is shown in Fig. 5.3.2. Mo-CCR is set up the upper of capsule as a reference. Al-CCR as a irradiation specimen is set up the lower of capsule. Photograph of two-axis driving device is shown in Fig. 5.3.3.

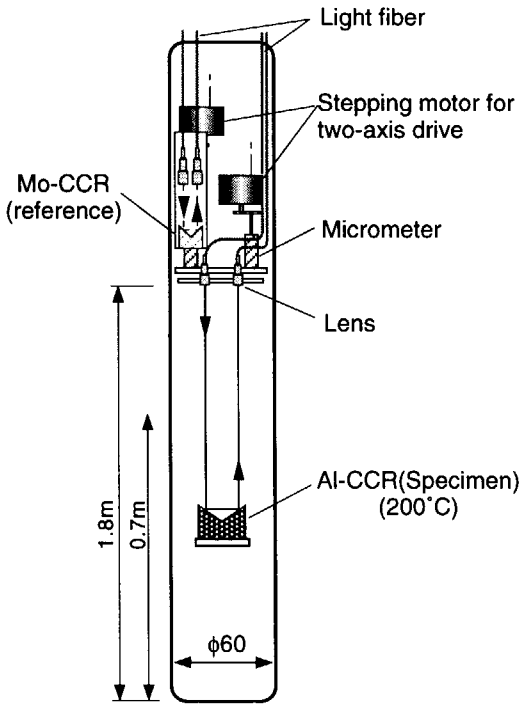

Fig. 5.3.2 In-situ reflection spectrum measuring capsule.

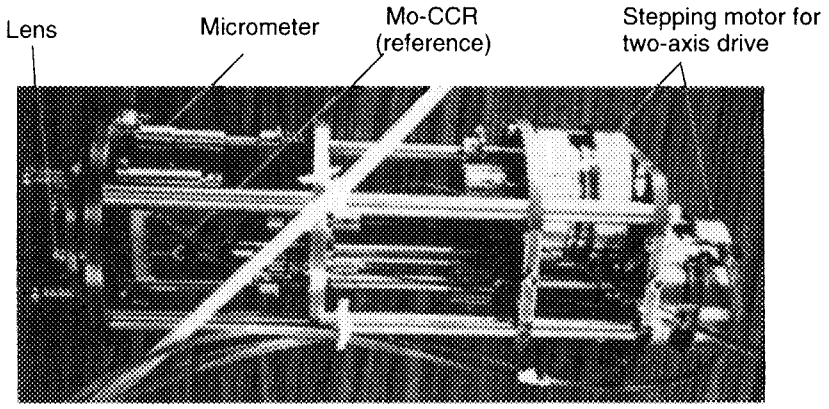

Fig. 5.3.3 Photograph of two-axis driving device.

(4) Measurement

White light source (AQ-4303B, Ando Electric CO., LTD.) and optical spectrum analyzer (AQ-6315, Ando Electric CO., LTD.) were used as measurement equipment.

5.3.4 Experimental results

Results is shown in Fig. 5.3.4. Reflectivity for Al-CCR decreased from low fluence (reactor start up). However, this decreasing is presumably caused by vibration of Al-CCR. Oscillated light intensity at 660 nm is shown in Fig. 5.3.5. Oscillation of the light intensity was presumably caused by the trouble of connecting system for Al-CCR which caused by unexpected thermal expansion from capsule structure. After all, the change of reflectivity for Al-CCR by neutron irradiation could not observed (see the line of shut down, induced loss at short wavelength might be caused to induced loss of fiber).

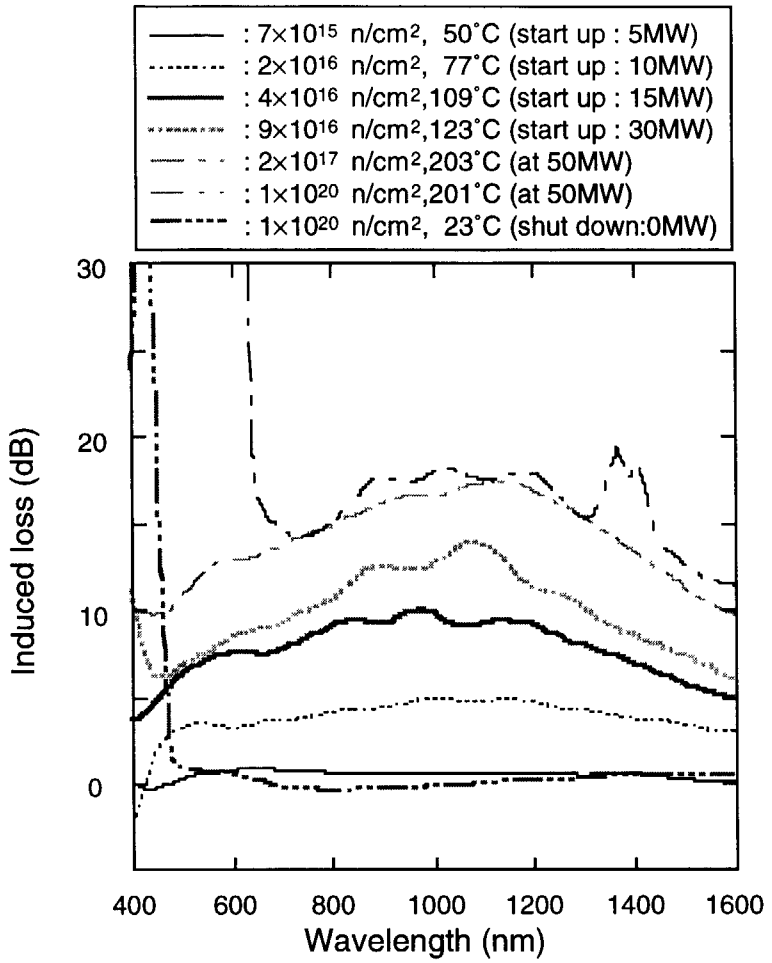

Fig. 5.3.4 Induced loss of reflectivity for Al-CCR.

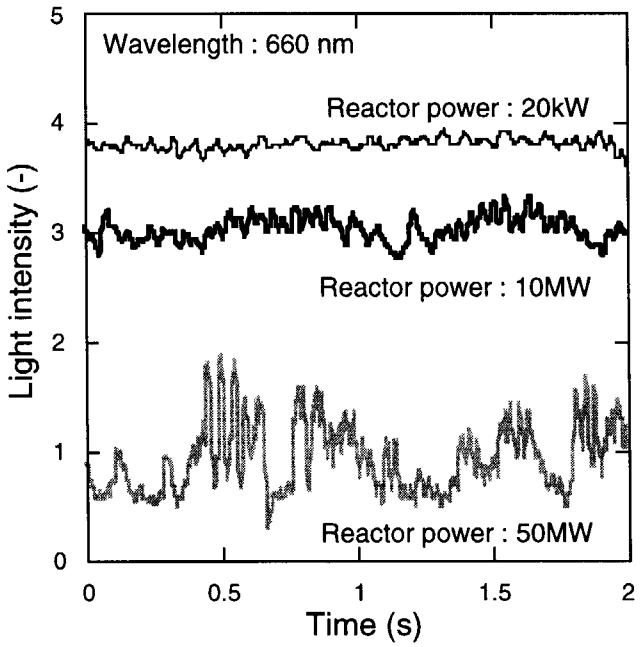

Fig. 5.3.5 Vibulation of Al-CCR at reactor start up.

5.3.5 Discussions

Main nuclear reaction of ^{27}Al by neutron is as follows.

^{27}Al (n, γ) ^{28}Al , ^{28}Al ---- $\beta^-(t_{1/2}=2.241min)$ ---> ^{28}Si

By the ORIGEN code, amount of generation rate for ^{28}Si during reactor operation are about 1/1000 of Al atom. This amount is very small, and effect on reflectivity by neutron irradiation might be negligible.

5.3.6 Conclusion

Change of reflectivity for Al-CCR by neutron irradiation could not observed. Utilization of Al as a optical mirror maybe no problem in the neutron fluence up to 1×10^{20} n/cm^2 (E>1MeV).

5.3.7 Remaing issues and future plan

None.

6. Bolometer

6.1 ^{60}Co-gamma Irradiation Test on Polyimide Substrate Bolometer

Takeo Nishitani, Tatsuo Sugie, Yosuke Morita and Satoshi Kasai

6.1.1 Experimental object

The gold resister bolometer with polyimide substrate[6.1.1] was developed for the radiation loss measurements in JT-60 and JT-60U. Polyimide substrate is not so resistive to high temperature and neutron irradiation that it could not be used in ITER. Main object of this irradiation test if to confirm the bolometer performance in the ITER relevant radiation environment. In ITER, nuclear heating is much larger than that from plasma radiation in bolometers. We have to confirm whether the bolometer can measure the plasma radiation eliminating the nuclear heating. Other objects are to establish the *in-situ* irradiation test technique for bolometers and to find the operation limit of the polyimide substrate bolometer in the gamma radiation.

6.1.2 Experimental conditions

(1) Material

JT-60 type gold resistor bolometer is irradiated. A schematic diagram of the bolometer is shown in Fig. 6.1.1. The sensor consists of three layers. A 11 × 16 mm^2, 5-mm-thick gold absorber is laminated on the front of 7-μm-thick polyimide sheet. A 0.1-μm-thick gold resistor is laminated on the back of the polyimide sheet. The manufacturing process of the resistor pattern is photo etching technique. The sensor foil is mounted on the stainless-steel frame. The bolometer is composed of two identical sensors. One is mounted behind the other via 1-mm-thick ceramics sheet. Front sensor faces to plasma. The backside sensor is shielded by front one and the ceramics sheet, so that it operates as a reference sensor to compensate the change of room temperature.

(2) Irradiation facility

The bolometer was irradiated in the ^{60}Co irradiation facility in JAERI Takasaki. The experimental set-up is shown in Fig.6.1.2. The ^{60}Co irradiation with the intensity of 115 kCi (4286 TBq) is stored in a water pool. The source is lifted into the irradiation room. The irradiation room is shielded with 1.3 m-thick heavy concrete walls.

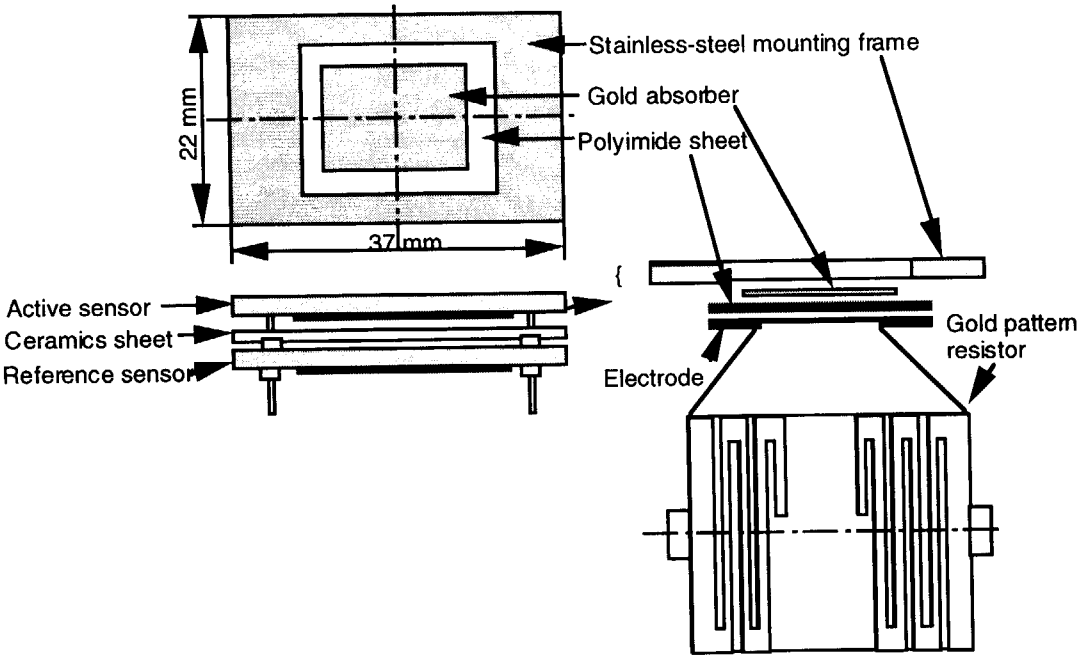

Fig. 6.1.1 Schematics of the JT-60 type gold resistor bolometer with polyimide substrate.

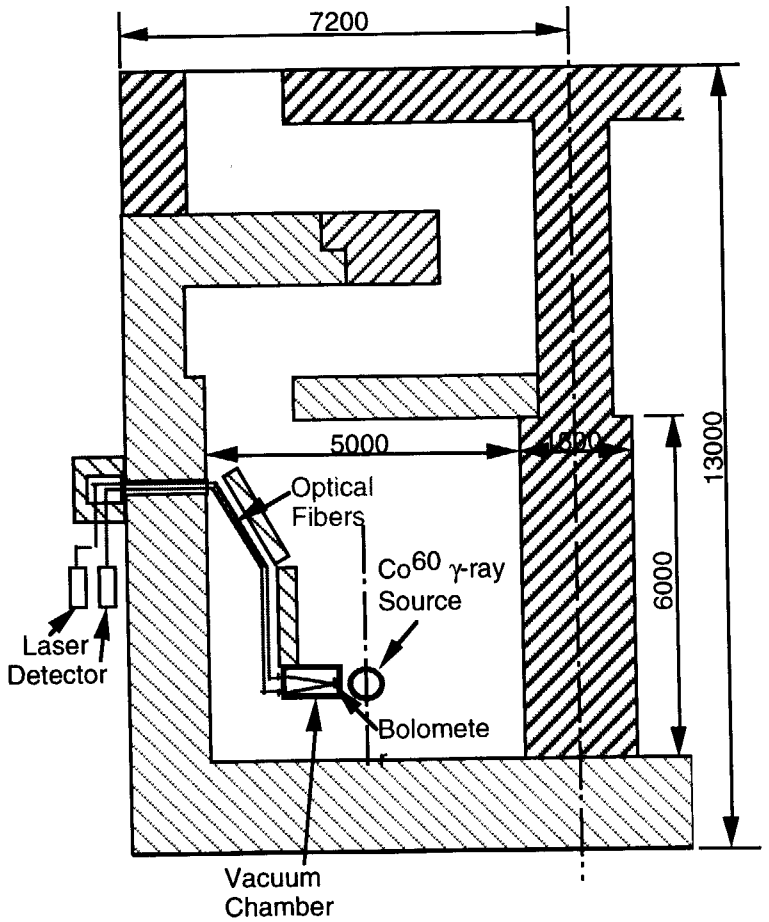

Fig. 6.1.2 Schematics of ^{60}Co irradiation facility used for the bolometer irradiation test.

(3) Irradiation conditions

Gamma dose rate at the bolometer position is evaluated to be 1.6×10^6 R/h (~4 Gy/s) by the gamma dose meter. Temperature of the bolometer is ~40°C which is room temperature and temperature rise due to gamma heating. The bolometer is mounted in a vacuum chamber. The chamber is pumped out to be $\sim 10^{-5}$ Torr ($\sim 10^{-3}$ Pa) by the turbo-molecular pump.

(4) Experimental devices

Diagram of the experimental set-up is shown in Fig.6.1.3. Pulsed Alexandrite laser was lunched on the bolometer surface via fiber optics. The wavelength is 752 nm and the maximum output is 2 J/pulse. The laser power was reduced by ND filters to prevent the damage of the fiber inlet. The power of the input laser pulse is monitored with a power meter via a beam splitter (half mirror). The loss of the laser light due to damages of window and fiber optics was evaluated by changing the bolometer to mirror routinely, typically one a month. We found that those losses were not so important. The laser and optical elements were set up on a optical bench with air insulators.

The transient response of the bolometer signal for pulsed laser light was recorded with a digital oscilloscope. Also the resistance are measured with digital ohm-meters. The measurement devices are listed in the Table 6.1.1.

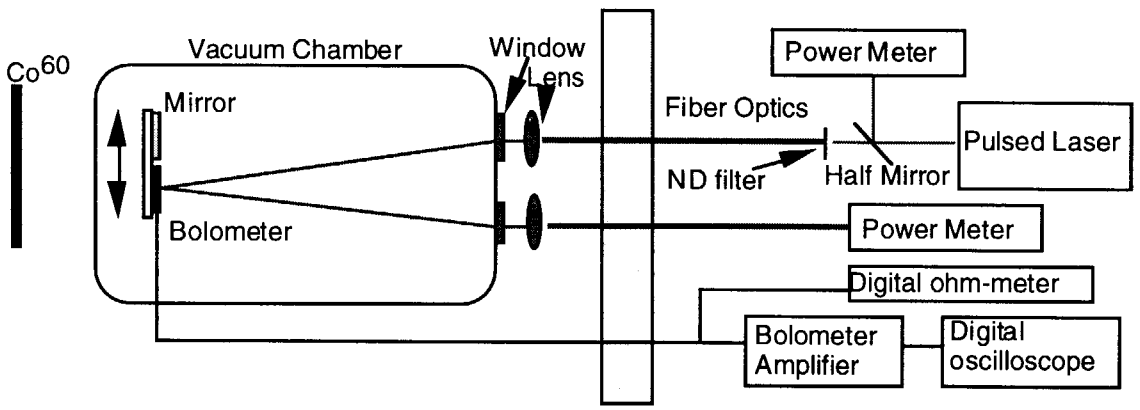

Fig. 6.1.3 Experimental set-up for the gamma irradiation test of the bolometer.

Table 6.1.1 Table of measurement devices for the bolometer irradiation test.

Item	Type
Alexandrite laser	Cynosure,Inc: CRD-1
Power meter	Scientech: MD 10
Bolometer amplifier	Toshiba: HNE 942
Digital ohm-meter	Tektronix: DM 2510G
Digital oscilloscope	Tektronix: TDS 524A

(5) Measurement

The resistance of the bolometer was measured. The in-situ measurement of the bolometer sensitivity for the pulsed laser was carried out in the Gamma-ray radiation environment. The wave form of the laser pulse is shown in Fig. 6.1.4. The pulse width is about 0.5 ms. The response of the bolometer for this laser pulse is shown in Fig.6.1.5. The sensitivity of the bolometer is derived from the set-up voltage in this waveform. The reflectivity of the bolometer surface was measured from the ratio of the reflected laser power by the metal mirror and bolometer. Here the reflectivity of the metal mirror was assumed to be constant during this irradiation experiment. So we confirmed this bolometer worked well under the gamma irradiation condition.

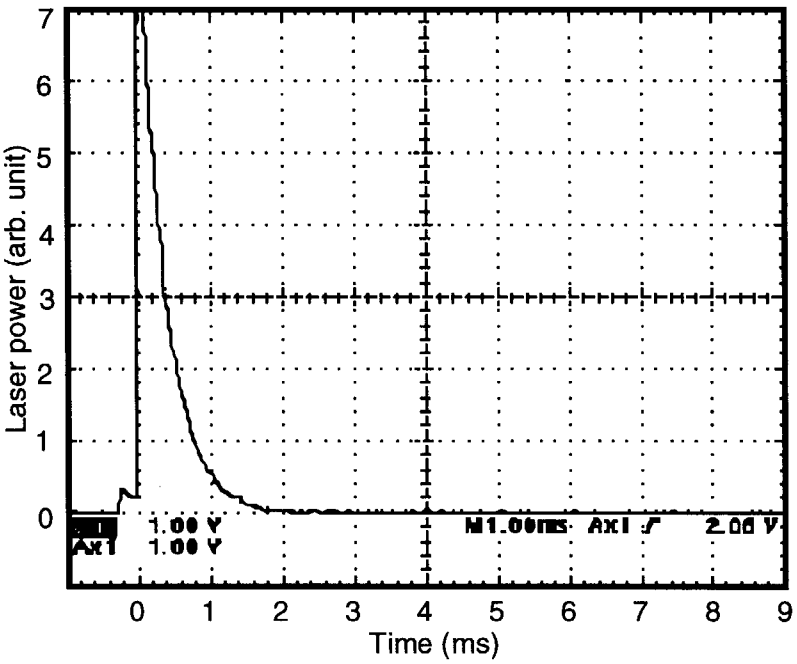

Fig. 6.1.4 Waveform of the Alexandrite laser pulse.

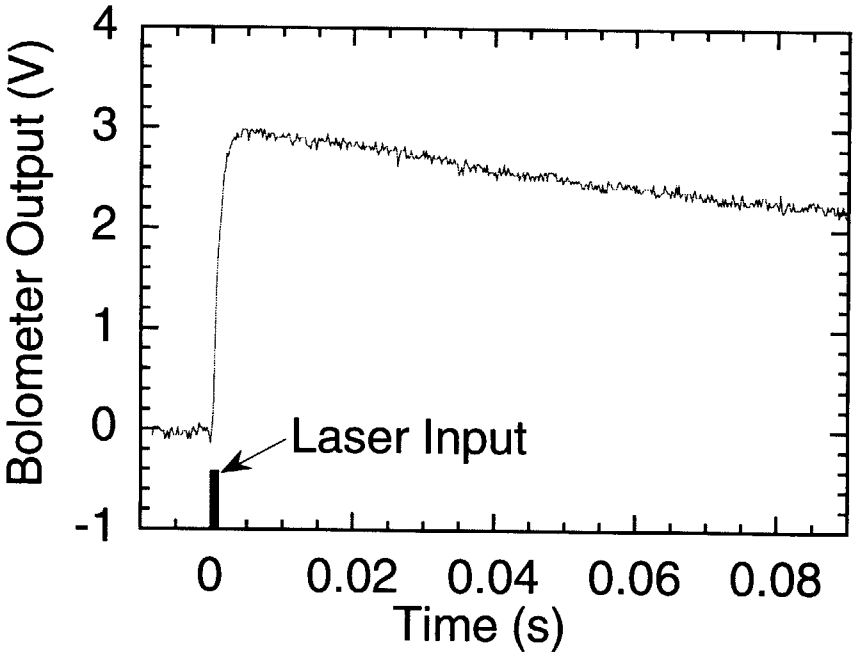

Fig. 6.1.5 Response waveform of the bolometer for the laser pulse input.

6.1.3 Experimental results

Figure 6.1.6 shows the bolometer resistivity as a function of the gamma dose. The bolometer resistivity decreased slightly until 100 MGy. The change is -0.8%. After 100 MGy up to 220 MGy, the resistivity is almost constant. The reason the resistivity change is still open.

Figures 6.1.8 shows the reflectivity of the bolometer surface and the bolometer sensitivity as a function of the gamma dose. We had a trouble of the slide mechanism of the bolometer and mirror at the dose of 170 MGy. Within the dose, there were no significant change in the reflectivity of the bolometer surface. Also significant change of the sensitivity has not been observed for the gamma dose up to 220 MGy as shown in Fig.6.1.9.

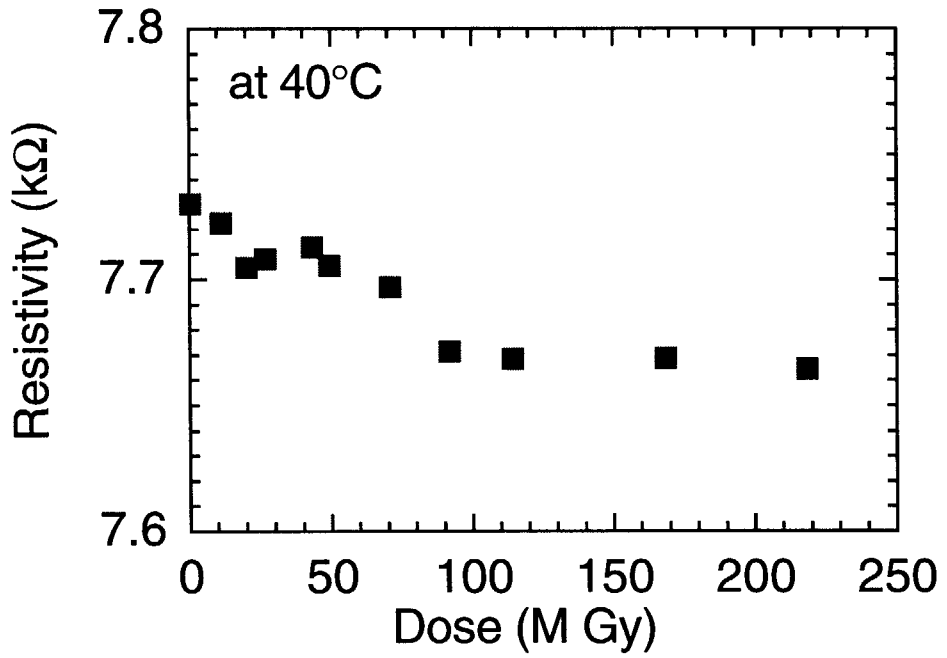

Fig. 6.1.6 Resistance of the bolometer as a function of the gamma dose.

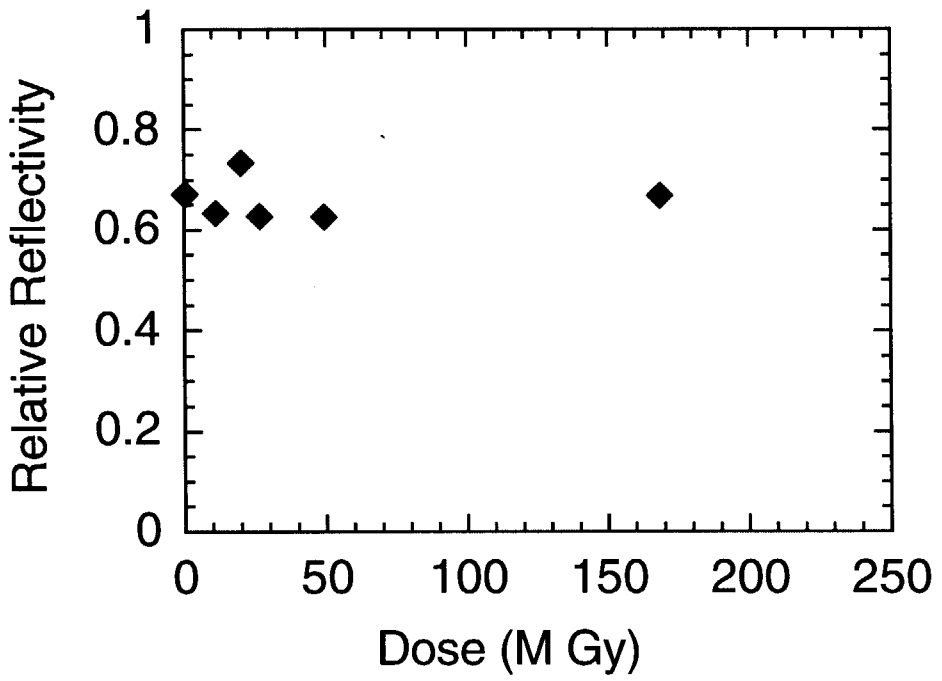

Fig. 6.1.8 Reflectivity of the bolometer as a function of the gamma dose.

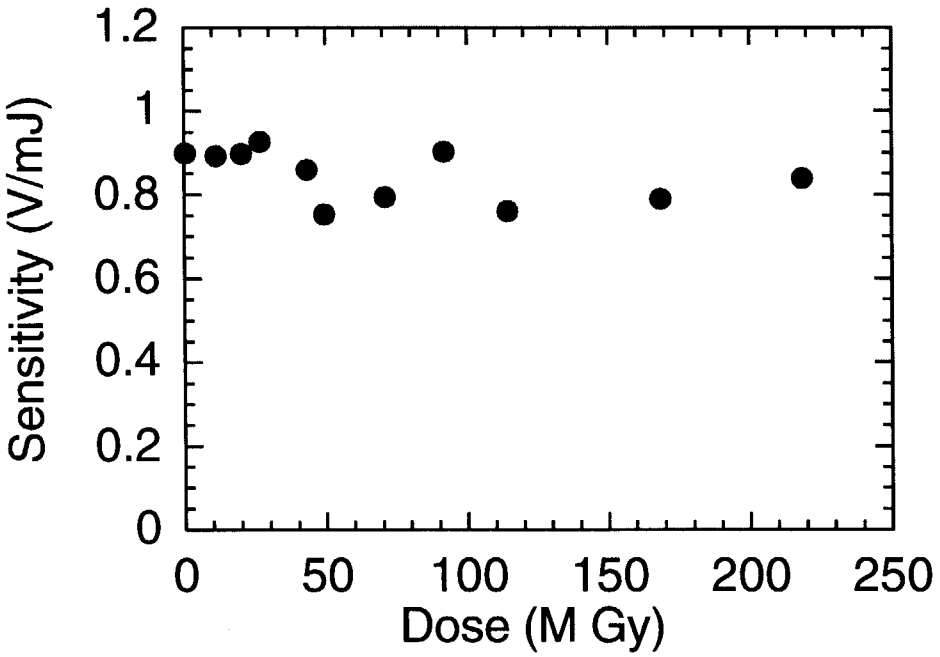

Fig. 6.1.9 Bolometer sensitivity as a function of the gamma dose.

6.1.4 Conclusion

The in-situ test technique for bolometers was established for gamma irradiation. We confirmed the polyimide substrate bolometer operated well under the gamma irradiation condition which is almost equivalent to gamma dose rate on the bolometer location (in the gap between adjacent blanket modules) in ITER.

References

[6.1.1] T. Nishitani, K. Nagashima, et al., Rev. Sci. Instrum. 59 (1988) 1866.

6.2 ^{60}Co-gamma Irradiation Test on Ceramics Substrate Bolometer

Takeo Nishitani, Yosuke Morita and Satoshi Kasai

6.2.1 Experimental object

We confirmed the performance of the polyimide substrate bolometer under the gamma irradiation as described in Section 6.1. However the bolometer could not be used in ITER due to the high temperature circumstances. So we propose the ceramic substrate bolometer for ITER. As one of the candidate, we developed the AlN substrate bolometer. Here we carried out the irradiation test on the bolometer to get the basic characteristics under the ITER relevant radiation environment.

6.2.2 Experimental conditions

(1) Material

Material of the bolometer substrate should have high thermal conductivity, high electric resistivity and mechanical robustness. Diamond, Al_2O_3, SiN, and AlN have relatively high thermal conductivity among ceramics. Diamond has the highest thermal conductivity, but may be changed to graphite under heavy neutron irradiation. Thin foil of is very fragile to use as the bolometer substrate. Here we employed AlN as the bolometer substrate to investigate the characteristics in radiation condition.

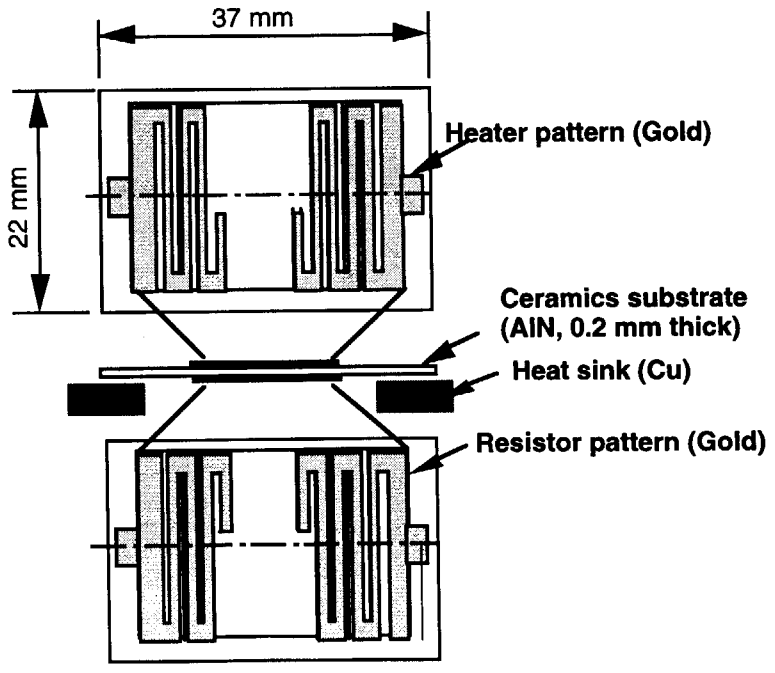

Fig. 6.2.1 Schematics of the AlN substrate bolometer with gold resistor pattern.

A schematic diagram of the AlN substrate bolometer is shown in Fig. 6.2.1. The sensor consists of three layers. A 0.1-μm-thick gold resistor pattern is laminated on the both side of AlN substrate with 0.2-mm thickness. The substrate is relatively thick to investigate the characteristics. The manufacturing process of the resistor pattern is photo etching technique. One side gold resistor is a bolometer sensor, and another is a heater to simulate the plasma radiation in the irradiation test.

(2) Irradiation facility

See Section 6.1.1 (2)

(3) Irradiation conditions

See Section 6.1.1 (3)

(4) Experimental devices

Diagram of the experimental set-up is shown in Fig.6.2.2. The bolometer is mounted in the vacuum vessel. The heater is turned on by step input voltage of ~12V from the pulse generator. The response of the bolometer sensor is measured by a oscilloscope via a bolometer amplifier. The resistivity of the gold pattern is monitored by a digital ohm-meter. Those equipment is same as Section 6.1 (See Table 6.1.1).

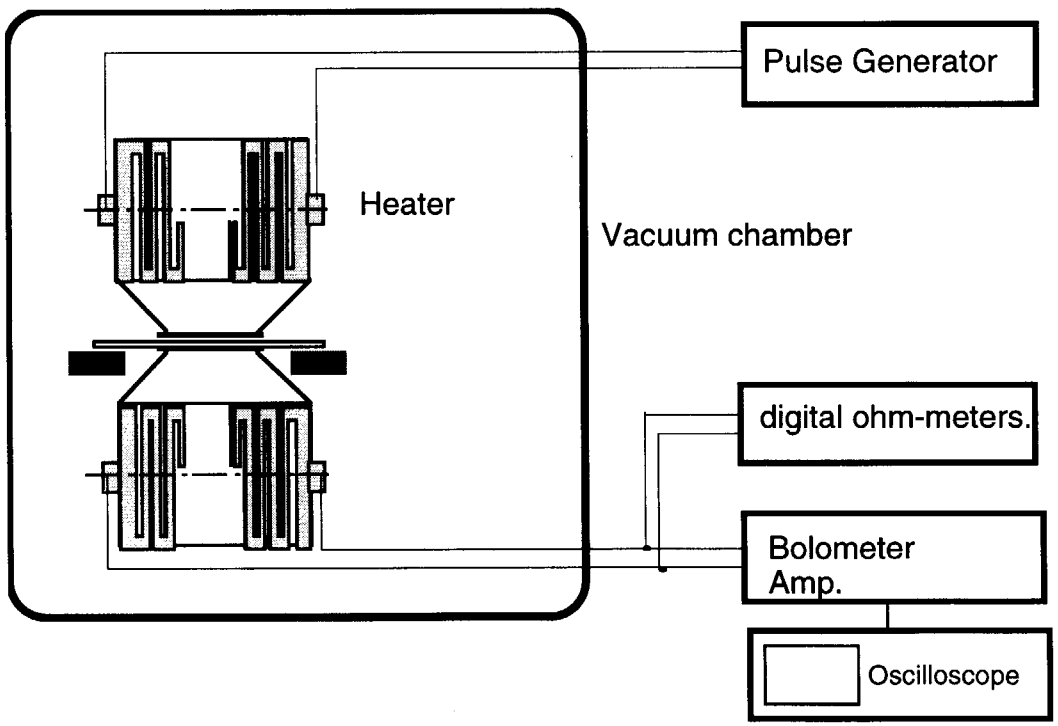

Fig. 6.2.2 Experimental set-up for the gamma irradiation test of the AlN substrate bolometer.

(5) Measurement

Before the irradiation experiment, the temperature dependence of the resistance and the sensitivity of the bolometer are measured in the vacuum vessel with baking heater. After that, the in-situ measurement of the bolometer resistivity and sensitivity for the heat input was carried out in the Gamma-ray radiation environment. The typical response of the bolometer for step heat input measured before irradiation in is shown in Fig.6.2.3. The spikes at the heater turn-on and -off seem to be due the high frequency component passing through the substrate from the heater to sensor. From this waveform, the sensitivity of 0.10 V/mW and cooling time of 1.27 sec were evaluated.

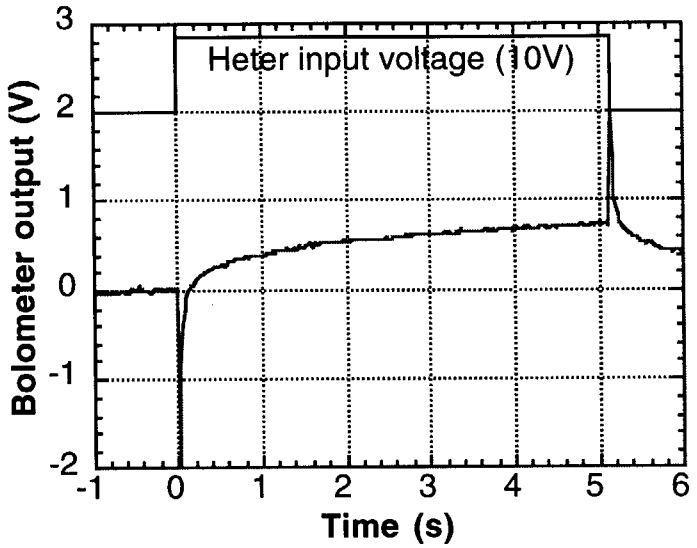

Fig. 6.2.3 Typical waveform of the bolometer output for the step input on the heater.

6.2.3 Experimental results

(1) Cold test of the bolometer characteristics before irradiation

Figure 6.2.4 shows the bolometer resistivity as a function of the temperature. The bolometer resistivity has good linearity for the temperature.

Figure 6.2.5 shows the bolometer sensitivity as a function of the temperature. The bolometer resistivity has good linearity for the temperature. The sensitivity decreases about 5% in high temperature higher than 120°C.

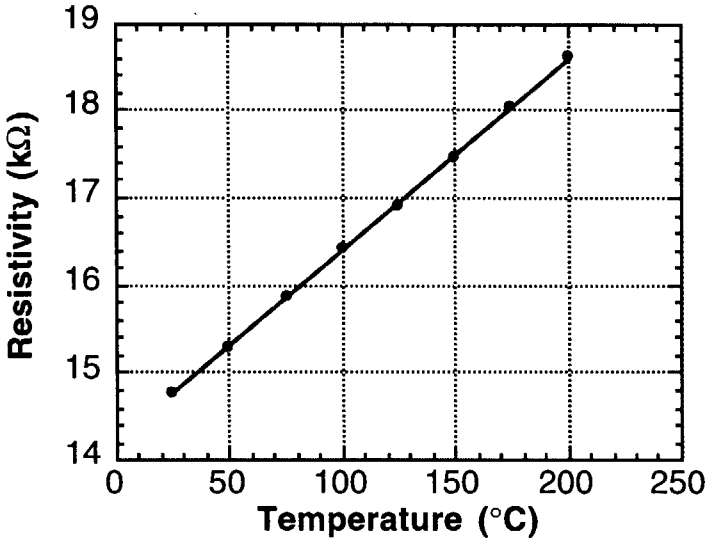

Fig. 6.2.4 Bolometer resistance as a function of the temperature.

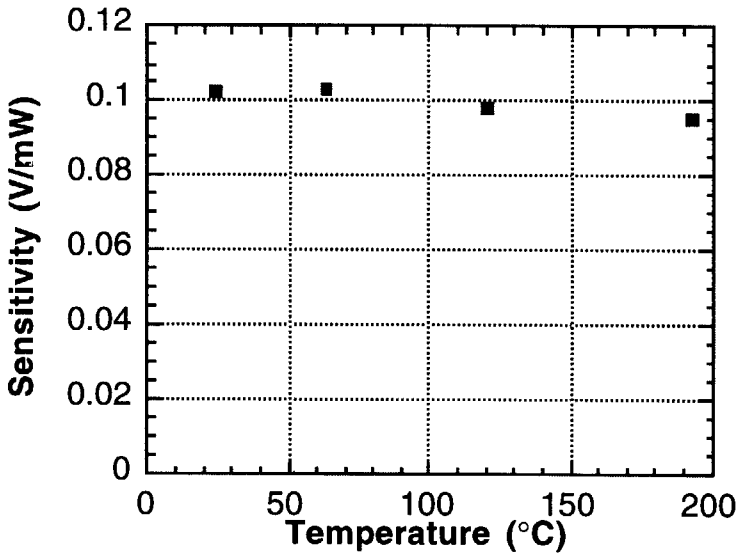

Fig. 6.2.5 Bolometer sensitivity as a function of the temperature.

(2) Gamma irradiation test

Figure 6.2.6 shows the response of the bolometer for the step input on the heater in the gamma irradiation. There is not significant deference among those response waveforms. We derived bolometer sensitivities from those waveforms. Figure 6.2.7 shows the bolometer resistivity as a function of the gamma dose. The bolometer resistivity decreased slightly until 10 MGy. The change is -0.3%. After 10

MGy up to 30 MGy, the resistivity is almost constant. The reason the resistivity change is still open. One of the possible explanation is the resistivity degradation due to the surface contamination.

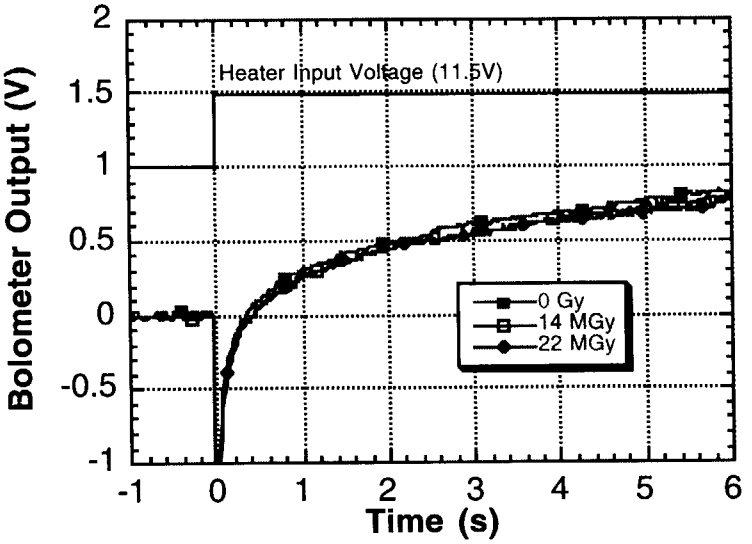

Fig. 6.2.6 Response of the bolometer for the step input on the heater in the gamma irradiation.

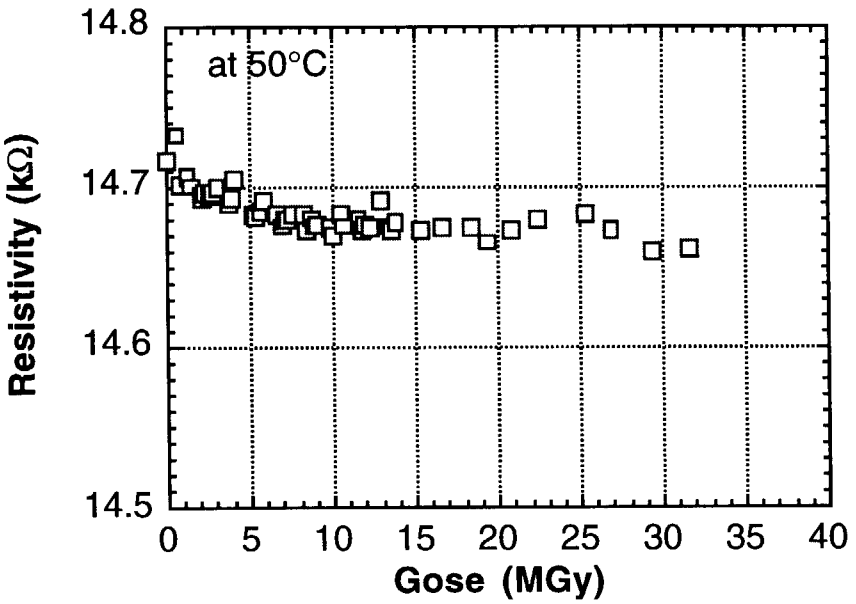

Fig. 6.2.7 Resistivity of the AlN substrate bolometer as a function of the gamma dose.

Figures 6.2.8 shows the sensitivity of the AlN substrate bolometer as a function of the gamma dose. Significant change of the sensitivity has not been observed for the gamma dose up to 22 MGy.

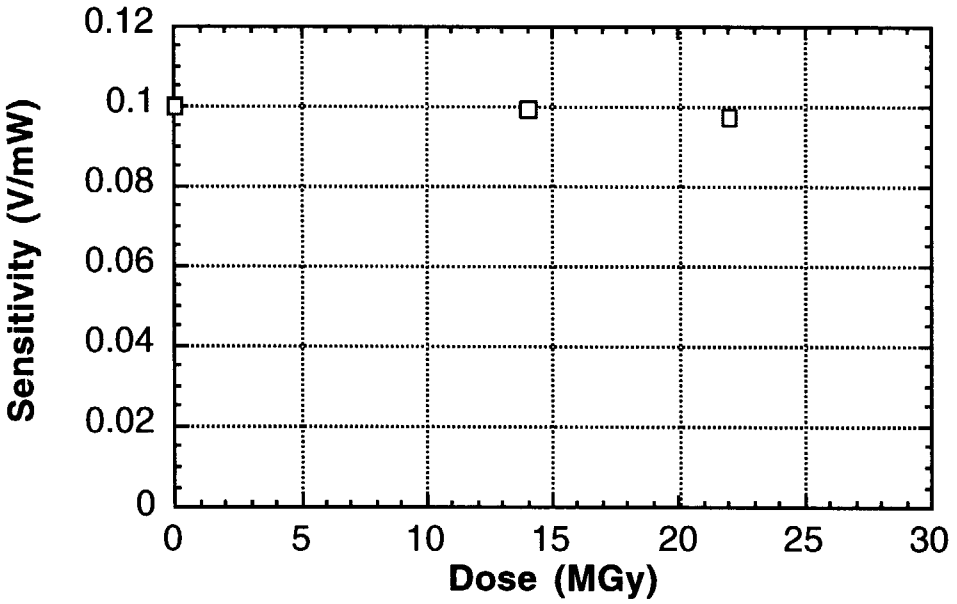

Fig. 6.2.8 Sensitivity of the AlN substrate bolometer as a function of the gamma dose.

6.2.4 Conclusion

A ceramics substrate bolometer has been developed for one of the candidate of the ITER bolometer. We carried out the irradiation test of the bolometer under the gamma irradiation. Significant change of the bolometer characteristics has not been observed for the gamma dose up to 22 MGy.

6.3 Irradiation Test on Ceramics Substrate Bolometer in JMTR

Takeo Nishitani, Hisashi Sagawa and Etsuo Ishitsuka

6.3.1 Experimental object

We carried out the irradiation test on the AlN substrate bolometer to get the basic characteristcs under the neutron radiation with ITER relevant neutron flux and fluence.

6.3.2 Experimental conditions

(1) Material
See Section 6.2.2 (1)

(2) Irradiation facility
JMTR in JAERI Oarai.

(3) Irradiation conditions
- Irradiation period : January 1998 - April 1998
- Neutron flux (E> 1MeV) : 9.3×10^{12} n/cm^2•s
- Neutron fluence (E> 1 MeV) : 6.0×10^{19} n/cm^2
- Irradiation environment : He gas
- Irradiation temperature : 140 °C

(4) Experimental devices

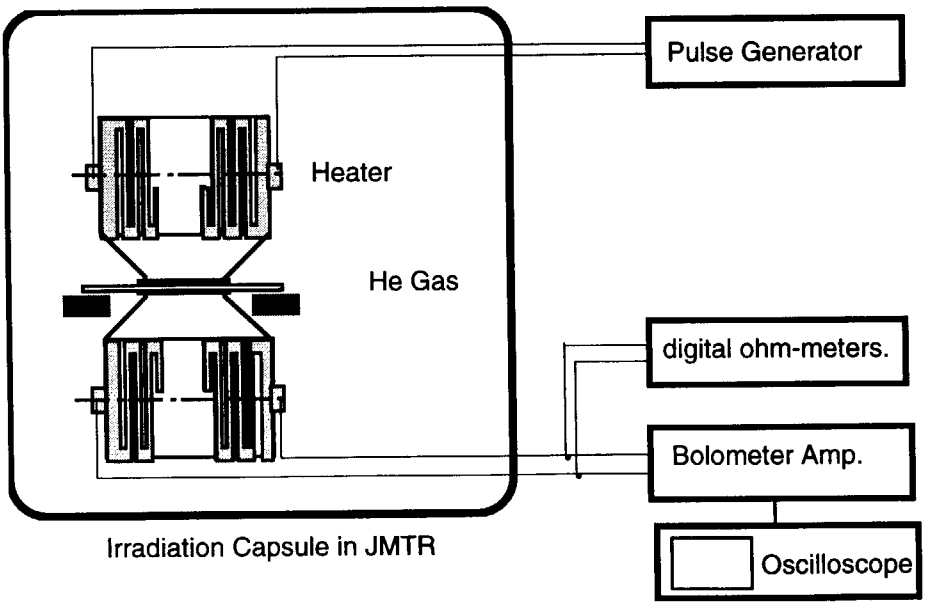

Fig. 6.3.1 Experimental set-up for the JMTR irradiation test of the AlN substrate bolometer.

Diagram of the experimental set-up is shown in Fig.6.3.1. The bolometer is mounted in the irradiation capsule filled with He gas in order to cool the nuclear heat. The heater is turned on by bipolar step input voltage of ± 5.7 V with 1 kHz frequency from the pulse generator. The response of the bolometer sensor is measured by a oscilloscope via a bolometer amplifier with a low pass filter to reject the ripple of the heater input. The temperature of the bolometer is monitored by the thermo-couple embedded in the heat sink. The resistivity of the gold pattern is measured by a digital ohm-meter. The outlet cables from the irradiation capsule are MI cables. Those equipment is same as Section 6.1 (See Table 6.1.1).

(5) Measurement

The typical response of the bolometer for bipolar heat input measured before irradiation in JMTR is shown in Fig.6.3.2. The waveform is rather noisy comparing with that of the gamma irradiation test. From this waveform, the sensitivity of 0.23V/mW and cooling time of 1.41 sec were evaluated. During the JMTR operation, the noise is so enhanced that we could not evaluate the bolometer characteristics with sufficient accuracy from the waveforms. We should use twisted pair MI cable from the bolometer to the electronics in order to reduce the noise.

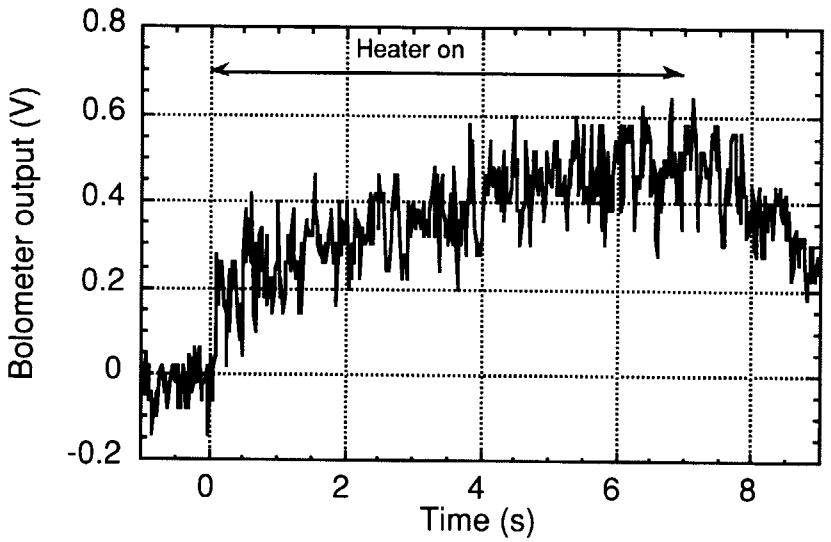

Fig. 6.3.2 Typical waveform of the bolometer for bipolar heat input with 1 kHz frequency measured before irradiation in JMTR.

6.3.3 Experimental results

Figure 6.3.3 shows the bolometer resistance as a function of the fast neutron fluence whose energy is larger than 1 MeV. The bolometer resistivity increased with the fluence up to 22 % for the neutron fluence of 4.1×10^{19} n/cm^2, which is ~0.5 of that in the gap of shielding blankets during the ITER life time where bolometers will be installed. The change of the resistance is much larger than that of the bulk material.

Figure 6.3.4 shows the substrate resistance as a function of the fast neutron flux whose energy is larger than 1 MeV. Before irradiation, the resistance is lager than the measurement range of the Ohm mater (~25 MΩ). The resistance decreased dramatically in the neutron flux larger than ~1 × 10^{12} n/cm^2•s. The change of the resistance may be due to RIC of the substrate. In the ITER 1st wall, ceramics conductivity is estimated to be ~1 × 10^{-6} S/m. The neutron flux in the capsule (~1 × 10^{13} n/cm^2•s) is ~ 0.1 of that in the ITER 1st wall, so that the conductivity is estimated to be ~1 × 10^{-7} S/m. From this value, the resistance of the AlN substrate is estimated to be ~2 MW, which is consistent with measured resistance.

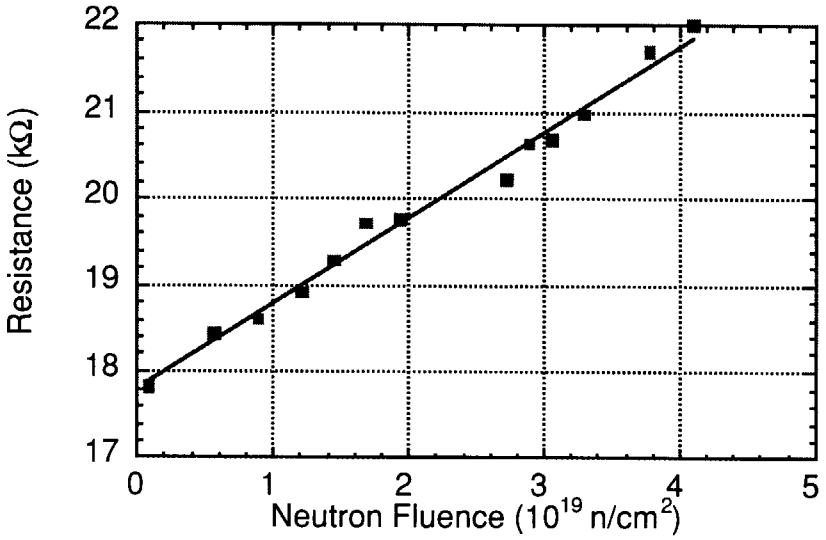

Fig. 6.3.3 Bolometer resistance as a function of the neutron fluence (E > 1 MeV).

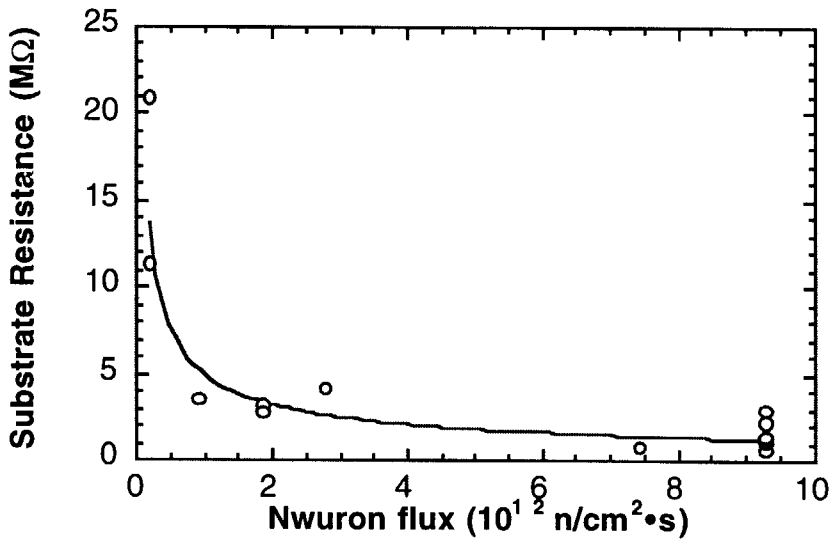

Fig. 6.3.4 Substrate resistance as a function of the neutron flux (E > 1 MeV).

As described in Section 6.3.2 (5), bolometer characteristics could dot evaluated from the bolometer response for the heater input. The bolometer sensitivity is proportional to the temperature coefficient of the resister pattern. So the temperature dependence of the resister pattern was measured as shown in Fig. 6.3.5. The temperature coefficient decreased 15% at the beginning of the 3rd cycle where the total fluence is ~4 × 10^{19} n/cm^2, which indicates that the sensitivity decreased 15% form the initial value.

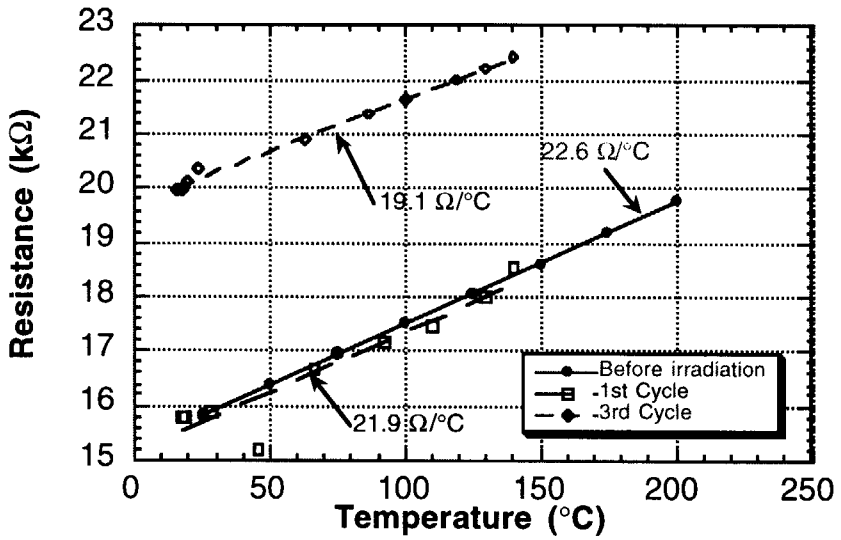

Fig. 6.3.5 Temperature dependence of the resister pattern.

6.3.4 Conclusion

Strong increase in the bolometer resistance has been observed, which suggests the necessity of the in-situ calibration of the bolometer in ITER. Bolometer response against the heater input could not be measured due to the noise. The temperature coefficient measurement of the bolometer resistance shows 15% decrease in the sensitivity at the fast neutron fluence of ~4 × 10^{19} n/cm^2.

6.3.5 Remaining issues and future plan

In-situ characteristics the bolometer such as the cooling time, heat conductivity of the substrate, etc. has not been measured in this experiment. The thermal and mechanical characteristics of the substrate should be investigated. Off line irradiation of the substrate using "rabbit" is easiest way to do this. Thickness of the AlN substrate used here is too thick for the real bolometer. Much more thin substrate of ~20 μm should be developed.

7. Magnetic Probe

7.1 In-situ irradiation test on a magnetic probe in JMTR

Hisashi Sagawa, Masaru Nakamichi and Hiroshi Kawamura

7.1.1 Experimental object

We carried out the irradiation test on the magnetic probe made of MI cable to get the electric characteristics under the neutron radiation with ITER relevant neutron flux and fluence.

7.1.2 Experimental conditions

(1) Material

The coil of the magnetic probe was made of 1.6 mm MI-cable, which has 280 turns around a ceramic bobbin. The sheath material and core material of the MI-cable were SS316 and oxygen free copper, respectively. The insulation material of MI-cable was MgO. The inner diameter and length of the coil were 9.0 mm and 50 mm, respectively. Helium gas was filled up in the probe outer container to exhaust heat of inner parts and to avoid oxidation, but the inner pressure of the helium gas could be changed to control irradiation temperature of the coil. Moreover, a chromel-constantan (CRC) thermocouple was installed between the ceramic bobbin and the coil to measure the coil temperature.

(2) Irradiation facility

JMTR in JAERI Oarai.

(3) Irradiation conditions

The magnetic probe was irradiated in the JMTR (Japan Materials Testing Reactor). The fast neutron flux (>1 MeV) and thermal neutron flux (<0.63 eV) were 9.3×10^{12} n/cm^2/s and 1.2×10^{14} n/cm^2/s, respectively. The fast neutron fluence and thermal neutron fluence were 3.9×10^{19} n/cm^2 and 5.0×10^{20} n/cm^2, respectively. The γ-ray heating rate of the probe was 1.5 W/g. The base irradiation temperature at JMTR 50MW operation was about 400°C.

(4) Measurement

As items to be measured, the inductance of the magnetic probe and insulation resistance and electric motive force (RIEMF) between sheath and core of the MI-cable were measured during reactor power-up and steady state operation. An impedance analyzer (HEWLETT PACKARD 4194A) was used to measure the inductance, a high resistance meter (HEWLETT PACKARD 4329A) was used to measure the insulation resistance and the electrometer (KEITHLEY 614) was used to measure RIEMF.

7.1.3 Experimental results

(1) Insulation resistance

The measurement result of the insulation resistance between sheath and core of MI-cable was shown in Fig.7.1.1. The insulation resistance which was in the order of about 10^{10} W during neutron non-irradiation decreased, but it was still kept in about 6×10^{6} W even under neutron irradiation with the fast neutron fluence of 4×10^{19} n/cm^2. Furthermore, the significant RIED of the MI-cable insulator was not observed up to 4×10^{19} n/cm^2.

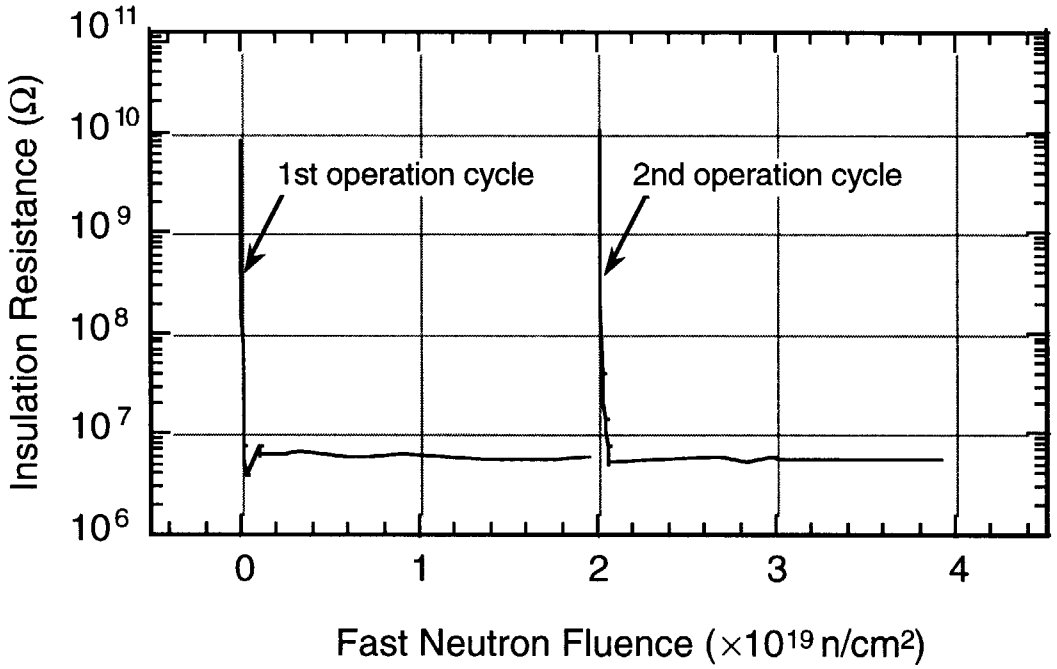

Fig.7.1.1 Effect of neutron fluence on insulation resistance of magnetic probe.

(2) Inductance

The measurement results of the inductance of the magnetic probe were shown in Fig.7.1.2 and Fig.7.1.3. The inductance increased with irradiation temperature rose as shown in Fig.7.1..2. However, the inductance at rated reactor power was constant as shown in Fig7.1.3, and the reproducibility of inductance was still maintained up to 4×10^{19} n/cm^2. Moreover, the measurement results of the inductance is shown in Fig. 7.1.4 when the irradiation temperature of the coil was changed up to 600 °C at the fast neutron fluences of 2.0×10^{19} n/cm^2 and 3.5×10^{19} n/cm^2. The inductance also increased with irradiation temperature rose.

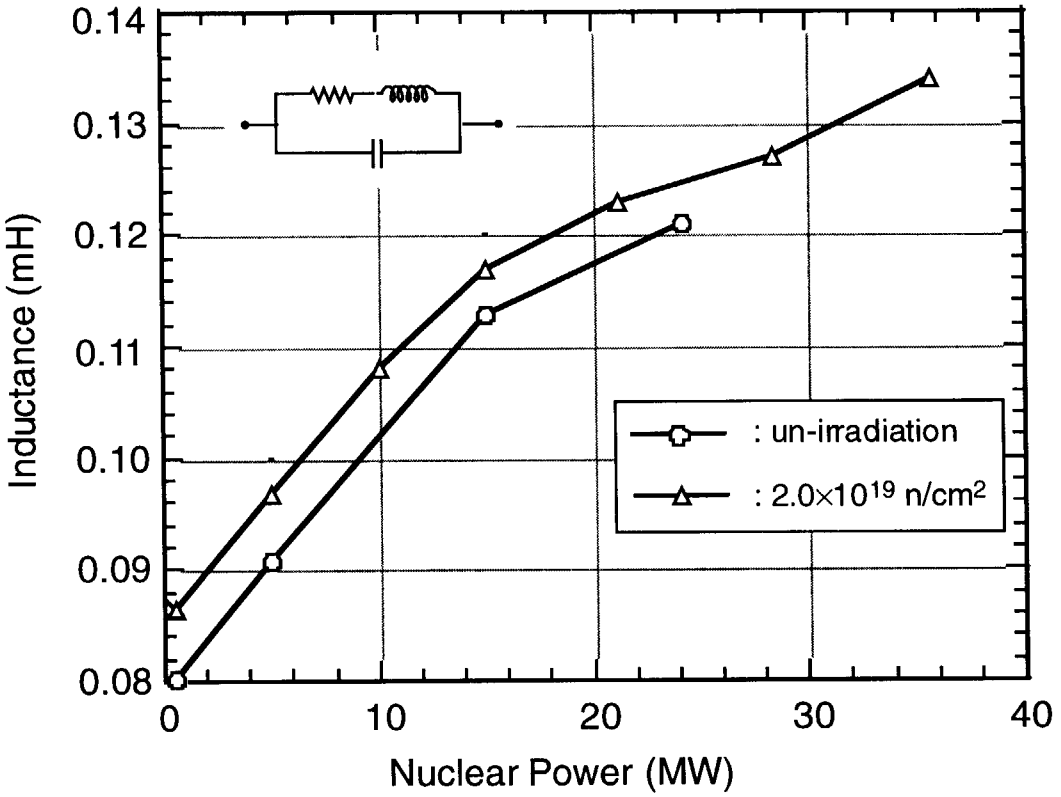

Fig.7.1.2 Inductance of magnetic probe during JMTR power up.

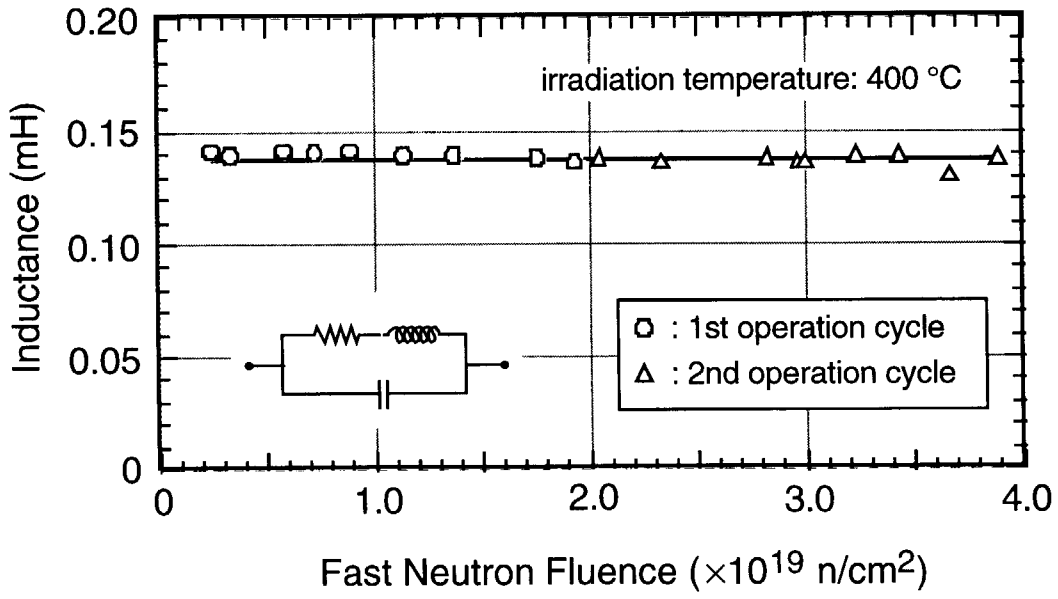

Fig. 7.1.3 Effect of neutron fluence on inductance of magnetic probe at rated reactor power.

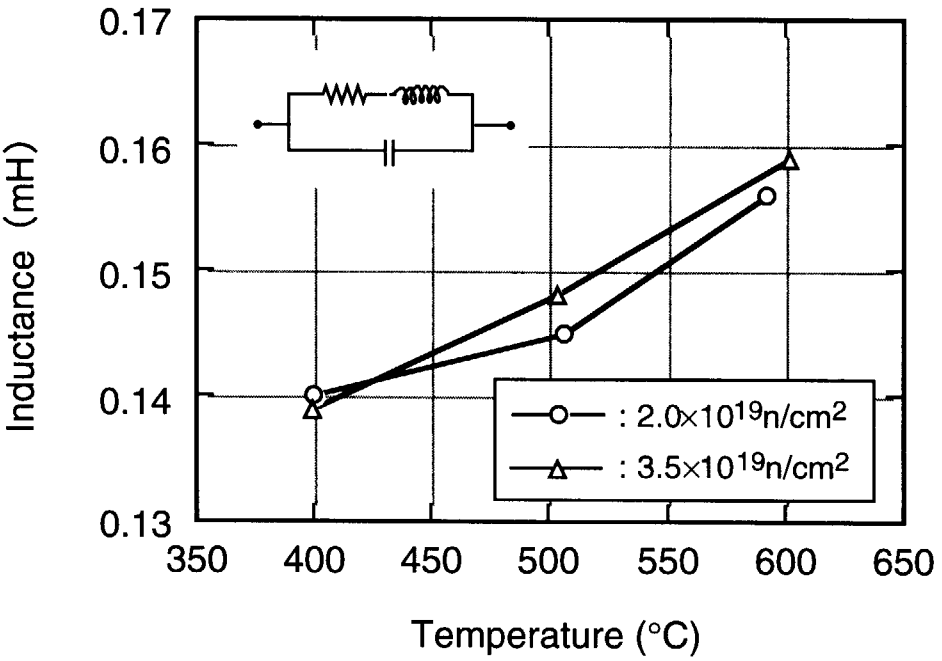

Fig. 7.1.4 Effect of coil temperature on inductance of magnetic probe at rated reactor power.

(3) RIEMF

The measurement result of RIEMF of the MI-cable insulator is shown in Fig.7.1.5. The RIEMF in the range of 4V-8V was observed under irradiation.

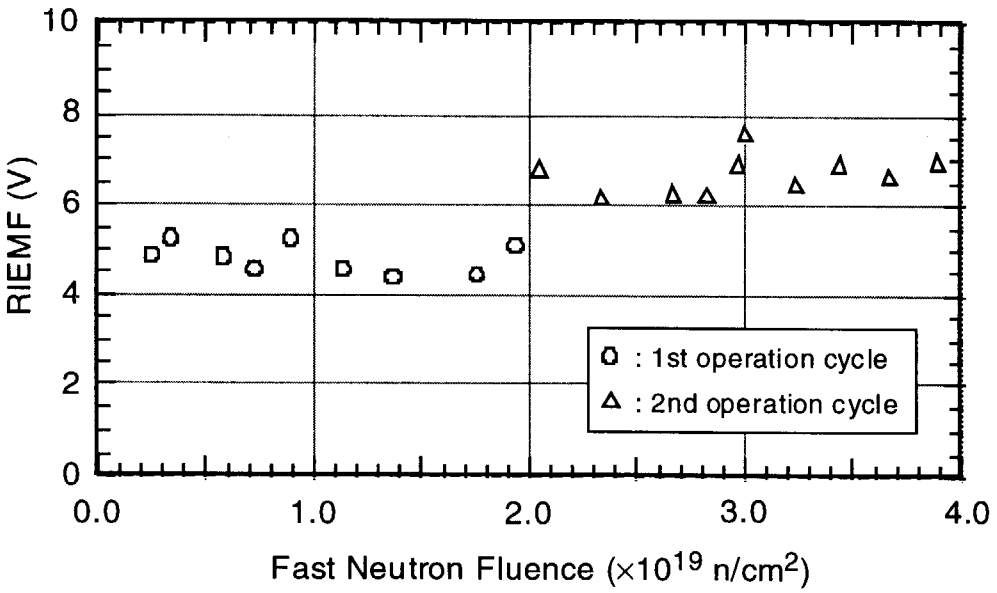

Fig.7.1.5 Effect of neutron fluence on RIEMF of magnetic probe at rated reactor power.

7.1.4. Conclusion

The magnetic probes made from MI-cable was irradiated in the JMTR to obtain data of electrical properties at high temperature and high neutron flux. The increase of inductance was observed with irradiation temperature risen, but it was constant at the steady temperature. Therefore, the irradiation temperature of magnetic probe should be constant when it uses in the ITER.

The reason why the inductance increases is not clear. The inductance was calculated automatically in the impedance analyzer. The equivalent circuit described in Fig.7.12 or Fig.7.13 does not consider the effect of MI-cable sheath material. It will be necessary to carry out further irradiation test in order to evaluate its effect.

8. Summary

Takeo Nishitani and Shin Yamamoto

In order to identify radiation hardened materials that can be used for diagnostics systems, an extensive data base of the impact of radiation on material characteristics must be constructed. In this report, the irradiation tests have been carried out on the basic materials of the transmission components such as ceramics, windows, fiber optics and mirrors, and in-vessel diagnostics sensors such as magnetic probes and bolometers. The in-situ measurement is essential for irradiation test on the In-Vessel Diagnostics Sensors and Transmission Components.

Ceramics
Ceramics will be used as general insulating materials. Here we investigated RIC (Radiation Induced Conductivity) effect of Al_2O_3 for 14 MeV neutrons. We confirmed that the RIC due to 14 MeV neutrons is similar to that due to other ionizing radiation such as electrons and gamma-rays. By extrapolating our results, the conductivity is estimated to be less than 10^{-6} S/m in the ITER 1st wall condition, which shows the availability of ceramics as an electrical insulator even in the vacuum vessel.

Windows
Light emission efficiency of window materials was measured for 14 MeV neutrons and ^{60}Co gammas. We found that the light emission efficiency for 14 MeV neutrons is less than 1/10 of that for gammas. So it is enough to take into account the light emission of the window due to gammas in the design of optical diagnostics.
In-situ measurement of transmission loss of windows was carried out in the JMTR reactor. High temperature is effective to reduce the induced loss of the windows. in the visible region.

Fiber optics
We carried out the irradiation test of pure silica and F-doped core fibers with Aluminum jack in JMTR, ^{60}Co gammas and 14 MeV neutrons. In the neutron fluence higher than 10^{20} n/m^2, there is no significant deference in those fibers. In gammas and neutron fluence lower than ~10^{19} n/m^2, the induce loss in F-doped core fiber is much less than pure silica core one, which suggests the viability of F-doped core fiber in the peripheral region inside the biological-shield.

Mirror/Reflector
Off-line irradiation of Mo reflector and in-situ test of Al one were performed in JMTR. There is no significant changes in those reflectors. Also Au coated mirror was irradiated. The surface was darkened maybe due to nuclear reaction of Au(n,γ)Hg.

Bolometers
We confirmed the performance of the JT-60 type bolometer with polyimide substrate under the ^{60}Co gamma-rays. The bolometer survived in gamma-rays up to 220 MGy which is almost equivalent dose of ITER life time at the bolometer location. We developed the AlN substrate bolometer and carried out irradiation tests in ^{60}Co gammas and JMTR. Significant increase in the bolometer resistance was observed, which should be considered in ITER.

Magnetic probes
The magnetic probe made of the MI cable has been irradiated in JMTR with in-situ measurements. The inductance kept constant up to 4×10^{23} n/m^2. The RIEMF(Radiation Induce Electrical Motive Force) of 5-8V was observed, which has weak dependence of the neutron fluence. We found that the RIEMF has high internal impedance, which suggests that we can neglect the RIEMF by using low impedance amplifier.

Acknowledgments

This report has been prepared as an account of work assigned to the Japanese Home Team under Task Agreement number G 55 TT 02 95-11-24 FJ within the Agreement among the European Atomic Energy Community, the Government of Japan, the Government of the Russian Federation, and the Government of the United States of America on Cooperation in the Engineering Design Activities for the International Thermonuclear Experimental Reactor ("ITER EDA Agreement") under the auspices of the International Atomic Energy Agency (IAEA).

This is a blank page.

国際単位系 (SI) と換算表

表 1　SI基本単位および補助単位

量	名称	記号
長さ	メートル	m
質量	キログラム	kg
時間	秒	s
電流	アンペア	A
熱力学温度	ケルビン	K
物質量	モル	mol
光度	カンデラ	cd
平面角	ラジアン	rad
立体角	ステラジアン	sr

表 2　SIと併用される単位

名称	記号
分，時，日	min，h，d
度，分，秒	°，′，″
リットル	l，L
トン	t
電子ボルト	eV
原子質量単位	u

1 eV = 1.60218 × 10^{-19} J

1 u = 1.66054 × 10^{-27} kg

表 5　SI接頭語

倍数	接頭語	記号
10^{18}	エクサ	E
10^{15}	ペタ	P
10^{12}	テラ	T
10^{9}	ギガ	G
10^{6}	メガ	M
10^{3}	キロ	k
10^{2}	ヘクト	h
10^{1}	デカ	da
10^{-1}	デシ	d
10^{-2}	センチ	c
10^{-3}	ミリ	m
10^{-6}	マイクロ	μ
10^{-9}	ナノ	n
10^{-12}	ピコ	p
10^{-15}	フェムト	f
10^{-18}	アト	a

表 3　固有の名称をもつSI組立単位

量	名称	記号	他のSI単位による表現
周波数	ヘルツ	Hz	s^{-1}
力	ニュートン	N	$m \cdot kg/s^2$
圧力，応力	パスカル	Pa	N/m^2
エネルギー，仕事，熱量	ジュール	J	N·m
工率，放射束	ワット	W	J/s
電気量，電荷	クーロン	C	A·s
電位，電圧，起電力	ボルト	V	W/A
静電容量	ファラド	F	C/V
電気抵抗	オーム	Ω	V/A
コンダクタンス	ジーメンス	S	A/V
磁束	ウェーバ	Wb	V·s
磁束密度	テスラ	T	Wb/m^2
インダクタンス	ヘンリー	H	Wb/A
セルシウス温度	セルシウス度	℃	
光束	ルーメン	lm	cd·sr
照度	ルクス	lx	lm/m^2
放射能	ベクレル	Bq	s^{-1}
吸収線量	グレイ	Gy	J/kg
線量当量	シーベルト	Sv	J/kg

表 4　SIと共に暫定的に維持される単位

名称	記号
オングストローム	Å
バーン	b
バール	bar
ガル	Gal
キュリー	Ci
レントゲン	R
ラド	rad
レム	rem

1 Å = 0.1 nm = 10^{-10} m

1 b = 100 fm^2 = 10^{-28} m^2

1 bar = 0.1 MPa = 10^5 Pa

1 Gal = 1 cm/s^2 = 10^{-2} m/s^2

1 Ci = 3.7 × 10^{10} Bq

1 R = 2.58 × 10^{-4} C/kg

1 rad = 1 cGy = 10^{-2} Gy

1 rem = 1 cSv = 10^{-2} Sv

（注）

1. 表1－5は「国際単位系」第5版，国際度量衡局 1985年刊行による。ただし，1 eVおよび1 uの値はCODATAの1986年推奨値によった。
2. 表4には海里，ノット，アール，ヘクタールも含まれているが日常の単位なのでここでは省略した。
3. barは，JISでは流体の圧力を表わす場合に限り表2のカテゴリーに分類されている。
4. EC閣僚理事会指令ではbar，barnおよび「血圧の単位」mmHgを表2のカテゴリーに入れている。

換算表

力	N(=10^5 dyn)	kgf	lbf
	1	0.101972	0.224809
	9.80665	1	2.20462
	4.44822	0.453592	1

粘度　1 Pa·s(N·s/m^2) = 10 P(ポアズ)(g/(cm·s))

動粘度　1 m^2/s = 10^4 St(ストークス)(cm^2/s)

圧力	MPa(=10 bar)	kgf/cm^2	atm	mmHg(Torr)	lbf/in^2(psi)
	1	10.1972	9.86923	7.50062 × 10^3	145.038
	0.0980665	1	0.967841	735.559	14.2233
	0.101325	1.03323	1	760	14.6959
	1.33322 × 10^{-4}	1.35951 × 10^{-3}	1.31579 × 10^{-3}	1	1.93368 × 10^{-2}
	6.89476 × 10^{-3}	7.03070 × 10^{-2}	6.80460 × 10^{-2}	51.7149	1

エネルギー・仕事・熱量	J(=10^7 erg)	kgf·m	kW·h	cal(計量法)	Btu	ft·lbf	eV
	1	0.101972	2.77778 × 10^{-7}	0.238889	9.47813 × 10^{-4}	0.737562	6.24150 × 10^{18}
	9.80665	1	2.72407 × 10^{-6}	2.34270	9.29487 × 10^{-3}	7.23301	6.12082 × 10^{19}
	3.6 × 10^6	3.67098 × 10^5	1	8.59999 × 10^5	3412.13	2.65522 × 10^6	2.24694 × 10^{25}
	4.18605	0.426858	1.16279 × 10^{-6}	1	3.96759 × 10^{-3}	3.08747	2.61272 × 10^{19}
	1055.06	107.586	2.93072 × 10^{-4}	252.042	1	778.172	6.58515 × 10^{21}
	1.35582	0.138255	3.76616 × 10^{-7}	0.323890	1.28506 × 10^{-3}	1	8.46233 × 10^{18}
	1.60218 × 10^{-19}	1.63377 × 10^{-20}	4.45050 × 10^{-26}	3.82743 × 10^{-20}	1.51857 × 10^{-22}	1.18171 × 10^{-19}	1

1 cal = 4.18605 J(計量法)
= 4.184 J　(熱化学)
= 4.1855 J　(15 °C)
= 4.1868 J(国際蒸気表)

仕事率　1 PS(仏馬力)
= 75 kgf·m/s
= 735.499 W

放射能	Bq	Ci
	1	2.70270 × 10^{-11}
	3.7 × 10^{10}	1

吸収線量	Gy	rad
	1	100
	0.01	1

照射線量	C/kg	R
	1	3876
	2.58 × 10^{-4}	1

線量当量	Sv	rem
	1	100
	0.01	1

（86年12月26日現在）